

https://dspace.org/

Characterization and leaching studies of cobalt and nickel-polysulfone nanocomposite membranes for potential water treatment

Enemuo, Ngozi Doris

2018

https://hdl.handle.net/10539/26951

Enemuo, Ngozi Doris (2018) Characterisation and leaching studies of cobalt and nickel-polysulfone nanocomposite membranes for potential water treatment, University of the Witwatersrand, Johannesburg, https://hdl.handle.net/10539/26951

Downloaded from a DSpace repository. https://dspace.org/

CHARACTERIZATION AND LEACHING STUDIES OF COBALT AND NICKEL-POLYSULFONE NANOCOMPOSITE MEMBRANES FOR POTENTIAL WATER TREATMENT



By

Ngozi Doris Enemuo

A dissertation submitted to the Faculty of Science, University of the Witwatersrand, Johannesburg, in fulfilment of the requirements for the degree of Master of Science

University of the Witwatersrand, Johannesburg.

DECLARATION

I declare that this dissertation is my own, unaided work. It is being submitted for the degree of Master of Science at the University of the Witwatersrand, Johannesburg. It has not been submitted before for any degree or examination at any other University.



(Signature of candidate)

1st November, 2018

(Date)

ABSTRACT

In spite of the undeniable importance of water for survival, a considerable number of people have no access to clean usable water as a result of high contamination of the water sources available to them. The consumption of the unclean water leads to epidemic diseases such as cholera and some other diseases whose adverse effect on the health of the people can range from mild to fatal. Although the conventional methods of water treatment are available, the challenges associated with their applications prompts researches towards finding more efficient alternatives. Application of nanotechnology in water treatment membranes is one of such unconditional means that is gaining ground in the field of membrane technology.

This work aimed at preparing nanocomposite membranes with a potential application in water treatment. This was done by modifying polysulfone using nickel and cobalt nanoparticles aimed at improving the polysulfone for effective usage in water treatment. The properties of the modified membranes were obtained and the stability of the embedded nanoparticles assessed. The synthesized nickel and cobalt nanoparticles were characterized using X-ray diffraction, and Transmission electron miscroscopy. The properties of the membranes were determined using Scanning electron miscroscopy, Atomic force miscroscopy, Thermogravimetric analysis, Contact angle measurements. The leaching of the nanoparticles from the nanocomposite polysulfone membranes was assessed using Inductively coupled plasma mass spectroscopy.

For the membranes modified with Ni, the hydrophilicity improved from 89.05^{o} to 75.49^{o}. Co nanoparticles also improved the hydrophicity from 89.05^{o} to 80.52^{o}, however the PSF-10 membrane exhibited contact angle of 89.45^{o} as a result of agglomeration at such high amount of Co. The pore sizes were increased from 0.307 μm to 0.833 μm and 0.307 μm to 1.79μm for the Co and Ni modified membranes respectively. In addition, the embedded nanoparticles were stable in the PSF matrix.

ACKNOWLEDGEMENTS

I would like to thank my amiable supervisor, Dr. Heidi Richards, for her immeasurable effort in impacting her knowledge and skills in me, and ensuring that I thrive as a young researcher in the field of membrane technology. To Dr. Somandla Ncube, words cannot express how grateful I am for the times you spent on assisting me despite your busy schedules.

The friendly postgraduate students in the Environmental Analytical Chemistry research group really made this journey plain sailing. From the deepest of my heart, I appreciate your help and sacrificing your time to listen and assist.

My gratitude also goes to my family for being a solid support to me throughout the duration of this program. To my exceptional husband, you made my dream of furthering my academic career a reality, and I am highly grateful. Special thanks to my beautiful daughters, Michelle and Chioma, for coping when I had to work late hours. I am also indebted to my mom and siblings for their prayers and support.

Table of Contents

DECLARATION I
ABSTRACT II
ACKNOWLEDGEMENTS III
TABLE OF CONTENTS IV
LIST OF FIGURES VII
LIST OF TABLES X
LIST OF ABBREVIATIONS XI
CHAPTER 1 1
1 INTRODUCTION 2
CHAPTER 2 5
2 LITERATURE REVIEW 6
2.1 Membranes 6
2.1.1 Classification of membranes 7
2.1.2 Fabrication of membranes 10
2.1.3 Fouling of membranes 13
2.2 Nanomaterials 15
2.2.1 Nanoparticles 15
2.2.2 Types of nanoparticles 17
2.2.3 Preparation route of nanoparticles 18
2.2.4 Safe use of nanoparticles 21
2.2.5 Modification of membranes using nanomaterials/nanoparticles 22
2.3 Recent works on nanocomposite membranes 23
2.3.1 Polysulfone-based nanocomposite membranes 23
2.4 Drawbacks of nanocomposite membranes 32
2.4.1 Agglomeration of nanoparticles in nanocomposite membranes 33
2.4.2 Leaching of nanocomposite membranes 36
2.5 Instrumental characterization of the prepared nanocomposite PSF membranes 37
2.5.1 Scanning Electron Miscroscopy (SEM) 38

2.5.2 Energy Dispersive X-ray (EDX) 41
2.5.3 Transmission Electron Microscopy (TEM) 42
2.5.4 Atomic Force Microscopy AFM 42
2.5.5 Contact Angle measurement 44
2.5.6 Thermogravimetric Analysis TGA 45
2.5.7 Inductively Coupled Plasma Mass Spectroscopy ICP-MS 46
CHAPTER 3 48
3 AIMS AND OBJECTIVES 49
3.1 Aims 49
3.2 Objectives 49
3.3 Research Questions 49
3.4 Motivation 50
CHAPTER 4 51
4 METHODOLOGY 52
4.1 Materials 52
4.1.1 Glassware 52
4.1.2 Chemical reagents 52
4.2 Methods 52
4.2.1 Synthesis of the Ni nanoparticles 52
4.2.2 Synthesis of the cobalt nanoparticles 53
4.2.3 Preparation of the Co and Ni-modified nanocomposite PSF membranes 54
CHAPTER 5 55
5 RESULTS AND DISCUSSION 56
5.1 The characterization of the nickel nanoparticles 56
5.2 The characterization of the cobalt nanoparticles 58
5.3 The characterization of the nickel modified-PSF membranes 60
5.3.1 The SEM result 60
5.3.2 The AFM result 63
5.3.3 The FTIR result 68
5.3.4 The TGA result 70

5.3.5 The contact angle result 71
5.3.6 The flux result 71
5.3.7 Leaching results 72
5.4 Characterization of the cobalt modified-PSF membranes 74
5.4.1 The SEM result 74
5.4.2 The AFM result 77
5.4.3 The FTIR result 82
5.4.4 The TGA result 84
5.4.5 The contact angle result 85
5.4.6 The flux result 85
5.4.7 Leaching results 88
CHAPTER 6 90
6 CONCLUSIONS AND RECOMMENDATIONS 91
6.1 Conclusions 91
6.2 Recommendations 92
REFERENCES 93

List of Figures

Figure 1 Schematic diagram of a membrane separation process 6
Figure 2 Classification of membranes according to structure (Bradley & Al-Shaeli 2017) 9
Figure 3 Schematic diagram of immersion precipitation. 11
Figure 4 Different pore pattern (a), and the irradiation setup (b), of track-etching techniques (Toimil-Molares 2012). 13
Figure 5 Selected-Area Electron Diffraction of an amorphous Ni-B alloy nanoparticles (Hoang & Ganguli 2012). 177
Figure 6 Water-in-oil microemulsion 20
Figure 7 The SEM image of the outer surface of (a) Neutral-PSF, (b) 0.25wt% Ag-PSF (c) 0.5wt% Ag-PSF, and (d) 1.0wt% Ag-PSF modified membranes (Koseoglu-Imer et al. 2013) 25
Figure 8 SEM cross-section image of (a) neutral-PSF, and (b) 0.01wt% (c) 0.05wt% (d) 0.1wt% (e) 1.0wt% zeolite-PSF hollow fiber membranes (Dahe et al. 2012) 27
Figure 9 The SEM image of (a) neutral membrane, (b) 0.5wt% TiO_2-PSF, (c) 0.75wt% TiO_2-PSF, (d) 1.0wt% TiO_2-PSF membranes (Emadzadeh et al. 2014) 28
Figure 10 The SEM image of the (a) neutral polysulfone, (b) PSF membrane modified through blending method, (c) PSF membrane modified through photopolymerization, and (d) PSF membrane modified through interfacial polymerization 29
Figure 11 The SEM image of the 0.02wt% (denoted NCM_1), and 0.03wt% (denoted NCM_2) alumina-PSF nanocomposite membranes 30
Figure 12 The SEM image of the PSF-Ni nanocomposite membrane showing uniform porosity (Phelane et al. 2014b) 31
Figure 13 SEM image of the cobalt- modified polysulfone membrane. 32
Figure 14 SEM cross-sectional image showing agglomeration in polyaniline/iron oxide nanoparticles modified polyethersulfone membrane (Daraei et al. 2012). 35
Figure 15 The basic components of SEM (JEOL) 40

Figure 16 Typical modern scanning electron microscope 41
Figure 17 Contact angle measurement of hydrophobic and hydrophilic surfaces (Jhaveri & Murthy 2016). 445
Figure 18 The TEM image of (a) big Ni particles of average size of 200nm, and (b) agglomerated Ni nanoparticles. 56
Figure 19 The XRD spectra of the Ni nanoparticles 57
Figure 20 The TEM image (a), and size distribution (b), of the Ni nanoparticles. 58
Figure 21 The TEM image (a), and size distribution (b), of the Co nanoparticles. 59
Figure 22 The SEM images of the top surface of the Ni-modified and unmodified PSF membranes 61
Figure 23 The SEM images of the inner structures of the Ni-modified and unmodified PSF membranes 62
Figure 24 The EDX spectra of the Ni-modified and unmodified PSF membranes 63
Figure 25 The 3D AFM images of the Ni-modified and unmodified PSF membranes 64
Figure 26 The 2D AFM images of the three different areas of the Ni modified PSF-3 membrane showing the quantitative roughness data of the membrane. 65
Figure 27 The 2D AFM images of the three different areas of the Ni modified PSF-5 membrane showing the quantitative roughness data of the membrane. 66
Figure 28 The 2D AFM image of the three different areas of the Ni modified PSF-10 membrane showing the quantitative roughness data of the membrane. 67
Figure 29 The FTIR spectra of (a) unmodified PSF-0, and the Ni modified (b) PSF-3,(c) PSF-5, and (d) PSF-10. 69
Figure 30 The TGA curve of the Ni-modified and unmodified PSF membranes. 70
Figure 31 The flux of the Ni-modified and unmodified membranes at different pressures. 72
Figure 32 (a) Concentration of the released Ni nanoparticles, and (b) EDX of the “after leaching” membranes. 73
Figure 33 The SEM image of the top surface of the Co-modified and unmodified PSF membranes 74

Figure 34 The SEM image inner structures of the Co-modified and unmodified PSF membranes 75
Figure 35 The EDX of the Co-modified PSF membranes 77
Figure 36 The 3D AFM image of the cobalt modified and unmodified PSF membranes. 78
Figure 37 The 2D AFM image of the three different areas of the Co modified PSF-3 membrane. 79
Figure 38 The 2D AFM image of the three different areas of the Co modified PSF-5 membrane. 80
Figure 39 The 2D AFM image of the three different areas of the PSF-10 membrane. 81
Figure 40 The FTIR spectra of (a) unmodified PSF-0, (b) Co modified PSF-3, (c) Co modified PSF-5, and (d) Co modified PSF-10. 83
Figure 41 The TGA curve of the Co-modified and unmodified PSF membrane..... 84
Figure 42 The flux of (a) unmodified PSF, (b) Co-modified PSF-3, (c) Co-modified PSF-5, (d) Co-modified PSF-10, (e) unmodified and modified Co-PSF membranes at 0.15MPa, and (f) agglomeration in PSF-10 membrane 87
Figure 43 (a)The concentration of the released Co nanoparticles, and (b) EDX of the "after leaching" Co-PSF membranes. 89

List of Tables

Table 1 Classification of porous membranes according to pore size (Van Der Bruggen et al. 2003). 8
Table 2 The benefits and limits of ceramic membranes over polymeric membranes (Basile & Gallucci 2011). 10
Table 3 Some synthetic methods of some armorphous nanoparticles (Sattler 2011). 20
Table 4 Some surface interactions that occur in particles in a liquid medium (Ng et al. 2013) 34
Table 5 Some differences between SEM and TEM. 42
Table 6 The composition of the casting solutions of the various prepared membranes 54
Table 7 The R_a and R_{RMS} values of the Ni-modified and unmodified PSF membranes. 68
Table 8 Contact angle results of the Ni-modified and unmodified PSF membranes. 71
Table 9 The pore sizes of the Co-modified and unmodified PSF membranes. 76
Table 10 The R_a and R_{RMS} values of the Co-modified and unmodified PSF membranes. 82
Table 11 Contact angle results of the Co-modified and unmodified PSF membranes. 85

List of Abbreviations

AFM	Atomic force microscopy
EDX	Energy dispersive X-ray
FTIR	Fourier-transform infrared spectroscopy
ICPMS	Inductively coupled plasma mass spectroscopy
NOAEL	No observable adverse effect level
NOM	Natural organic matter
PES	Polyethersulfone
PSF	Polysulfone
SAED	Selected-area electron diffraction
SEM	Scanning electron miscroscopy
TEM	Transmission electron microscopy
TGA	Thermogravimetric analysis
TFC	Thin-film composite
USEPA	United states environmental protection agency
WHO	World health organization
WRC	Water research commission
XRD	X-ray diffraction

CHAPTER 1

Chapter one provides a brief discussion into water scarcity as a global challenge. It introduces membrane technology and nanotechnology as promising in providing a solution to water scarcity. It also highlights leaching of incorporated nanoparticles from nanocomposite membranes as an inherent adverse effect in use of nanotechnology in membranes.

1 INTRODUCTION

Water is an essential part of life but its high demand limits its availability. The availability of water and its demand has a somewhat similar antagonistic relation as defined by the law of demand and supply, that is, the high usage of water by the ever-growing population leads to diminished availability or supply of water.

Apart from high population, contamination of water bodies is a contributing factor to water scarcity and availability. In cases where there are no amenities for the treatment of such polluted waters, the residents are left with no option than to use such contaminated water. For instance, an estimated 2 billion people drink water that are contaminated with faeces (World Health Organisation (WHO) 2017). The detrimental health effects resulting from the consumption of contaminated water includes cholera, hepatitis A, diarrhea, typhoid, dysentery, and polio.

Another factor that leads to water scarcity is the uneven distribution of water across the globe. This results in physical water scarcity where there is not enough natural water resources to meet the water demands. Some parts of the world are naturally water-stressed, while others have high abundance of water. About 1.2 billion people live in areas of physical water scarcity (UNDESA) 2014), and that is 16% of the current world population. An incidence of physical water scarcity is not far-fetched as South Africa is a case study with an average annual rainfall of 464 mm (South Africa Yearbook 2015), with less than 500 mm of rain received by 65% of the country per year (Water Research Commission (WRC) 2015).

To alleviate or eradicate the water scarcity problems, several policies have been implemented such as the Water Framework Directive (European Community 2000), World Health Organization (WHO) water quality guidelines (WHO) 2001), and the South Africa Department of Water Affairs (DWA) water policy (Department of

Water Affairs (DWA) 2013). In addition to the policies, techniques and methods for water and wastewater treatments have been developed. One of such methods is membrane technology.

Membrane technology is gaining momentum in the field of water treatment research as the number of journals published per year has been on the increase. This is attributed to the ease of preparation as well as ease of use of membranes. The application of membranes span across simple to advanced treatment of water and wastewater. The use of membranes for the removal of organic matter (Miaomiao Zhang et al. 2003), trace metal ions (Tian et al. 2011), salts (Ahmad et al. 2004), pharmaceutical residues (Radjenović et al. 2008), and virus (Zodrow et al. 2009) has been reported. Membranes frequently used for water and wastewater treatment are polysulfone (PSF), polyethersulfone (PES), and so forth.

Polysulfone is one of the leading polymers used in membrane technology. It has physical properties that favours its use in membrane preparation such as high strength, toughness, rigidity, and ability to maintain its properties over a wide range of temperatures (Liesl K. Massey 2003), however, the hydrophobicity of polysulfone is a limiting factor in its use in membrane technology because it reduces the adsorption of water to polysulfone, and also causes fouling of the membrane. Membrane fouling arises from adsorption as a result of chemical interaction between solutes and membranes, blockage of pores by solutes, and biofouling due to the growth and adhesion of bacteria and virus at the membrane's surface (Goosen et al. 2005). Decline in flux, permeate quality, and high energy requirement are some of the consequences of a fouled membrane. Fouled membranes can undergo physical cleaning such as backwashing, chemical cleaning and physio-chemical cleaning, however the cleaning process can be tedious and costly (Ning 2011).

To minimize fouling, most of the membranes used for the treatment of water and wastewater are usually modified and tailored towards efficiency, and selectivity of

the intended contaminants. Several approaches have been developed in modifying polysulfone and in general, polymer membranes. One of such approach is nanotechnology. Nanotechnology can be described as technology that is implemented at the nanoscale, and it includes nanomaterials (Bharat Bhushan 2017).

Nanomaterials are materials that are smaller than 100 nm in at less one dimension (Qu & Alvarez 2013). A typical nanomaterial has properties that are different from its larger counterpart. At this nano-size, there is increased surface area leading to enhanced properties of membranes modified with nanomaterials. Silver nanoparticles (Sawada et al. 2012a), carbon nanotubes (Zhao et al. 2014), nickel and cobalt nanoparticles (Phelane et al. 2014a) and several other nanomaterials have been used in modification of membranes for water treatment.

Despite the beneficial implication of the nanoparticles in modifying water treatment membranes, it is necessary that they are applied with caution as the incorporated nanoparticles might not be stable enough in the membrane matrix thereby leading to leaching of the nanoparticles from the membranes during their use in water treatment. Zhang et al. reported leaching of silver from bio-Ag/PES nanocomposite membranes, even though the observed amount of leached silver was still in the tolerance range stipulated by WHO (Zhang et al. 2012a). Reports on leaching and devising means of its minimization have been published (Li et al. 2014).

In this research, nickel and cobalt nanoparticles were used to modify polysulfone membranes, and the impact of the nanoparticles as well as their possible leaching from the modified membranes were studied.

CHAPTER 2

Chapter two gives a detailed literature review of the topics relevant to this work. These includes membranes, nanomaterials, nanocomposite membranes, the work done so far on nanocomposite membranes, and the research area that is ignored but is crucial to the application of nanocomposite membranes. The various instrumental characterizations employed in this work were also discussed here.

2 LITERATURE REVIEW

2.1 Membranes

The word membrane originates from the latin word “membrana” (Oxford University Press 2004). A membrane can be described as a separation barrier that separate two phases and has the ability to limit the transport of many components selectively (Wang et al. 2011). The separation process of a typical membrane involves the passage of a solution or mixture through the membrane, and the permeate passes through while the retentate is rejected. This is as a result of the difference in the physical and chemical properties of the membrane and the transported components. The driving force of the membrane separation process can be due to pressure gradient, concentration gradient, temperature gradient, and electrical voltage gradient (Beier Søren Prip 2015). A schematic depiction of the separation process of a membrane is shown in Figure 1.

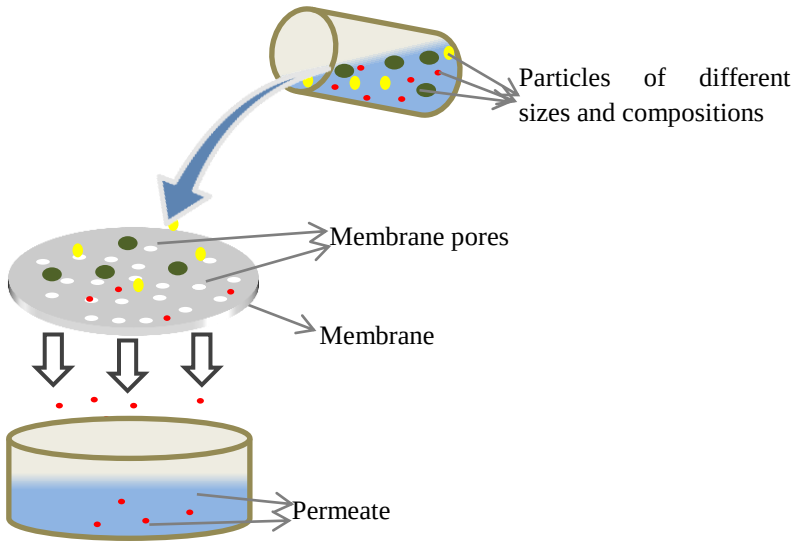


Figure 1 Schematic diagram of a membrane separation process

Different contaminated solutions or mixtures including water and wastewater can be purified using different varieties of membranes. The use of membranes as a separation technique has more preference than other convectional separation methods due to their ease of use and low operational cost. In addition, membrane separation process requires no chemical, biological, or thermal change of the component.

2.1.1 Classification of membranes

There are several different ways of classifying membranes. Two of the major ways are: classification according to their structure, and classification according to their materials. According to the structure or morphology, the classification of membranes are (Bradley & Al-Shaeli 2017):

- Dense homogenous membranes
- Porous membranes
- Composite membranes

The preparation of dense homogeneous membranes is done in two ways: through solvent evaporation of solution, or by the extrusion of the melted polymer (S.P. & Peinemann 2006). An example is a silicone polymer membrane.

The porous membranes, as the name suggests, have defined pores. They are divided into microfiltration, ultrafiltration, nanofiltration, and reverse osmosis. This classification of porous membranes is based on their pore sizes. Table 1 shows the pores sizes of the various porous membranes.

Table 1 Classification of porous membranes according to pore size (Van Der Bruggen et al. 2003)

Porous membranes	Pore size (nm)
Microfiltration	100-10000
Ultrafiltration	2-100
Nanofiltration	0.5-2
Reverse osmosis	< 0.5

Porous membranes can further be divided into symmetric and asymmetric membranes (Bradley & Al-Shaeli 2017). Few membranes have symmetric structure, and they are prepared by track etching and precipitation from the vapour phase (Khulbe et al. 2008). Majority of membranes have asymmetric structure, and consist of a top skin layer (thin dense layer) and a porous layer at the bottom of the membrane. The skin layer gives the membrane its permeation properties while the mechanical strength of the membrane is due to the porous layer (Khulbe et al. 2008).

The composite membrane, which is the third class of membrane according to structure, has a top layer that is dense and a porous inner layer. A schematic diagram of the classification of membranes according to structure is shown in Figure 2.

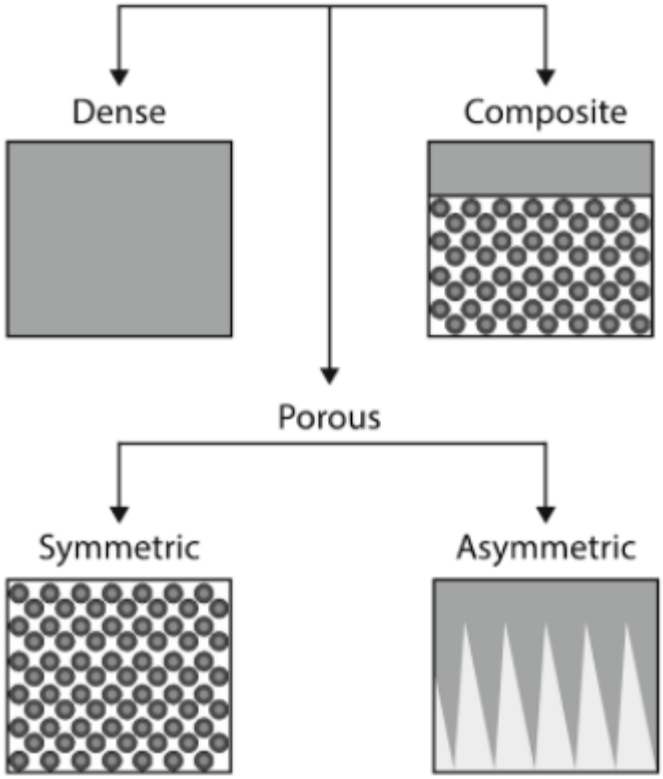


Figure 2 Classification of membranes according to structure (Bradley & Al-Shaeli 2017)

Membranes used in water and wastewater treatment are also classified according to their materials as polymeric (organic), and ceramic (inorganic) membranes (Cui & Muralidhara 2010). Commonly used polymeric membranes include polysulfone, polyethersulfone, cellulose acetate, and polyamide. They have properties which fronts them as the material of choice in membrane technology. Some of these properties include ease of preparation, low cost, availability, and ease of use.

Ceramic or inorganic membranes are more costly than polymeric membranes, however, they are used in applications that demands high thermal, chemical, and mechanical stability (Weber et al. 2003). The brittle nature of ceramic membranes also limits its use in membrane technology. The benefits and limits of ceramic membranes in comparison with polymeric membranes are listed in Table 2.

Table 2 The benefits and limits of ceramic membranes over polymeric membranes (Basile & Gallucci 2011).

Benefits	Limits
Good stability at high temperatures	Capital intensive
High resistance to extreme conditions such as pH	Embrittlement phenomenon
Resists high pressure drops	Limited membrane surface per volume of matrix
Resists degradation from microbes	Limitation in acquiring high selectivities in industries microporous membranes
Easy to clean fouled membrane	At low temperatures, permeability of dense membranes is low
Catalytic activation is easily achievable	Module sealing at high temperature is difficult

Polymeric membranes overcome the limitations associated with ceramic membranes, hence their high preference in water treatment membranes.

2.1.2 Fabrication of membranes

There are different ways of fabricating membranes for various applications. For a polymeric membrane, the choice of fabrication method depends on the type of polymer, and the intended application. The most common methods of polymeric membrane fabrications are (Lalia et al. 2013): Phase inversion, interfacial polymerization, track-etching, and electrospinning.

2.1.2.1 Phase inversion

Phase inversion involves the transformation of a thermodynamically stable polymer solution from liquid to solid state in a controlled manner (Hołda & Vankelecom 2015). Phase inversion can be achieved in different ways which are (Werber et al. 2016):

1. Non-solvent induced phase separation: it is also called immersion precipitation, and it involves immersing the polymer solution in a coagulation bath which is a non-solvent. The transformation of the polymer solution to a solid is as a result of exchange between the solvent of the polymer solution and the non-solvent. The most commonly used non-solvent is water. The non-solvent and solvent must be miscible for precipitation to occur. A schematic diagram of a typical immersion precipitation is shown in Figure 3. This method was employed in this study.

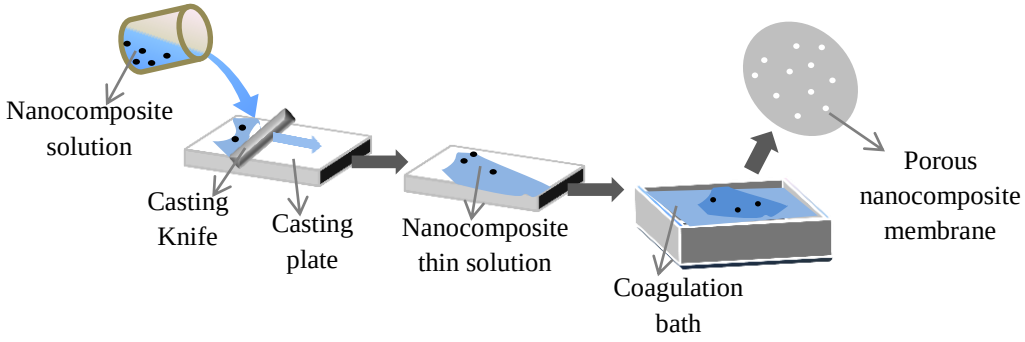


Figure 3 Schematic diagram of immersion precipitation.

2. Thermally-induced phase separation: This technique involves slowly cooling of a high temperature polymer solution until demixing occurs. It utilizes the fact that solvent quality decreases as the temperature decreases.

3. Controlled-solvent evaporation phase separation: In this technique, the solvent is evaporated from thin film polymer solution resulting in demixing of the polymer solution.

2.1.2.2 Interfacial polymerization

Interfacial polymerization is a technique for the preparation of ultrathin layers, hollow nanospheres, and nanofibers (Raaijmakers & Benes 2016). In this technique, a reactive set of monomers, such as amide, is interfacially polymerized on a microporous support surface, such as a polysulfone surface (Petersen 1993). The procedure involves immersing the microporous support membrane into an aqueous solution of the first reactant, and then placing the substrate to an organic solution containing the second reactant such that the reaction takes place at the interface of the two solutions (which are immiscible). The formation of a thin dense layer on the surface of the support membrane prevents the reaction from proceeding further. It is most commonly used to fabricate thin-film composite (TFC) reverse osmosis and nanofiltration membranes.

2.1.2.3 Track-etching

Track-etched membranes are thin-film membranes having fine, geometrically distinct pores. These membranes are formed by either irradiation with fragments resulting from heavy metal fission, or by ion beams from accelerators (Apel 2001). The preparation method involves two steps which are irradiation of a nonporous polymeric film, and etching of the damaged polymer chains that remains after the irradiation using appropriate chemical such as alkali solutions (Miyazaki & Takenaka 2017). The formed pores are usually cylindrical with pore diameter depending on the etching time. The most important advantage of this technique is the ability to control the pore size distribution of the membranes. A schematic diagram showing the different pore pattern(a), and the irradiation setup (b) of track-etching technique is presented in Figure 4 (Toimil-Molares 2012).

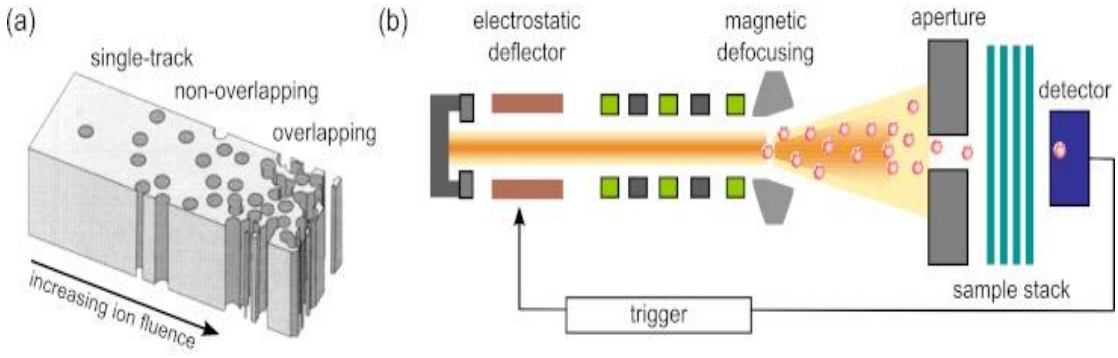


Figure 4 Different pore pattern (a), and the irradiation setup (b), of track-etching techniques (Toimil-Molares 2012).

2.1.2.4 Electrospinnning

Eletrospinning is a relatively new technique that is gaining ground as membrane fabrication process which involves using an electrically charged jet of polymer solution to produce polymeric membranes (Gopal et al. 2006). The principle of the technique is basically the interaction between the electrostatic field and the conducting fluid (Chu et al. 2001). High porosity and large surface area per unit volume are the major advantages of an electrospun membrane. The disadvantage is the difficulty in handling such membranes as a result of its tendency to accumulate electrostatic charges during the electrospinning process.

2.1.3 Fouling of membranes

Fouling is a serious setback in the application of membranes in water treatment. Fouling is the phenomenon whereby particles, colloids, salts, macromolecules, bacteria, virus, etc. are deposited on the surface and/or inside of the pores of the membrane (Jhaveri & Murthy 2016). It is brought about by the physical and chemical interaction of the foulant with the membrane. The major consequences of a fouled membrane are reduction in permeability, and its lifespan, as well as, increase in cost of operation as a result of high operational energy demand. Fouled membranes can be

cleaned with chemical but the cost and procedures involved is economically draining. The rate of fouling is determined by various conditions such as the nature and concentration of solutes and solvents, type of membrane, the distribution of pore size, and the surface properties and nature of membrane (Peinemann & Nunes 2010). There are different types of fouling based on the origin of the foulant. The membrane fouling types are defined below (Guo et al. 2012):

1. Organic fouling: This is as a result of colloids such as proteins which adsorbed on the membranes. Fouling caused by natural organic matter (NOM) has been considered to be the main cause of membrane fouling (Rana & Matsuura 2010).

2. Inorganic fouling: This type of fouling is as a result of the precipitation of dissolved inorganic components such as silica onto the surface of the membrane as a result of oxidation or pH scaling.

3. Biological fouling: fouling of this type is called biofouling. It caused by the presence of algae, bacteria, virus, etc. in the feed water. These microorganisms adhere or penetrate to the membrane thereby leading to fouled membrane.

4. Particulates: Particulate matters can block the pores of the membrane and cause fouling of the membrane. This type of fouling can also arise from cake layer formation on the surface by particulate matter thereby obstructing the effective permeation of the feed water.

Over the years, parameters such as hydrophilicity, roughness, and surface charge have been used as basis for finding solution to membrane fouling (Li et al. 2017). Two of the methods of dealing with membrane fouling are (Chun et al. 2017):

- Cleaning of the fouled membrane using appropriate chemical such as sodium hydroxide.

- Modification of the membrane so as to eradicate or minimize fouling tendency of the modified membrane. Such modification can be achieved by the incorporation of nanomaterials to the membrane material.

2.2 Nanomaterials

The word "Nano" is a prefix that describes something that has a factor of 10^{-9}. It originated from the Greek word "nanos" meaning "dwarf". In relation to length, "nano" is a billionth of a meter. Therefore for a material to be "nano", at least one of its dimensions has to be in this range. In the field of nanotechology, different approaches are used to classify nanomaterials. One of these approaches is classification according to the form of products, and they are listed as (Cao & Wang 2011):

- Nanoparticles
- Nanorods or nanowires
- Thin films
- Nanostructured bulk materials

2.2.1 Nanoparticles

The nanomaterial of our interest is nanoparticles. The size of this type of nanomaterial is less than the wavelength of visible light (400nm). Nanoparticle is defined as material whose size is between 1-100nm (Hosokawa 2012). The small size of nanoparticles gives them unique properties which are different from their bulky counterparts.

These properties include (Hosokawa 2012):

1. Activated particle surface

All the different states of matters, solids, liquids, and gases, consist of atoms or molecules bonded together, and exhibit characteristic properties. Some solids consist of network of atoms bonded together. When the solid is broken to the size in the nano-range, the solid tends to be affected by the characteristic of the atoms or molecules, and exhibit different properties from their bulky counterparts as a result of change in the bonding state of the atoms or molecules that made up the solid. This is the reason behind the unique characteristics exhibited by nanoparticles which includes better interaction between nanoparticles and any contacting material.

2. Increased surface area

As the size of the nanoparticles approaches the nano-range, there is increase in the specific surface area of the particles. Increased surface area is directly related to reaction rates, therefore nanoparticles has greater reaction or interaction with any contacting medium than their bulky equivalent.

These unique properties of nanoparticles have led to broadened research field employing nanoparticles. These areas cover almost all fields of science which include medicine, cosmetics, agriculture, and environmental science. In medicine, nanoparticles have been reported, to control the formation of oral biofilm (Allaker 2010), to enhance radiotherapy in mice (Hainfeld et al. 2004), and as antimicrobials (Hernández-Sierra et al. 2008). Many reports have also been published on the use of nanoparticles in cosmetics, an example is the use of solid lipid nanoparticles to enhance penetration of retinyl palmitate in porcine skin (Jenning et al. 2000). The use of nanoparticles in agriculture is also an emerging research field. (S. W. Kim et al. 2012) reported silver nanoparticles as an antifungal for eighteen different plant

pathogenic fungi, and novaluron nanoparticles have been reported as a potential insecticide (Elek et al. 2010). In the environmental science, specifically in water treatment, the use of nanoparticles is a very active research field where they are mainly employed in the modification of the membranes for water treatment purposes. A more detailed discussion on the use of nanoparticles in membrane modification is discussed in section 2.2.5.

2.2.2 Types of nanoparticles

The various classification of nanoparticles includes (Sattler 2011):

1. Amorphous nanoparticles

This is the type of nanoparticles whose structure is disordered. The parts of an amorphous nanoparticle can be grouped into the core, and the surface of the nanoparticles. The different parts of an amorphous nanoparticle have distinct characteristics. The core has properties similar to the bulky equivalent of the amorphous nanoparticles, while the surface has structure characterized with defeats and high porosity. This type of nanoparticle is usually difficult to produce because of the high tendency of many materials to crystallize (Amstad et al. 2015). A typical selected-area electron diffraction (SAED) image of an amorphous nanoparticle is shown in Figure 5 below.



Figure 5 Selected-Area Electron Diffraction of an amorphous Ni-B alloy nanoparticles (Hoang & Ganguli 2012).

2. Magnetic nanoparticles

They are highly crystalline nanoparticles whose characteristics are contributed by their intrinsic properties and the interaction between the particles (Kodama 1999). The size of a magnetic nanoparticle is similar to the size of a magnetic domain. As a result, two types of magnetic behavior arises from magnetic nanoparticles, which are (Kodama 1999):

- Single domain ferromagnetic nanoparticles
- Superparamagnetic nanoparticles

The major difference in the magnetic behavior of a bulky magnetic nanoparticle and a collection of single domain ferromagnetic nanoparticles is the magnetization cycle mechanism through the hysteresis loop. The superparamagnetic nanoparticles have properties varying from high saturation magnetization accompanied by a low saturation field, and no remnant magnetization. There are no magnetic interactions between the particles of a superparamagnetic nanoparticles (Mahmoudi et al. 2011), therefore there is better control on the aggregation of the nanoparticles.

2.2.3 Preparation route of nanoparticles

Magnetic nanoparticles can be synthesized using three different ways, namely:

1. Coprecipitation: This is one of the major methods used in preparing magnetic nanoparticles. It usually involves preparation from aqueous salt solutions by adding a base in a room or elevated temperature under inert conditions (Sattler 2011). Parameters such as pH, the precursor concentration, stirring speed, temperature can be used to control the size and magnetic properties of the nanoparticles (Kim et al. 2003). (Suh et al. 2012) prepared non-spherical nanoparticles by using coprecipitation to grow the crystals. (Houshiar et al. 2014) also synthesized $CoFe_2O_4$ nanoparticles using salt solutions of iron chloride and cobalt by the coprecipitation method.

2. Thermal decomposition: Nanoparticles can also be synthesized in the presence of surfactants by the thermal decomposition of organometallic compounds in high boiling organic solvents. The surfactant acts as the stabilizing agent to control the size of the nanoparticles during the synthesis. (Chin et al. 2011) employed the method of thermal decomposition to synthesize magnetite nanoparticles. They controlled the shape and size of the magnetite nanoparticles by optimizing the concentration of the precursor, the reaction times, and the surfactants. They took a step further by using reagents that are environmentally friendly in the synthesis of the Fe_3O_4 nanoparticles. (Herrera et al. 2013) also used thermal decomposition to synthesize cobalt ferrite nanoparticles using iron-cobalt oleate precursor dissolved in high boiling 1-octadecene solvent.

3. Microemulsion: In this method, the synthesis of the nanoparticles is done in a water-in-oil microemulsion media. A surfactant is dispersed in an oil phase, where there is an entrapment of the microdroplets of the aqueous phase (Tartaj et al. 2003). Lakshmanan et al. prepared nanoparticles of magnetic iron oxide using this method (Lakshmanan et al. 2014). In their study, magnetic iron oxide was nanoparticles applied in removing phosphate from sewage wastewater. (Okoli et al. 2011) also prepared magnetic iron oxide nanoparticle by the water-in-oil microemulsion, and they applied the nanoparticles in protein purification. A typical water-in-oil microemulsion is illustrated in Figure 6.

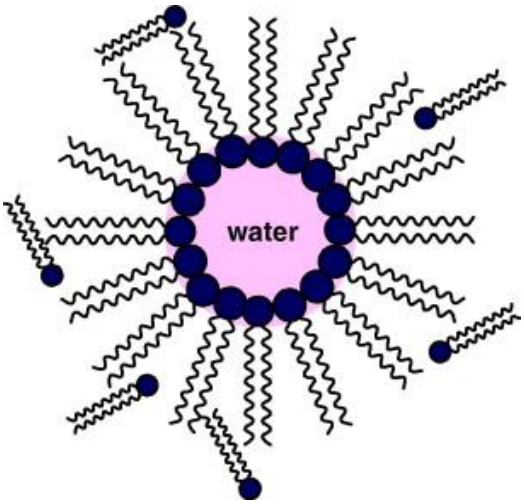


Figure 6 Water-in-oil microemulsion.

Table 3 Some synthetic methods of some amorphous nanoparticles (Sattler 2011).

Synthetic methods	Substances
Hydrolysis, and then condensation	Fe_2O_3, GeO_2
Thermally induced solid-state decomposition	Fe_2O_3, Ni-B
Sol-gel method	TiO_2
Precipitation	Fe_2O_3
Microwave pyrolysis	Fe_2O_3
Sonochemical synthesis	Fe_2O_3, Fe_3O_4, Ni, Ag
Microwave irradiation	Fe_2O_3
Chemical reduction	(Fe, Co, Ni)-(B,P)
Electroless deposition	Ni-W-P
Gas phase condensation	SnO_2
Laser ablation condensation	Al_2O_3

2.2.4 Safe use of nanoparticles

In spite of the beneficial application of nanoparticles, precautions must be exercised during their use as nanoparticles can be detrimental to both human and environmental health. Cobalt-chromium nanoparticles have been reported to damage human fibroblast cells by the transmission of purine nucleotides and intercellular signaling within the barrier resulting in DNA damage (Bhabra et al. 2009). Du et al. reported that TiO_2 and ZnO can hinder the growth of wheat, and TiO_2 has the capability of adhering to the cell walls of the wheat (Du et al. 2011). They found that TiO_2 can be held in the soil for an extended period of time, and the ZnO can be dissolved in the soil leading to much uptake of unsafe Zn by the plant. Li et al. reported leaching of a TiO_2-modified polyethersulfone membrane (Li et al. 2014). Therefore, to ensure safe use of nanoparticles, it is important to consult and have deep knowledge of the cons and pros of the nanoparticles, as well as the stipulated tolerance limit of the nanoparticles with regard to the body and environment.

Different health and environmental bodies such as World Health Organization (WHO), and United States Environmental Protection Agency (US EPA) have policies that should be followed in this regard. For instance, the world health organization stipulated that 0.1mg/litre of silver in drinking water can be tolerated by the human without health risk (WHO 2003). Also, total intake of 10g of silver is stipulated for the entire lifetime of human, and this is known as the "no observable adverse effect level" (NOAEL). The guideline value for nickel in drinking water is 12µg/kg of body weight (WHO 2005). Cobalt guidance limit for freshwater was set at 8µg/litre (WHO 2006), and no guideline has been set by WHO for cobalt in drinking water.

2.2.5 Modification of membranes using nanomaterials/nanoparticles

Several methods can be utilized in modifying polymeric membranes. The modification to be discussed in this section will be specifically for incorporating nanomaterials to polymeric membranes. The aim of incorporating nanomaterial is to harness the unique properties of nanomaterial into the polymeric membranes, with the resulting modified membranes exhibiting improved properties. The number of reports on improved properties of polymeric membranes due to nanaomaterials' incorporation is overwhelming. The enhancement in porosity, hydrophilicity, antifouling, and roughness are many but few of the results (Cao et al. 2006; Razmjou et al. 2011). Two main strategies/methods have been devised for modification using nanomaterials. These are:

- Coating/deposition
- Blending

Coating/deposition of nanomaterials is done by placing the nanomaterials on the surface of the membrane through self-assembly leading to rapid interaction of the coated nanomaterials and the membrane material (Al Aani et al. 2017). The procedure involves immersing the membrane in a solution of the nanomaterial. This modification method has been widely used such as the coating TiO_2 on polysulfone (Bae & Tak 2005), polyethersulfone (Luo et al. 2005), and anionic sulfonated polyethersufone (Bae et al. 2006). Coating/deposition is an easy method, however the interaction between the deposited nanomaterial and the membrane surface is usually not strong, leading to high possibility of losing the nanomaterials with time (Yin & Deng 2015). This will seriously jeopardize the effectiveness of the modified membrane in water treatment.

Blending of nanomaterial in a polymeric membrane involves the impregnation of the nanomaterial on the inner matrix of the polymer. This is achieved by simply adding a

measured amount of the nanomaterial in the polymer casting solution, and stirring appropriately until the nanomaterial is well dispersed in the casting solution. In contrast to the coating method, the nanomaterial is well embedded in the polymer other than the surface of the polymer. The outrageous number of reports on blending fronts it as the preferred method of incorporating nanomaterials. This includes blending of ZnO nanoparticles to polyvinylidene fluoride (Liang et al. 2012), to polysulfone (Leo et al. 2012), carbon nanotube to polyethersufone (Celik et al. 2011), and TiO_2 to polyvinylidene fluoride (Oh et al. 2009).

Agglomeration of the incorporated nanoparticles in the polymer matrix has been a major drawback in blending modification technique. Agglomeration results from the uneven dispersion of nanomaterials in the membrane. The adverse effect of agglomeration includes clogging of pores, and change in the expected properties of the modified membrane. Many means have been introduced to minimize agglomeration such as mechanical and chemical treatment of the nanomaterial (Razmjou et al. 2012; Razmjou et al. 2011), and use of low concentration of nanomaterial (Sotto et al. 2011).

2.3 Recent works on nanocomposite membranes

There is an active and growing research on membranes modified with nanoparticles. This is attributed to the favourable transition that is observed when a neutral polymer membrane is incorporated with nanoparticles. Some of the works done on some membranes with various nanoparticles will be discussed in the following sections.

2.3.1 Polysulfone-based nanocomposite membranes

1. Polysulfone-silver nanocomposite membranes

Silver nanoparticles are the most commonly used nanoparticles for modification of polysulfone membranes. Due to their antibacterial property, silver nanoparticles are

used to control biofouling of membranes. In addition to anti-biofouling impact, silver nanoparticles also improve the hydrophilicity, porosity, and roughness of membranes. Koseoglu-Imer et al. modified polysulfone (PSF) membranes by incorporating different ratios (0.25, 0.5, 1.0 w/w) of silver nanoparticles to the polysulfone solutions (Koseoglu-Imer et al. 2013). It was found in the study that the incorporation of the nanoparticles enhanced the porosity of the outer surface of the various membranes. Improved porosity is linked to improved permeability of membranes. Agglomerates of the Ag nanoparticles were observed on the surface of the different modified membranes. It was also observed in the study that the agglomerates increase as the amount of incorporated Ag increases. Figure 7 shows the SEM image of the outer surface of their neutral and modified membranes.

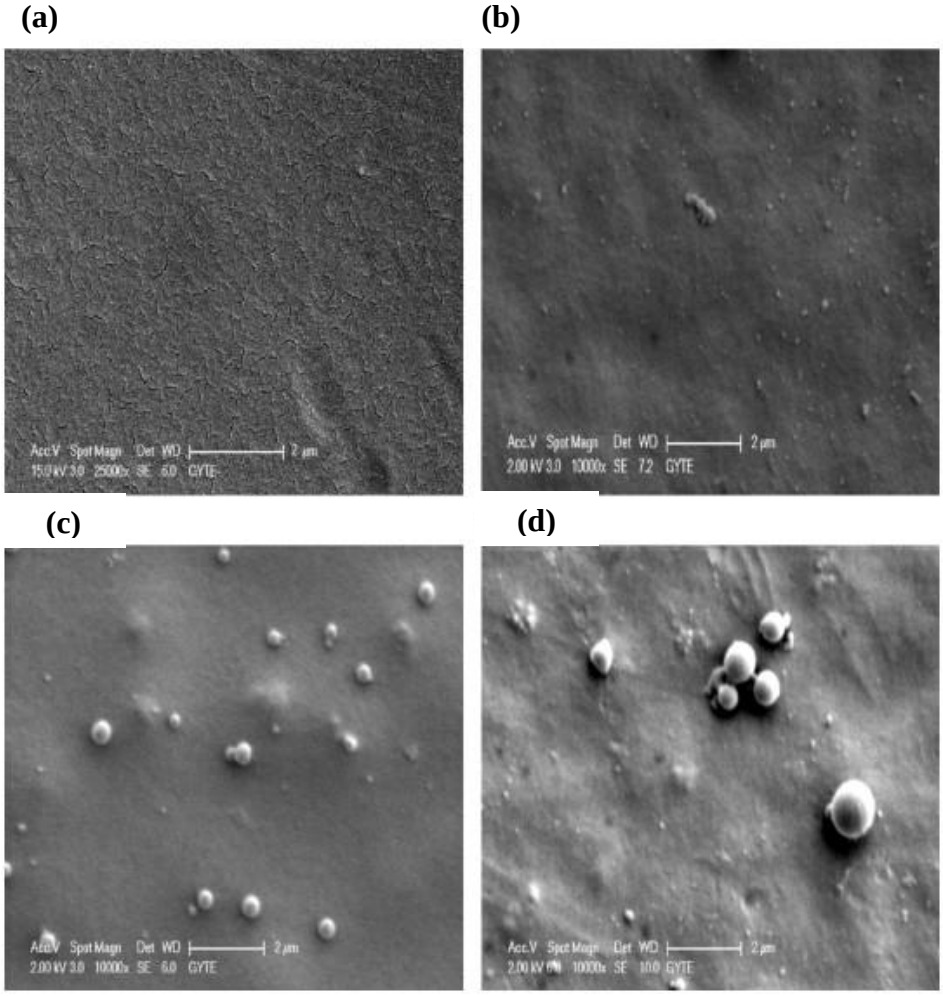


Figure 7 The SEM image of the outer surface of (a) Neutral-PSF, (b) 0.25wt% Ag-PSF (c) 0.5wt% Ag-PSF, and (d) 1.0wt% Ag-PSF modified membranes (Koseoglu-Imer et al. 2013)

The SEM result showed that as the concentration of the silver nanoparticles increases, the porosity and agglomeration increases. Therefore, it is of utmost importance to consider both the desired and the undesired effect of increasing the amount of nanoparticles used in modification of membranes. In terms of biofouling, it was found that the presence of the Ag nanoparticles decreased the growth of bacteria. From the AFM, and permeability result, the study found that roughness and permeability were favoured due to the Ag incorporation. Some other reported

modifications of polysulfone using Ag nanoparticles include (Andrade et al. 2015), (Zhang et al. 2012b), and (Sawada et al. 2012b).

2. Polysulfone-zeolite nanocomposite membranes

Dahe et al. used different compositions (0.01, 0.05, 0.1, and 1.0wt%) of zeolite nanoparticles to prepare modified polysulfone hollow fiber membranes (Dahe et al. 2012). The results of their study showed that the incorporation of the zeolite up to 0.05wt% increases the diameters and the wall thickness of the modified membranes, while further addition of the zeolite led to a decrease of the diameter and wall thickness of the membranes. From the results, a model was postulated relating flux to the zeolite incorporation, and proposed that the nucleation and nodule formation in the membrane were improved by the addition of the zeolite nanoparticles thereby leading to increased flux. The decrease in flux at high zeolite concentration was reported to be as a result of zeolite agglomeration which led to reduced pore number in the membranes. Figure 8 shows the SEM cross-sectional image of the various zeolite modified polysulfone hollow fiber membranes. The reported negative effect on flux as a result of agglomeration at higher zeolite concentration also proves the importance of balancing nanoparticle's concentration with desired and undesired effects on the membrane performance.

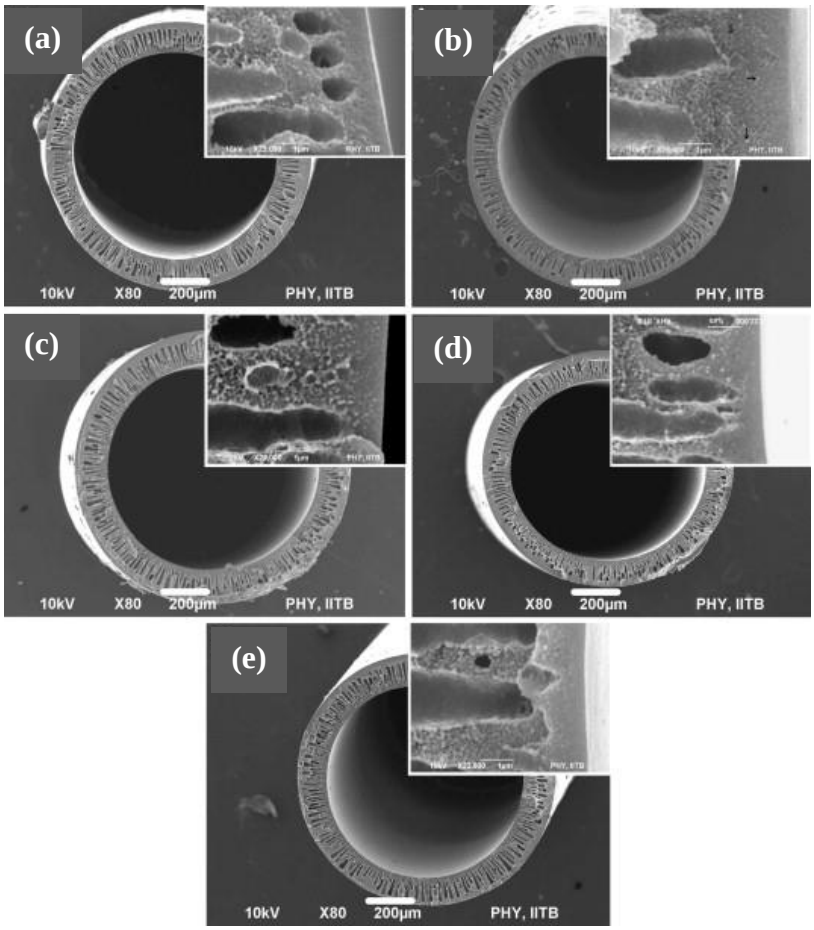


Figure 8 SEM cross-section image of (a) neutral-PSF, and (b) 0.01wt% (c) 0.05wt% (d) 0.1wt% (e) 1.0wt% zeolite-PSF hollow fiber membranes (Dahe et al. 2012)

3. Polysulfone-titanium dioxide nanocomposite membranes

Emadzadeh et al. prepared nanocomposite membranes by adding different proportions (0.5wt%, 0.75wt%, and 1.0wt%) of TiO_2 nanoparticles to polysulfone (Emadzadeh et al. 2014). The prepared nanocomposite membranes were applied in desalination of water. The SEM image of the TiO_2-PSF membranes showed that the morphology of the membranes was enhanced on subsequent addition of the TiO_2 nanoparticles. Similar to the Ag and zeolite nanoparticles modified membranes,

agglomeration of the TiO_2 nanoparticles were also found to increase as the nanoparticles composition increases. The SEM images of the various modified membranes are shown in Figure 9.

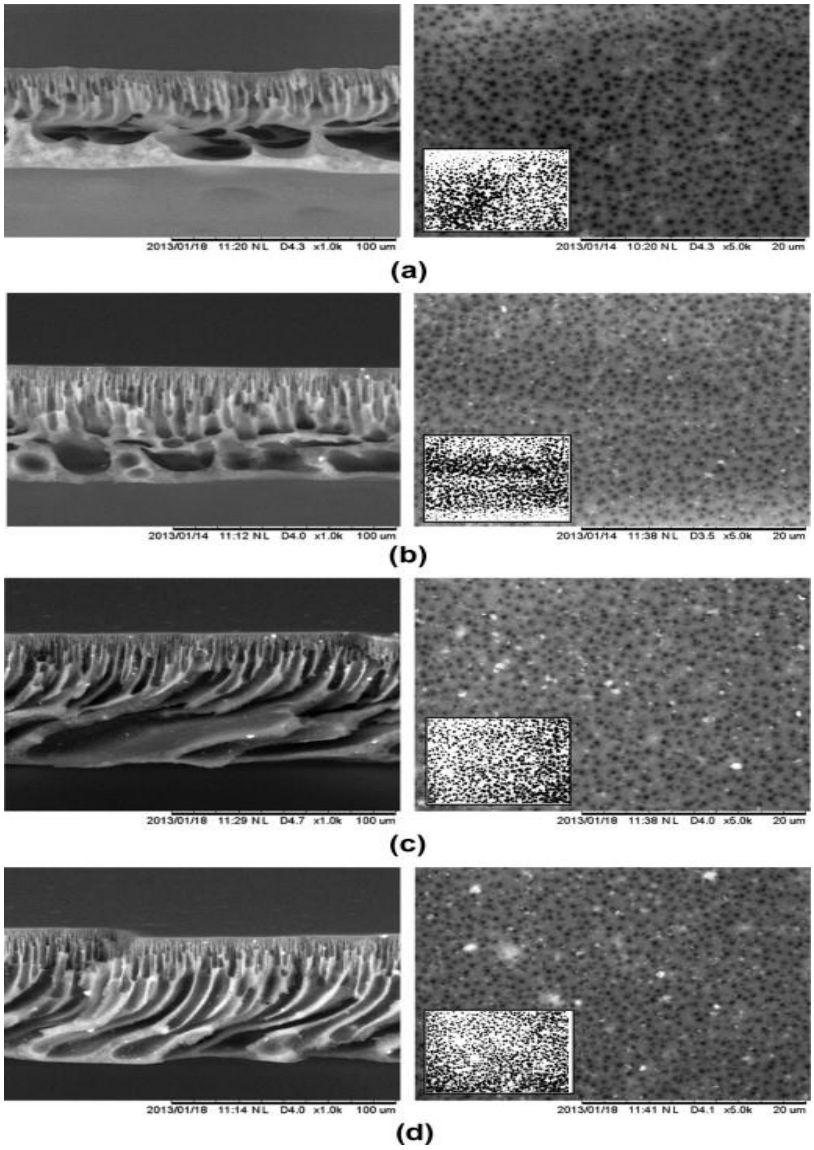


Figure 9 The SEM image of (a) neutral membrane, (b) 0.5wt% TiO_2-PSF, (c) 0.75wt% TiO_2-PSF, (d) 1.0wt% TiO_2-PSF membranes (Emadzadeh et al. 2014)

Other parameters such as the hydrophilicity, roughness, and permeability were also reported to have been favoured by the various additions of the TiO_2 nanoparticles.

The salt rejection however decreased with the subsequent incorporation of the nanoparticles. It was concluded that for optimium result and performance of the TiO_2-polysulfone nanocomposite membrane, 0.5wt% nanoparticle is the ideal composition to use for the modification. Several other reports on polysulfone-TiO_2 nanocomposite membranes have also been written such as (Hamid et al. 2011), (G. Zhang et al. 2013), (Yang et al. 2007), and (Jyothi et al. 2016).

4. Polysulfone-iron oxide nanocomposite membranes

Iron oxide is also among the nanoparticles used in modification of polysulfone membrane for enhanced properties. Homayoonfal et al. reported the incorporation of iron oxide nanoparticles to polysulfone using the blending, photopolymerization and interfacial polymerization method (Homayoonfal et al. 2014). The morphology of the modified membranes, irrespective of the method of incorporation of the nanoparticles, was enhanced. Figure 10 shows the SEM image of the modified membranes prepared by the various methods.

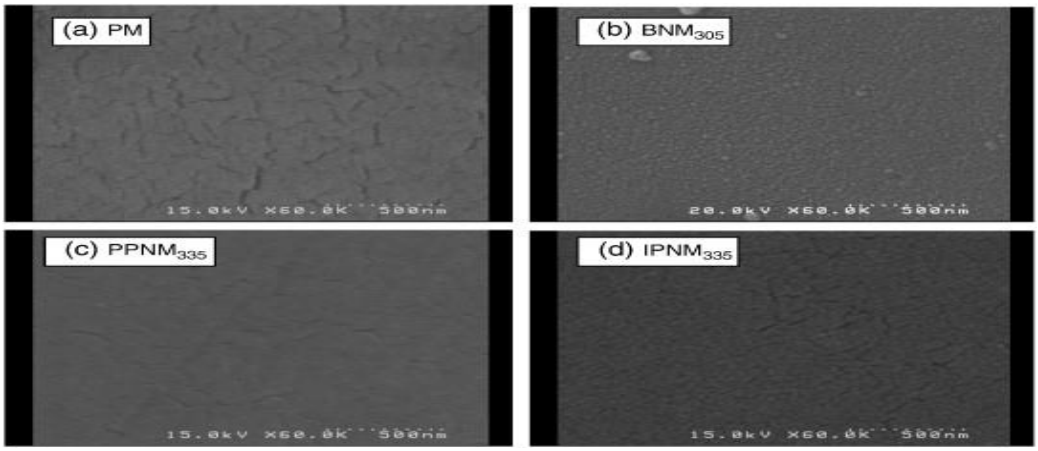


Figure 10 The SEM image of the (a) neutral polysulfone, (b) PSF membrane modified through blending method, (c) PSF membrane modified through photopolymerization, and (d) PSF membrane modified through interfacial polymerization (Homayoonfal et al. 2014).

It was also found from the study that other parameters such as hydrophilicity and roughness were also improved by the incorporation of the iron oxide nanoparticles to the polysulfone membranes.

5. Polysulfone-alumina nanocomposite membranes

The preparation of a polysulfone nanocomposite membranes using alumina was reported by Homayoonfal et al. (Homayoonfal et al. 2015). They modified the polysulfone with 0.02wt%, and 0.03wt% of alumina separately. Interestingly, they found that increasing the alumina concentration from 0.02wt% to 0.03wt% decreased the porosity of the membranes. This was unusual behavior since the incorporation of a nanoparticle to a polymeric membrane is expected to increase the porosity with increase in the concentration of the nanoparticles. The decreased porosity observed with increased concentration of the nanoparticles was explained by the increase in the viscosity of the dope solution. The increased viscosity of the dope solution on addition of more nanoparticles decreased the phase inversion process thereby decreasing the porosity. Figure 11 shows the SEM image of the 0.02wt%, and 0.03 wt% alumina modified polysulfone membranes.

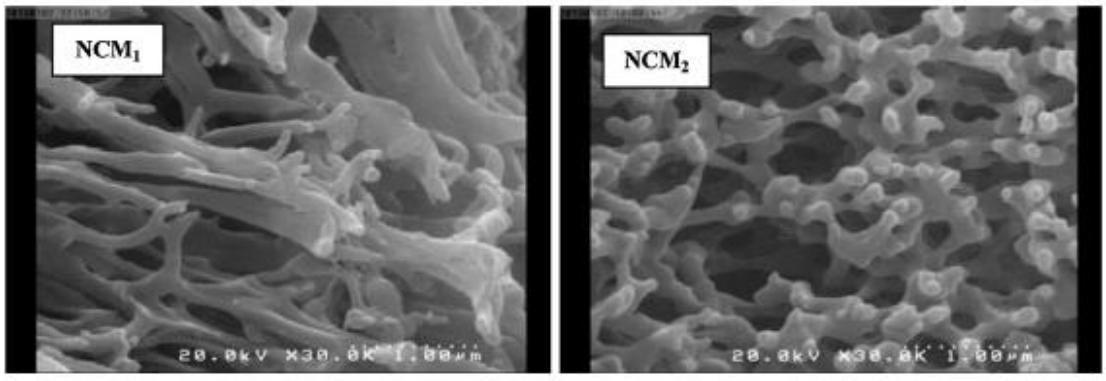


Figure 11 The SEM image of the 0.02wt% (denoted NCM_1), and 0.03wt% (denoted NCM_2) alumina-PSF nanocomposite membranes (Homayoonfal et al. 2015).

The hydrophilicity, roughness, and the mechanical strength of the nanocomposite membranes were enhanced on increasing the concentration of the alumina nanoparticles. Modification of a polysulfone hollow fiber membrane using alumina has also been reported (Choi et al. 2006).

6. Polysulfone-nickel nanocomposite membranes

There are very few reports on the use of nickel nanoparticles in the modification of polysulfone membranes. Phelane et al. reported preparation of a polysulfone membrane modified with nickel nanoparticles (Phelane et al. 2014b). They found that the incorporation of the nickel nanoparticles to the polysulfone led to a uniformly porous nanocomposite membrane. Figure 12 shows the SEM result of the polysulfone-nickel nanocomposite membrane.

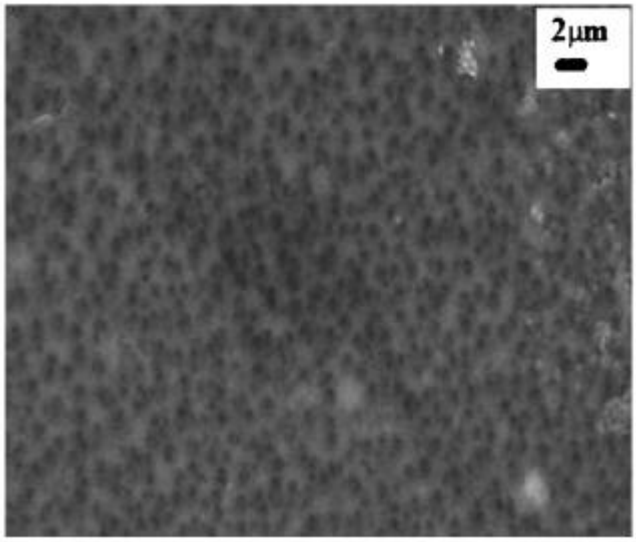


Figure 12 The SEM image of the PSF-Ni nanocomposite membrane showing uniform porosity (Phelane et al. 2014b)

The contact angle of the Nickel modified membrane was found to decrease on the addition of the nanoparticle, and thus the hydrophilicity was enhanced. Lee et al. also

reported successful modification of polysulfone with nickel powders (Lee et al. 2008).

7. Polysulfone-cobalt nanocomposite membranes

Phelane et al. also modified a polysulfone membrane using cobalt nanoparticles (Phelane et al. 2014b). They found that a uniformly distributed porous nanocomposite was formed on incorporation of the cobalt nanoparticles. Figure 13 shows the SEM image of the cobalt modified polysulfone membrane. The formal potential from the electrochemical analysis of the modified membrane was measured to be 1.20V. The hydrophilicity was also found to increase on addition of the cobalt nanoparticle.

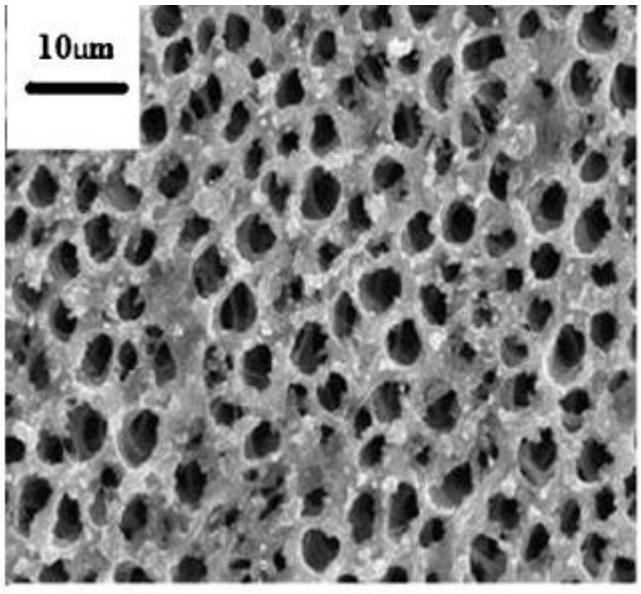


Figure 13 SEM image of the cobalt- modified polysulfone membrane (Phelane et al. 2014b).

2.4 Drawbacks of nanocomposite membranes

Two major pitfalls are normally encountered in membrane modification using nanoparticles. These are agglomeration of the incorporated nanoparticles in the

membrane matrix, and the leaching of the incorporated nanoparticles from the modified membrane.

2.4.1 Agglomeration of nanoparticles in nanocomposite membranes

Agglomeration of nanoparticles arises from the surface interaction between the nanoparticles. The surface interaction is primarily as a result of the van der waals forces that exist in the nanoparticles (Min et al. 2008). However, other forms of interactions can lead to agglomeration, and they are presented in Table 4. The sizes of the nanoparticles are so small, hence it is difficult to avoid aggregation of the nanoparticles. At this nanosize, there is high possibility of collision between the particles since the distance between the particles is minimized due to the reduced particle size. Agglomeration of nanoparticles can occur during the synthesis of the nanoparticles, or incorporation of the nanoparticles in the polymer solution (Zare 2016). The intended improvement in the properties of the nanocomposite membranes is jeopardized by agglomeration of the nanoparticles, and such negative impact includes formation of holes and defeats in the modified membranes (Saleh & Gupta 2016).

Table 4 Some surface interactions that occur in particles in a liquid medium (Ng et al. 2013)

Surface interaction	Description
Van der Waals interaction	Electromagnetic interaction between atoms and/or molecules
Hydration force	Overlap of water molecules on the surface of an hydrophilic particle
Steric interaction of adsorbed polymer	Interaction by adsorption of polymer layer on particles
Overlap of electric double layer	Interaction by overlap of electric double layer around particles
Bridge force	Production of the bridge of polymer binder and/ or surfactant between particles

Several reports of agglomeration of incorporated nanoparticles have been presented in various studies of nanocomposite membranes. Razmjou et al. found that use of higher concentration of TiO_2 nanoparticles led to agglomeration even after modification of the nanoparticles prior to incorporation (Razmjou et al. 2011). The incorporation of 5 wt% of TiO_2 nanoparticles to a PVDF membrane was found to lead to agglomeration of the incorporated nanoparticles, however no agglomeration was observed when lower concentration was used (F. Zhang et al. 2013). SEM image of polyaniline/iron oxide nanoparticles modified polyethersulfone membranes prepared by Daraei et al. showed severe agglomeration of the incorporated nanoparticles (Daraei et al. 2012). In the study, the adverse effect of the agglomeration includes low ion rejection. The study also found that agglomeration increases with increased concentration of the nanoparticles. Figure 14 shows the agglomeration of the incorporated polyaniline/iron oxide nanoparticles as seen in the cross sectional SEM image of the nanocomposite membrane.

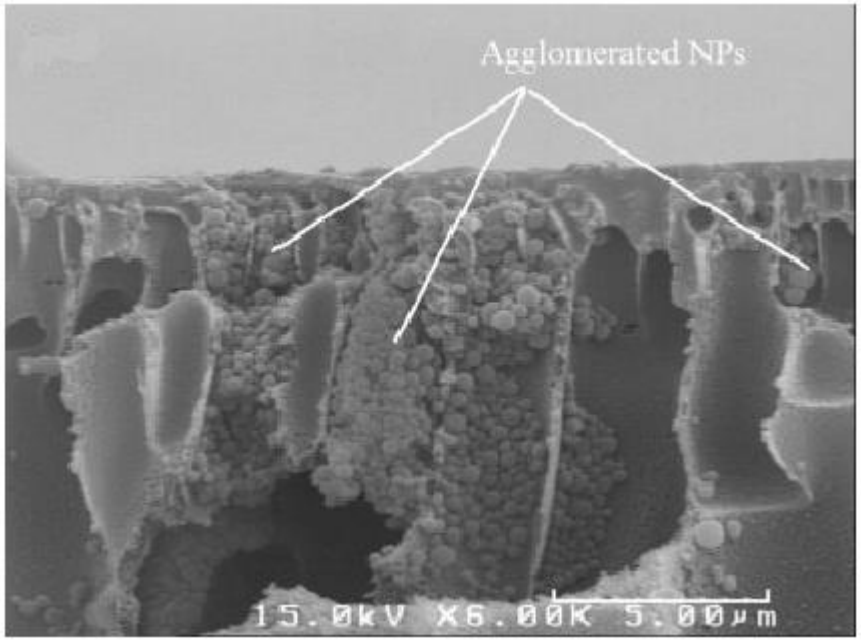


Figure 14 SEM cross-sectional image showing agglomeration in polyaniline/iron oxide nanoparticles modified polyethersulfone membrane (Daraei et al. 2012).

From the above mentioned studies, it can be concluded that the modification of polymer membranes with higher concentration of the incorporated nanoparticles will lead to greater possibility of agglomeration in the nanocomposite matrix.

Several methods have been proposed to combat agglomeration. The carboxylation of TiO_2 nanoparticles was used as a strategy to minimize agglomeration in polyvinyl alcohol nanocomposite membranes (Rajaeian et al. 2015). Rajaeian et al. used silane coupling agent to minimize agglomeration of TiO_2 nanoparticles in a polyamide nanocomposite membrane (Rajaeian et al. 2013). Chemical and mechanical modification of TiO_2 was used by Razmjou et al. to mitigate agglomeration (Razmjou et al. 2011).

2.4.2 Leaching of nanocomposite membranes

This aspect of research is usually ignored in studies regarding nanocomposite membranes. It is a crucial part of the modification protocol of nanocomposite membranes. It is beyond the bounds of possibility to put into application any nanocomposite membrane whose nanoparticles' stability was not tested. Leaching of incorporated nanoparticles from the nanocomposite membranes typically occurs when there is lack or minimum chemical interaction between the nanoparticles and the polymer, and as a result the stability of the nanoparticles in the matrix is weak. The weak stability makes the nanocomposite membrane prone to leaching during filtration. Two major consequences of leaching are (Saleh & Gupta 2016):

i. Ineffectiveness of the nanocomposite membranes
ii. Inefficiency of the incorporated nanoparticles.

In order to assess leaching, different criteria has been employed. Zhang et al. filtered ultrapure water through Ag-modified PES nanocomposite membrane using dead-end filtration cell (Zhang et al. 2012c). The filtration was done for 12 hours, and the permeate was collected every 30 minutes. The Ag concentration in the permeate was analyzed using Inductively Coupled Plasma Mass Spectroscopy, ICP-MS. It was found that the Ag nanoparticles slowly leached from the modified PES membranes, and the amount of leached Ag decreases as more water was filtered. One of the most significant information from the study was that leaching increases with increase in incorporated nanoparticles. Although the study reported leaching, the amount of Ag leached was below the tolerance limit stipulated by the WHO.

Silver leaching was also assessed by Kim et al. (Kim et al. 2012). In the study, the modified membrane was soaked in water for three days, and the concentration of Ag in the water measured after the three days. The soaked membrane was also used to filter milli-Q water, and the concentration of Ag in the permeate measured. In both

cases, the concentration of Ag was quantified using ICP-MS. The result showed that about 0,04% of the incorporated Ag leached, and the leaching diminished as more water was filtered. It was concluded from the study that the incorporated silver was stable in the matrix of the modified membrane.

The leaching of silver was also investigated in a cellulose acetate hollow fiber membrane by Chou et al. (Chou et al. 2005). In this study, the modified membrane was soaked in a stirring water bath for 180 days. It was found that after 180 days, 90% of the Ag on the surface of the modified membrane leached while 39% of Ag on the bulk of the modified membrane was leached.

The above mentioned examples emphasized the importance of assessing leaching of embedded nanoparticles in nanocomposite membranes. The information obtained from the leaching study will help to determine whether a nanoparticle-modified membrane is suitable for use in water treatment.

2.5 Instrumental characterization of the prepared nanocomposite PSF membranes

The various properties of the cobalt and nickel modified-PSF membranes such as porosity, roughness, thermal stability, flux, and hydrophilicity was evaluated with specialized techniques and instruments. In addition, characterization of the nanoparticles was done prior to their incorporation to the PSF solutions. The characterization techniques used include Scanning Electron Microscopy SEM, Energy Dispersive X-ray EDX, Transmission Electron Miscroscopy TEM, Atomic Force Microscopy AFM, Contact angle measurements, Thermogravimetric Analysis TGA, and X-ray Diffraction XRD. The following subsections will give brief description of the characterization techniques.

2.5.1 Scanning Electron Miscroscopy (SEM)

Scanning Electron Microscopy, SEM, employs finely focused beam of electrons to give microscopic information of the surface of a specimen (Webb & Holgate 2003). This microscopic information cannot be seen by the human eye because the eye is only responsive to radiation in the visible region of the electromagnetic spectrum, which corresponds to 400-700 nm. The two most important features of SEM are the high resolution obtained when samples are examined, and its ability to provide three-dimensional images of the samples (Goldstein & Yakowitz 1975).

SEM works by focusing a beam of electrons on the surface of the sample, during which emission of secondary and back scattered primary electrons occurs. These emissions are collected and amplified to give an image of the surface topology as well as the composition of the sample (Webb & Holgate 2003). The electron beam is "raster scanned" across the samples, and higher magnification is obtained by reducing the area of the sample scanned by the beam of electrons. Scanning electron microscope can have magnification as high as ×30,000, and resolution in the range of 2-4 nm or even higher resolution. The microscope has very good depth of focus which is as a result of the convergence angle of the primary electron beam and the long working distance between the final lens and the sample. The ability of the microscope to produce three-dimensional image of the sample arises from its good depth of focus. The operation of the microscope requires high vacuum to avoid collision of the electron beam with gases when travelling to the sample.

The basic components of SEM are:

i. Electron guns: The electron gun is the source of the electron beam. For good operation of SEM, the electron beam produced by the electron gun must be of high current, small spot size, and have small energy dispersion. There are different types of electron guns which are: tungsten, lanthanum hexaboride, and field emission

electron guns. Most modern SEM uses field emission guns. In field emission electron guns, a single crystal tungsten wire with a very sharp tip is used to generate the electron beams. Strong electric field is produced on the perfectly oriented tip, and the electrons are attracted towards the anodes.

ii. Electron lenses: The diameter of the electron beam is magnified or demagnified using the electron lenses. In SEM, the electron lenses demagnify the image of the emission source thereby obtaining a narrow probe on the surface of the sample. There are two different basic electron lenses, which are:

- Condenser lenses: After passing through the anode plate from the emission source, the electron beam diverges. The condenser lenses are used to converge and collimate into a somewhat parallel stream.
- Objective lenses: Below the condenser aperture, the electron beam also diverges. The electron beam is focused into a probe point on the surface of the sample by the objective lenses. The objective lenses are also used to provide further demagnification.

iii. Column: The components in the column include the aperture, and stigmator. The aperture removes scattered electrons, and controls the spherical aberrations in the final lens. There are two different types of aperture, which are, real aperture and virtual aperture.

The stigmator is a string of coils that surrounds the electron beam. They are used to correct astigmation, and obtain images with good resolution. Astigmation arises from the undesirable effects on the electromagnetic lens.

iv. Scanning coil: The scanning coils are used to make the electron beam scan on the surface of the sample along x-or y-axis by deflecting the electron beam.

v. Detector: Several types of detectors are used to detect the various signals in SEM.

The detectors are:

- Solid state back scattered electron detectors for back scattered electrons.
- Everhart-Thornley detectors for secondary and back scattered electrons.
- Energy-dispersive x-ray spectrometer for characteristic x-ray.
- Wavelength-dispersive x-ray spectrometer also for characteristic x-ray.

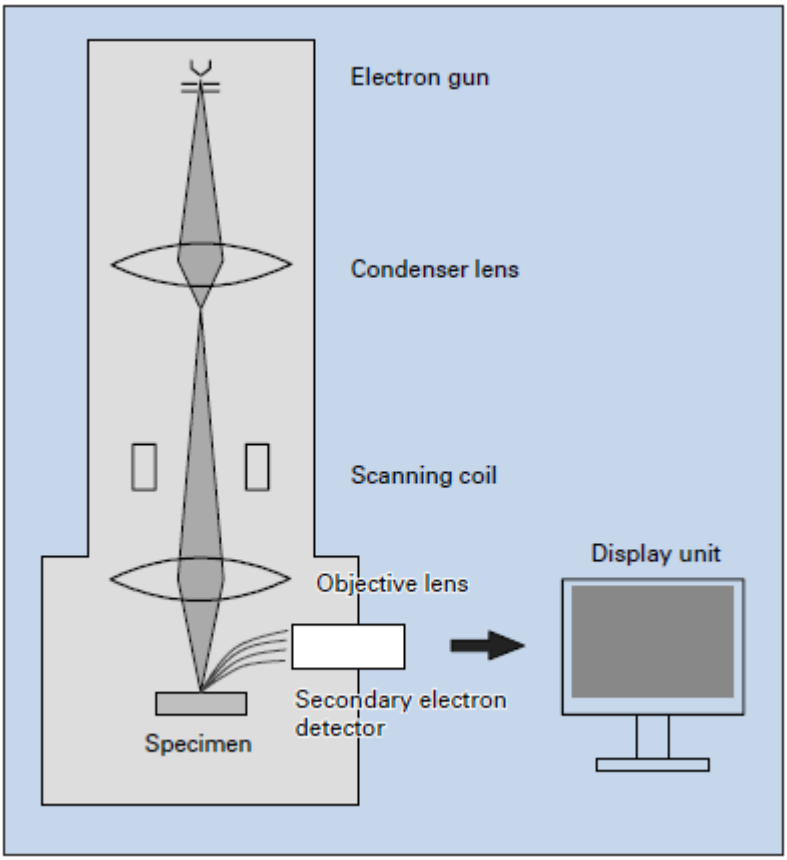


Figure 15 The basic components of SEM (JEOL)

SEM is used to analyze the surface morphology of nanocomposite membranes. For the characterization of nanocomposite membranes, the SEM result of unmodified membrane is compared with that of modified membrane, and the difference is attributed to the presence of the nanoparticles. The SEM was done on a SEM (Carl Zeiss Sigma FESEM equipped with oxford x-act EDS detector). The samples were

prepared on a SEM mount , and coated with gold/palladium prior to the SEM analysis. Figure 16 shows a modern scanning electron microscope.



Figure 16 Typical modern scanning electron microscope

2.5.2 Energy Dispersive X-ray (EDX)

Most SEMs are equipped with EDX, and are capable of identifying and quantifying all elements except hydrogen, helium, and lithium. The identification and quantification of the elements is done by using the information provided by electron-excited characteristic X-ray. The characteristic X-rays are generated when the atoms in the sample are ionized by the electron beam. The ionization results in vacancy or holes in the core shell. The holes are filled by electrons from the outer shells, and in the process energy is emitted in the form of X-ray. The characteristic X-ray is detected by the EDX detector.

A typical EDX detector is a semiconductor device which comprises of the collimator, and the electron trap. The collimator makes sure that the X-rays collected are from the interaction of the primary electron beam and the sample. The electron trap is used to ensure that only X-ray, but no electron, enters the detector.

The elemental compositions of nanocomposite membranes were obtained using EDX. Such results can be presented as EDX spectra, EDX mapping, and so forth.

2.5.3 Transmission Electron Microscopy (TEM)

Transmission electron microscopy TEM uses the same principle as SEM, but the electron beams is transmitted through a thin sample in TEM analysis. One major limitation of TEM is that the sample has to be very thin, otherwise the electrons are scattered within the sample, or absorbed rather than transmitted (Egerton 2016). The major differences between SEM and TEM are presented in Table 5.

Table 5 Some differences between SEM and TEM.

SEM	TEM
Images the surface, or near surface of the sample	Images ultrathin structure of the sample
The electron beam scans over the sample surface	The electron beam penetrate through the sample
Produces three-dimensional images	Produces two-dimensional images
Relatively lower resolution than TEM	Higher resolution
High depth of field	Moderate depth of field

The sizes of the nanoparticles used in modification of membranes are determined using TEM. The TEM can also be used to determine the shape of nanoparticles.

2.5.4 Atomic Force Microscopy AFM

This is another microscopic tool useful in characterization of nanocomposite membranes. AFM scans the surface of the sample using a probe, and gradually

accumulate the map of the height or topology of the surface of the sample (Eaton & West 2010). The principle of the AFM involves attaching a probing tip to a cantilever (Meyer 1992). The tip and the sample interact leading to the deflection of the cantilever in response to the force of the interaction. Images are generated by scanning the sample relative to the probing tip and digitizing the deflection of the cantilver. The AFM can be operated in contact, and non-contact mode. In the contact mode, ionic repulsion forces are used to give details on the surface topology with high resolution. In the non-contact mode, forces such as Van der Waals, electrostatic, magnetic or capillary forces are sensed and used to give information on the surface topology of the sample. The AFM analysis of membranes is done in non-contact mode.

The AFM is basically composed of (Rugar & Hansma 1990) :

- A sharp tip mounted on a soft cantilever spring
- A way of sensing the deflection of the cantilever
- A feedback system that monitors and controls the deflection
- A mechanical scanning system that moves the sample with respect to the tip in a raster pattern
- A display system that converts the data measured into an image

The AFM analysis was performed on the Ni-modified and unmodified membranes to ascertain the effect of the various amounts of the Ni nanoparticles on the surface roughness of the modified membranes. The AFM was carried out on a Veeco Di3100 AFM. The graphical, as well as the quantitative AFM results were obtained. The graphical images were presented in the form of 3D images, while the quantitative measurements consists of the R_a (average roughness), and the R_{RMS}. The quantitative results provide details that may not be easily visualized in the graphical images.

Three different areas of each of the membranes were measured, and the mean R_a, and R_{RMS} calculated to obtain better representative values of the roughness parameters of

these membranes. An area of 1µm×1µm of each of the membrane surfaces was scanned.

2.5.5 Contact Angle measurement

The contact angle of a liquid on a surface is a measure of the interfacial energies of the solid/liquid interfaces. Contact angle measurement is the best way to obtain the surface energetics of a solid/liquid interface (Kwok et al. 1997). It is used to assess the wettability of a solid surface. There are basically two types of contact angle, and they are (Gu et al. 2016):

- Static contact angle
- Dynamic contact angle

The static contact angle is the most popular method because it is somewhat easy to measure. It consists of sessile drop method, and pendant drop method.

Surfaces are classified as high energy surfaces, or low energy surfaces (Kohli & Mittal 2016). Metals, metal oxides, glasses, and ceramics are examples of high energy surfaces. High energy surfaces normally have good spread of liquid on them, that is, they have high wettability. The high wettability is as a result of the high surface free energy which is considerably more than the surface tension of the liquids. Polymers are considered to have low surface energy.

Contact angle measurements are used to determine the wettability of a nanocomposite membrane. Membranes can be classified as being hydrophobic or hydrophilic. Water droplets does not easily spread on hydrophobic membranes, thus they have high water contact angle. Hydrophilic membranes have lower water contact angle. The incorporation of nanoparticles into polymer membranes is expected to increase the surface energy of the membranes thereby reducing the contact angle of the nanocomposite membranes. Figure 17 shows a depiction of the contact angle of hydrophobic and hydrophilic surfaces.

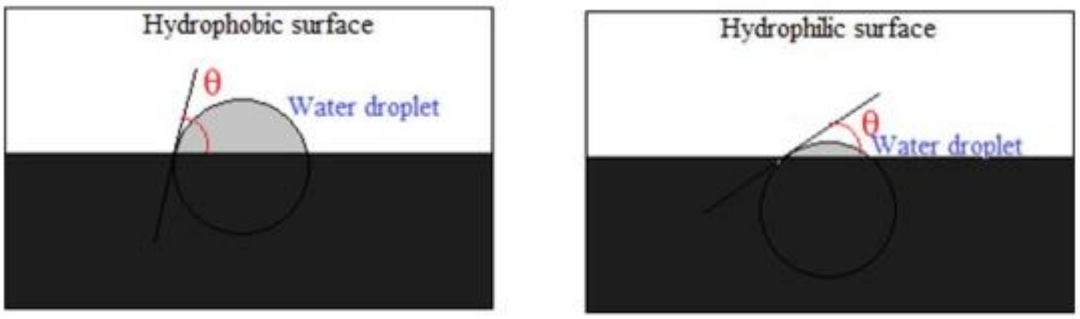


Figure 17 Contact angle measurement of hydrophobic and hydrophilic surfaces (Jhaveri & Murthy 2016).

2.5.6 Thermogravimetric Analysis TGA

This is also one of the characterization technique employed to assess the influence of nanoparticles in nanocomposite membranes. In TGA, the changes in mass of a sample in response to temperature changes are measured. The mass changes occurs as a result of decomposition, degradation, desorption, adsorption, reduction, oxidation, sublimation, and vaporization of the sample during the temperature changes (Vyazovkin 2012). Put simply, TGA is used to measure the weight of a sample as the sample is heated or cooled in a furnace.

The basic procedure of TGA involves placing the sample in a sample pan that is held by a precision balance. The sample is heated or cooled in the furnace, and the mass changes are recorded. The sample purge gas which could be either inert or reactive is used to keep the sample's environment stable. The sample purse gas surrounds the sample during the analysis and exits through the exhaust of the instrument.

The TGA result is analyzed from the TGA curve. The curve is shown from left to right of the graph, and a weight loss is shown by a descending curve. First, the onset temperature is obtained from the curve. The onset temperature is the temperature where the weight loss begins. Other data such as the endset temperature, the first derivative peak temperature, and the final residue are also obtained from the curve and used to characterize the sample.

The chemical structure of a membrane modified with nanoparticles is expected to change. TGA is used to determine change in thermal stability as a result of change in chemical structure of the nanocomposite membranes as the nanoparticle is incorporated. A comparison is made between the unmodified membrane and the modified membrane. The TGA was performed on a Mode-SDT Q 600 model.

2.5.7 Inductively Coupled Plasma Mass Spectroscopy ICP-MS

ICP-MS is currently the most powerful instrument used in the detection of many elements, with a wide linear dynamic range, low detection limit, and ability to measure isotopic ratios (Beauchemin 2010). ICP-MS measures elements in concentrations as low as parts per billion (ppb), and parts per trillion (ppt). The principle of the technique involves ionization of the atoms of the elements in the sample, and then the ions are separated and detected according to their mass-to-charge ratio. The source of the ionization is inductively coupled plasma, while the separation and detection of the ions are done by a mass spectrometer. The basic components of an ICP-MS include (Barshik et al. 2000):

- Nebulizer and spray chamber
- Inductively coupled plasma (ICP) source
- Differentially pumped interface
- Ion optics
- Mass spectrometer
- Detector

The analysis of a sample using ICP-MS involves introducing the sample to the instrument using the peristaltic pumps. The solution is then pumped to the nebulizer where they are transformed to aerosol. Some aerosol drops that are too big to be vaporized in the plasma are removed in the spray chamber. The total amount of the aerosol and vapour that enters the plasma is also controlled by the spray chamber. The aerosol from the spray chamber is then passed to the inductively coupled plasma

source. The plasma is produced in a stream of hot gas (mainly argon gas) flowing through a set of three concentric quartz tubes known as the plasma torch.

In the plasma, the solvent in the aerosol evaporates thereby leaving a particle. The particles is then vaporized and ionized. The ions travel towards the sampling orifice. A positive ion beam is formed as the electrons diffuse and charge separation occurs. The positive ions are focused into the mass spectrometer by a series of ion optics. Ions of same mass-to-charge ratio leave the mass spectrometer and they are detected by the detector.

The ICP-MS is used to investigate leaching of nanocomposite membranes. Filtration of water is usually done using the modified membrane. The amount of nanoparticles in the permeate is then quantified using ICP-MS.

ICP-OES can also be used to quantify the leached nanoparticles. ICP-OES is like a "twin" to ICP-MS, but the ICP is coupled to an optical spectrometer. ICP-OES is cheaper than ICP-MS, however ICP-MS is usually preferred in assessing leaching of nanocomposite membranes. The reason for the high preference of ICP-MS over ICP-OES is because of some drawbacks of ICP-OES. Some of these drawbacks are:

- Lower detection limit
- High potential for spectral interference
- High volume gas installation needed

Chapter 3

This chapter presents the aims of this research, as well as the objectives that were achieved.

3 AIMS AND OBJECTIVES

3.1 Aims

This study focused on preparing nickel, and cobalt nanocomposite PSF membranes with improved properties, characterizing the prepared modified membranes and determining possible leaching of the incorporated nanoparticles from the nanocomposite PSF matrix.

3.2 Objectives

The objectives of the research were:

- Synthesize and characterize nickel and cobalt nanoparticles.

- Prepare modified PSF membranes using the synthesized nanoparticles.

- Characterize the prepared nanocomposite PSF membranes using Atomic Force Microscopy (AFM), Scanning Electron Microscopy (SEM), Thermogravimetric Analysis (TGA), and Contact angle measurements.

- Investigate the possible leaching of the embedded nanoparticles from the prepared nanocomposite polysulfone membranes using Inductively Coupled Plasma Mass Spectroscopy (ICPMS).

3.3 Research Questions

This work tends to answer these two key questions:

1. Can Ni and Co nanoparticles be ideal for the modification of PSF membranes?

2. Are embedded Ni and Co nanoparticles stable in the matrix of the modified PSF membranes?

3.4 Motivation

The use of Ni and Co nanoparticles in the modification of PSF membranes is fairly new with only very few reported researches previously done on the topic. The previous work focused on modifying PSF with 10 wt % Ni and Co nanoparticles, as well as the electrochemical studies of the modified membranes (Phelane et al. 2014c). The stability of the incorporated Ni and Co nanoparticles in modified PSF matrix has never been tested.

The driving force of this work is the need to pinpoint the amount of Ni and Co nanoparticles that gives the optimum effects on modified PSF membranes, including better stability in the modified PSF membranes. Different amounts of the Ni and Co nanoparticles were used to modify the PSF membranes in this work, and the modification that gave the best characteristic and performance results was identified.

CHAPTER 4

The materials and experimental methods used in this study are detailed in this chapter.

4 METHODOLOGY

4.1 Materials

4.1.1 Glassware

All glassware used in this work were thoroughly washed with detergent and rinsed properly with water and acetone. The glasswares used include beakers, graduated cylinders, round bottom flasks, and Erlenmeyer flasks.

4.1.2 Chemical reagents

The nickel nanoparticles were synthesized using nickel(II)chloride ($NiCl_2$), ethylene glycol, and hydrazine monohydrate ($N_2H_4.H_2O$) purchased from Sigma-Aldrich. Sodium hydroxide was purchased from ACE chemicals.

The cobalt nanoparticles were synthesized using cobalt acetate tetrahydrate, ethylene glycol, polyvinylpyrrolidone (PVP) and hydrazine monohydrate also from Sigma-Aldrich.

The membranes solutions were prepared using polysulfone (PSF), and dimethylacetamide (DMAc) from Sigma-Aldrich.

4.2 Methods

4.2.1 Synthesis of the Ni nanoparticles

The synthesis of the Ni nanoparticles was done using a method similar to the procedure employed by Wu & Chen (Wu & Chen 2003). 0.60 g of $NiCl_2$ was dissolved in 200 mL ethylene glycol at a temperature of 60^oC under stirring until the $NiCl_2$ was well dissolved. The colour of the solution changed from yellow to light green when the $NiCl_2$ was properly dissolved in the solvent. 2 mL of $N_2H_4.H_2O$ was added to the $NiCl_2$ solution, followed by the addition of 4 mL of NaOH (1 M) under

vigorous stirring. The colour of the reaction mixture changed from light green to blue, and then to black. It took about 1 hour for the reaction to be complete.

The black particles obtained from the reaction were washed thoroughly with ethanol during centrifugation. The washing was done three times, and each wash was performed in 10 minutes at a 7000 rpm in the centrifuge. The washed black particles was sonicated for 90 minutes and stored in ethanol.

The size of the nickel nanoparticles was determined using TEM. The TEM was done on a JEOL JEM 2100F TEM model. The Ni nanoparticles were diluted with ethanol and sonicated for 1 hour, and then drop-coated on a copper grid and analyzed on the TEM instrument. The size was measured using imageJ software.

4.2.2 Synthesis of the cobalt nanoparticles

The synthesis of cobalt nanoparticles was carried out using a method by Kaylan et al. (Kalyan Kamal et al. 2009). 1 g of cobalt acetate tetrahydrate was dissolved in 25 mL of ethylene glycol until it is well dissolved. In a separate flask, 1 mL of $N_2H_4.H_2O$ was mixed with 25 mL of ethylene glycol. In another beaker, 1 g of PVP was dissolved in 50 mL of ethylene glycol. The solution of PVP was added to the hydrazine solution, followed by the dropwise addition (at a rate of 2 ml/minute) of the solution of the cobalt acetate tetrahydrate to the reaction mixture. The reaction mixture was refluxed at a temperature of 190^oC. The reaction was completed in about 30 minutes. The product was washed three times with ethanol while centrifuging. The final product was sonicated for 90 minutes and stored in ethanol.

Prior to the TEM analysis, the sample of the Co nanoparticles was diluted with ethanol, and sonicated for 1 hour to ensure good dispersion, and minimal agglomeration of the nanoparticles. The sample was drop coated on a copper grid,

and analyzed using a JEOL JEM 2100F TEM model. The size was also measured using imageJ software.

4.2.3 Preparation of the Co and Ni-modified nanocomposite PSF membranes

The polysulfone pellets were dried in the oven at temperature of 40^{o}C. The polysulfone pellets were dissolved in the solvent, DMAc, under heated stirring, and left to cool. The nanoparticles were sonicated, dried and grinded with a mortar and pestle, and added to the polysulfone solutions. The polysulfone nanocomposite solutions were properly mixed and sonicated until the nanoparticles were found to be well dispersed in the solutions.

The nanocomposite solutions were manually casted on a clean and dried glass plate and immersed in water until the nanocomposite membranes were solidified. The solidification of the membrane was achieved through phase inversion. The prepared nanocomposite membranes were left to dry at room temperature. The compositions of the various prepared PSF membranes are shown in Table 5.

Table 6 The composition of the casting solutions of the various prepared membranes

Membrane	PSF (g)	Co/Ni (g)	DMAc (ml)
PSF-0	0.800	0.000	8.0
PSF-3	0.800	0.024	8.0
PSF-5	0.800	0.033	8.0
PSF-10	0.800	0.080	8.0

CHAPTER 5

In this chapter, the results obtained in this work are presented and discussed.

5 RESULTS AND DISCUSSION

5.1 The characterization of the nickel nanoparticles

The work focused on obtaining Ni nanoparticles with size in the nano-range. Many syntheses were done but only the procedure employed for the synthesis of the Ni nanoparticles used in this work was presented as is described in section 4.2.1. Most of the nanoparticles synthesized using different methods from the one described in section 4.2.1 were found to be too big or highly agglomerated or both. The TEM result of one of such "big" Ni nanoparticles is shown in Figure 18 (a), and agglomerated Ni nanoparticles 18 (b), and they were synthesized using a method by Wu et al. (Wu et al. 2010). Some parameters different from the ones employed by Wu et al. such as concentration of the precursor, reaction temperature, and reaction time were optimized during the synthesis.

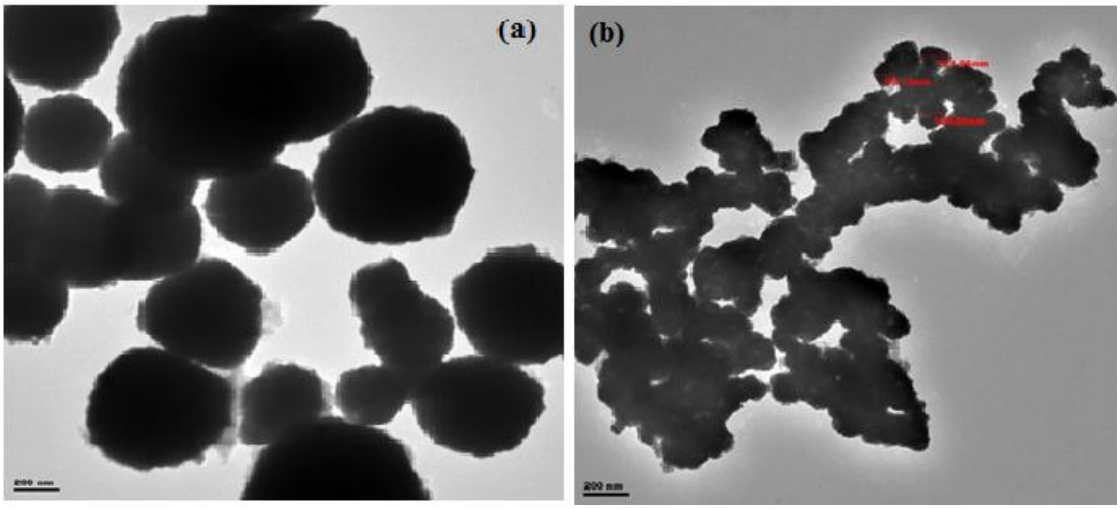


Figure 18 The TEM image of (a) big Ni particles of average size of 200nm, and (b) agglomerated Ni nanoparticles.

The average size of the Ni nanoparticles used in this work was found to be 58.3± 3.1 nm. The XRD spectra showed peaks at 56.5, 62.3, and 91.2 corresponding to miller

indexes of (111), (200), and (220) respectively which are characteristic of pure nickel. Figure 19 shows the XRD result of the Ni nanoparticles. The TEM image (a), and size distribution (b), of the Ni nanoparticles are shown in Figure 20.

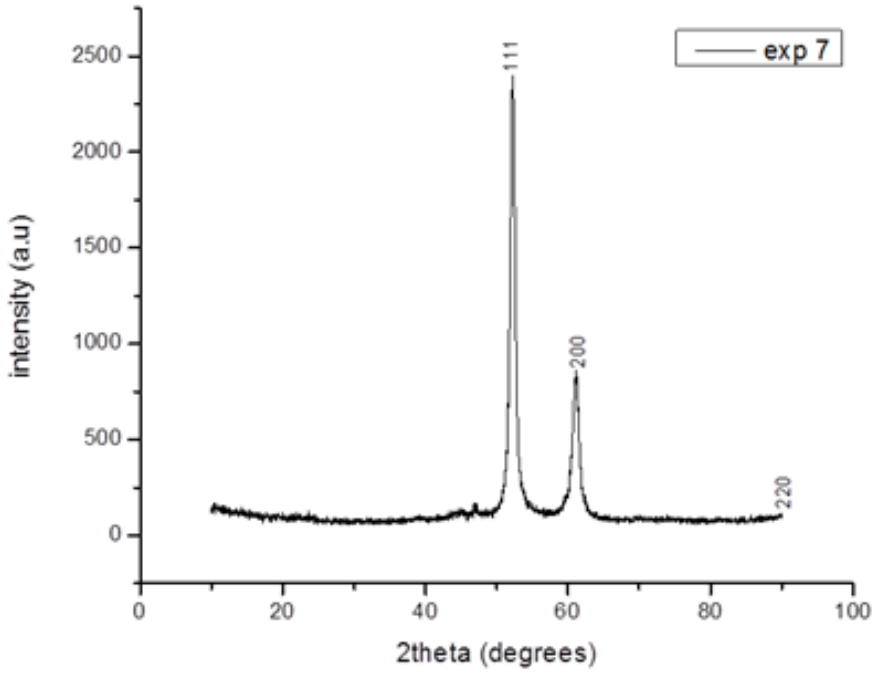


Figure 19 The XRD spectra of the Ni nanoparticles

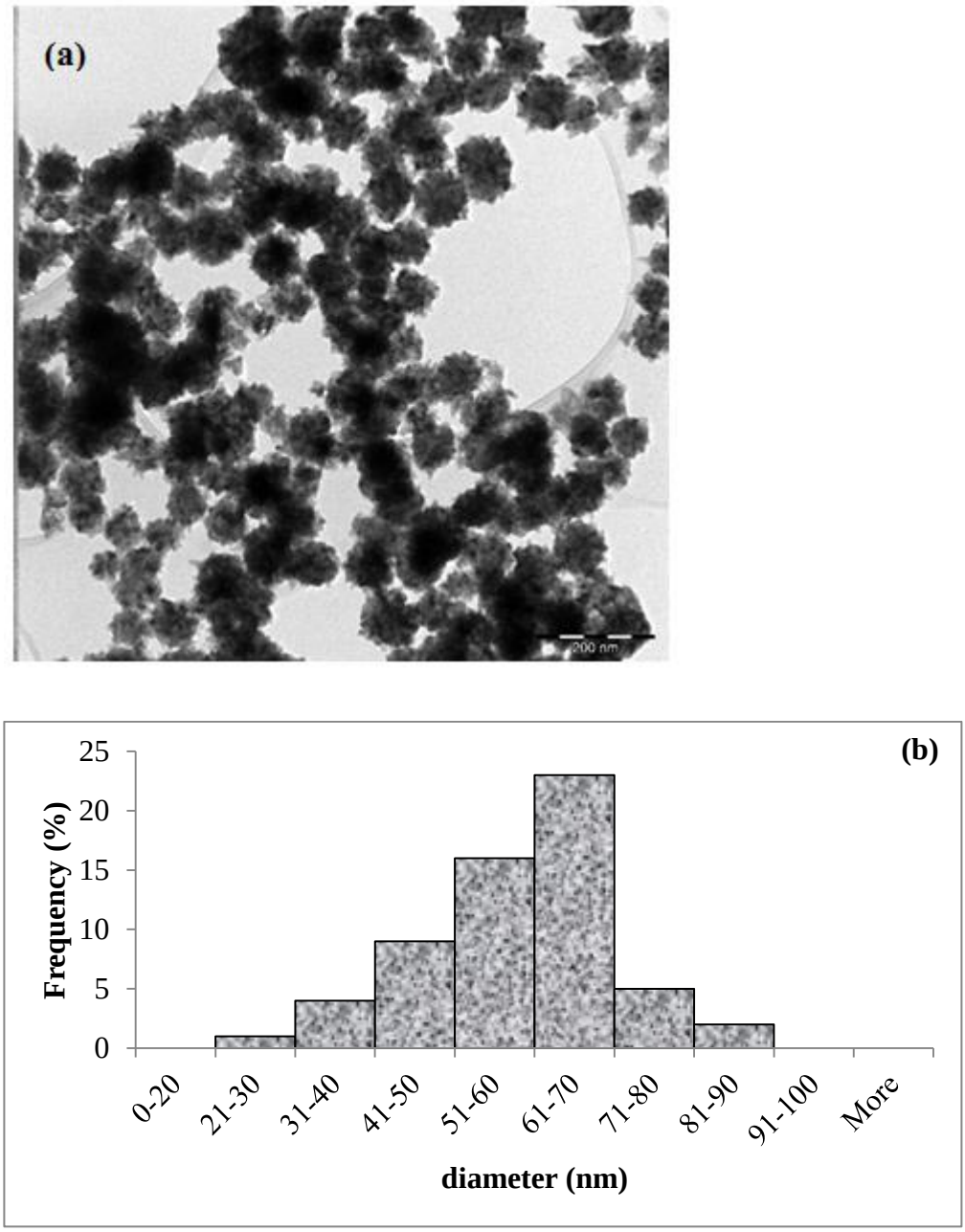


Figure 20 (a) TEM image and (b) size distribution of the Ni nanoparticles.

5.2 The characterization of the cobalt nanoparticles

The TEM result shows agglomeration of the Co nanoparticles. The agglomeration is as a result of the surface interaction between the nanoparticles as described in section

2.4.1. The agglomeration of nanoparticles is difficult to control. However, the distinct spherical shape of the Co nanoparticles can be seen from the TEM image, and the agglomeration is considered minimal for the purpose of membrane modification.

The micrograph of the Co nanoparticles shows that the particle sizes are distributed in a narrow range of 5-30 nm with an average size of 17.3±2.1 nm. Figure 21 shows the TEM image (a), and the size distribution (b) of the Co nanoparticles.

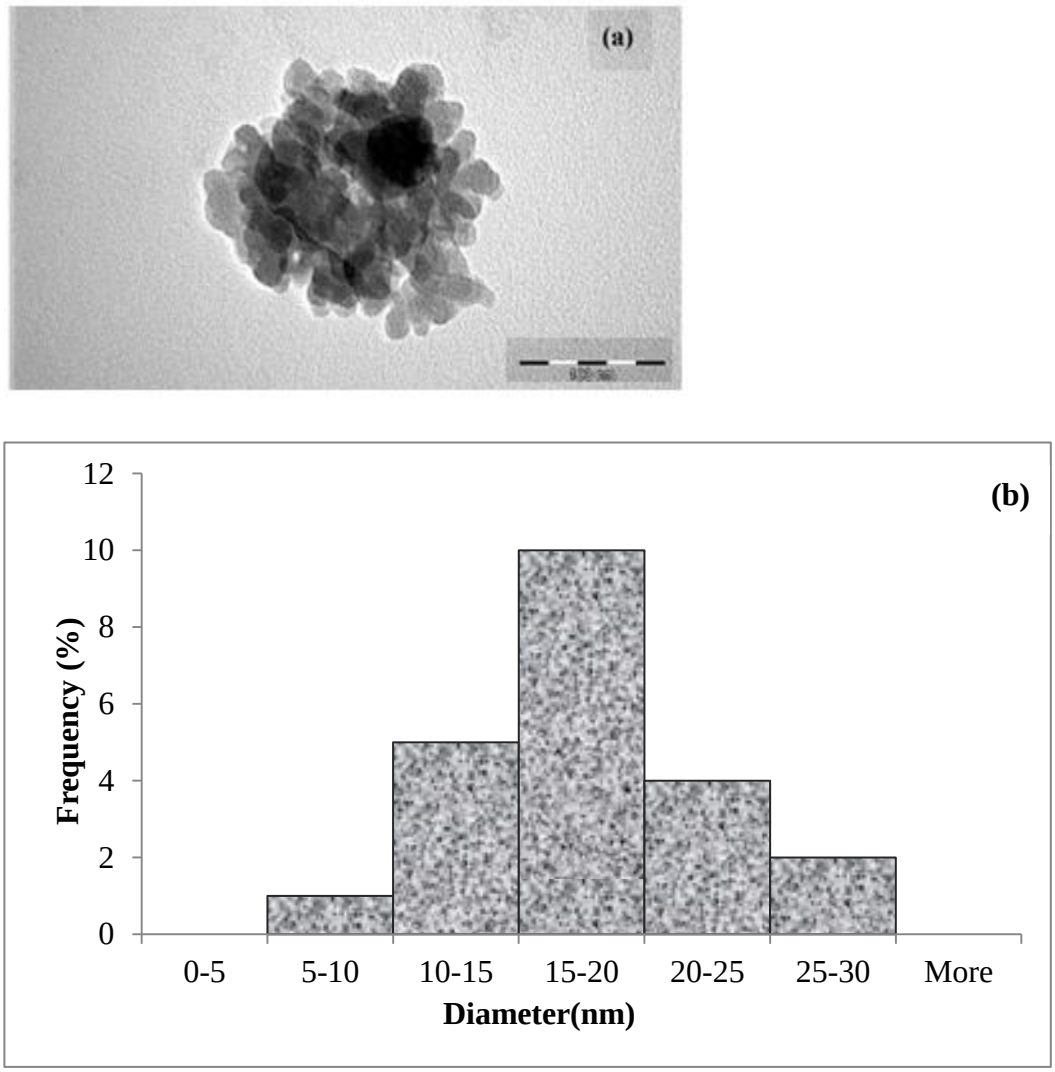


Figure 21 The TEM image (a), and size distribution (b), of the Co nanoparticles.

5.3 The characterization of the nickel modified-PSF membranes

5.3.1 The SEM result

Figure 22 shows the SEM image of the top surface of the modified and unmodified membranes. From the images, it can be seen that the top surfaces of the various membranes were relatively dense consisting of more polymer rich phase and less polymer poor phase (pores). The dense layer seen in the top surface can be explained by the very fast phase inversion process that occurred at the top surface since the top surface is directly in contact with the non-solvent (water). The pore sizes and porosity on the top surface were also enhanced by incorporation of the subsequent amounts of the Ni nanoparticles. The top surface of a membrane is responsible for the selectivity of the membrane, therefore the improvement seen with the addition of the various amount of the Ni nanoparticles was considered to be advantageous in the selectivity of the Ni-modified membranes.

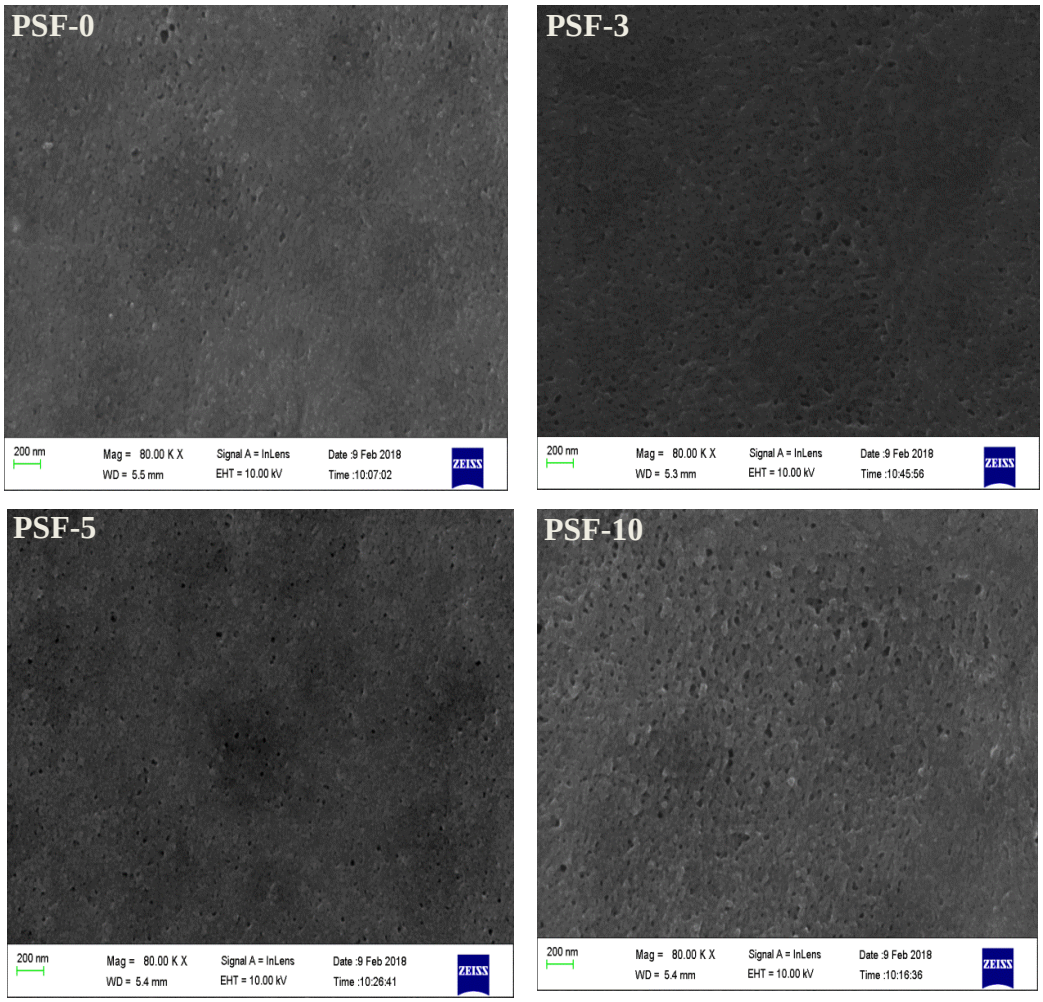


Figure 22 The SEM images of the top surface of the Ni-modified and unmodified PSF membranes

Unlike the top layer, the inner structure of both the modified and unmodified membranes are highly porous. This can be explained by the fact that the phase inversion process was not as fast as it was in the top surface. During this process, the nonsolvent was transported into the nanocomposite polymer solution and the solvent was transported out leading to formation of the sponge-like inner layer with mostly polymer-poor phase (pores). The addition of the Ni nanoparticles led to increase in the pore sizes as well as reduction in the number of pores, however, the PSF-3 membrane has higher pore size than the PSF-5 membrane. The pores sizes are 1.22,

0.79, 1.79 μm for PSF-3, PSF-5, and PSF-10 respectively. The pores of the PSF-3 and PSF-5 seem more regular patterned than the PSF-10 which seems to have many interconnected sponge-like structures in the pores making the pores irregular. Figure 23 shows the SEM image of the inner structure of the Ni modified and unmodified PSF membranes.

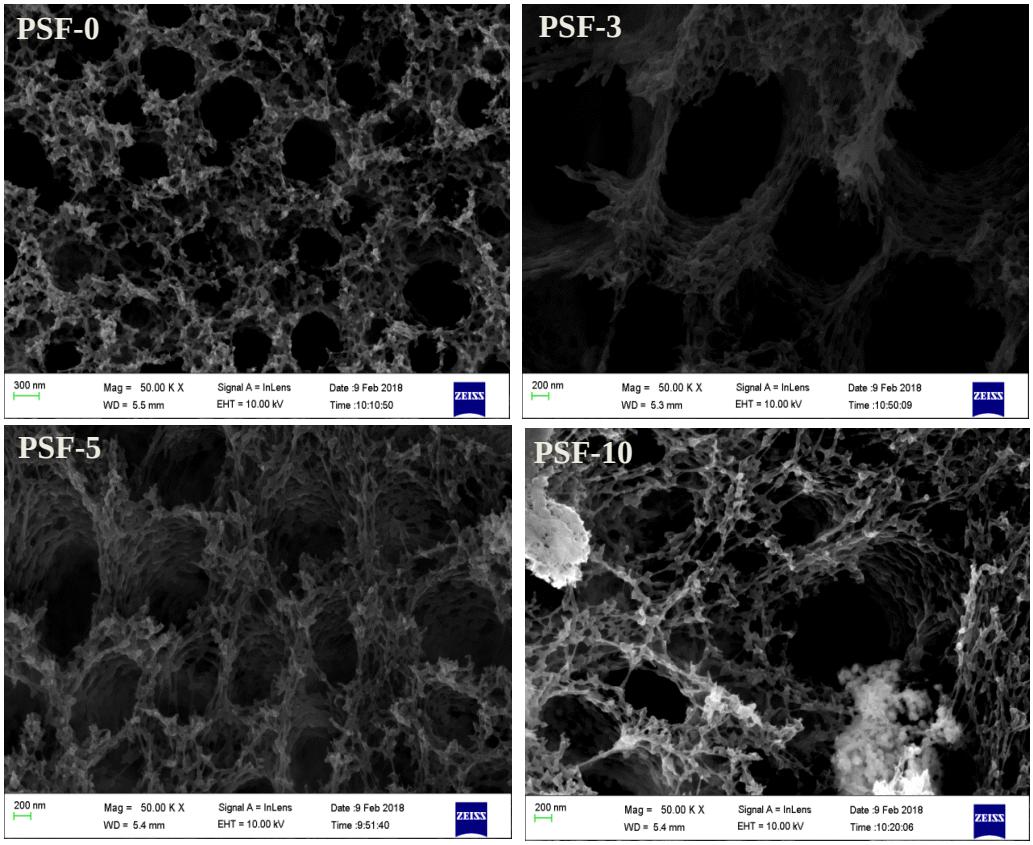


Figure 23 The SEM images of the inner structures of the Ni-modified and unmodified PSF membranes

The EDX results show the elemental composition of the membranes as presented in Figure 24. Carbon, oxygen, and sulfur which are the elemental constituents of the polysulfone were seen in all the spectra. The peak for Ni was seen in the modified membranes, and it increases as the incorporated Ni nanoparticles increases, and thus suggests the presence of Ni in the modified membranes.

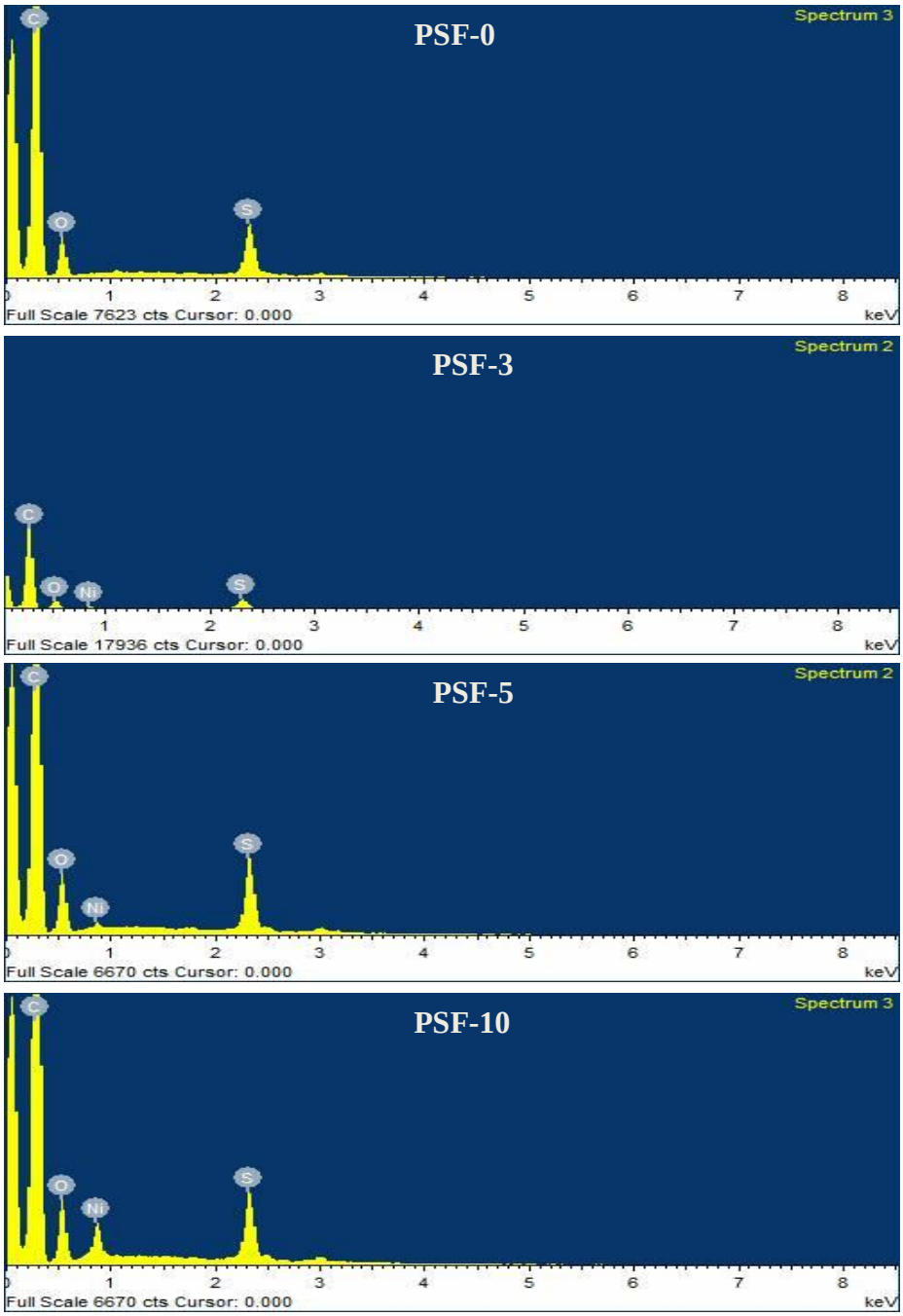


Figure 24 The EDX spectra of the Ni-modified and unmodified PSF membranes

5.3.2 The AFM result

The surface roughness was significantly improved by the incorporation of the Ni nanoparticles. The PSF-10 membrane has the highest roughness, followed by the

PSF-5 membrane while the PSF-3 has the least roughness among the modified membranes. The increased surface roughness was expected to contribute to the enhancement of the flux of the membranes since the surface area was increased. Figure 25 shows the 3D AFM images of the Ni-modified and unmodified PSF membranes.

The 2D AFM image, as well as the quantitative roughness data of the Ni modified PSF-3, PSF-5, and the PSF-10 membranes are shown in Figure 26, 27, and 28 respectively.

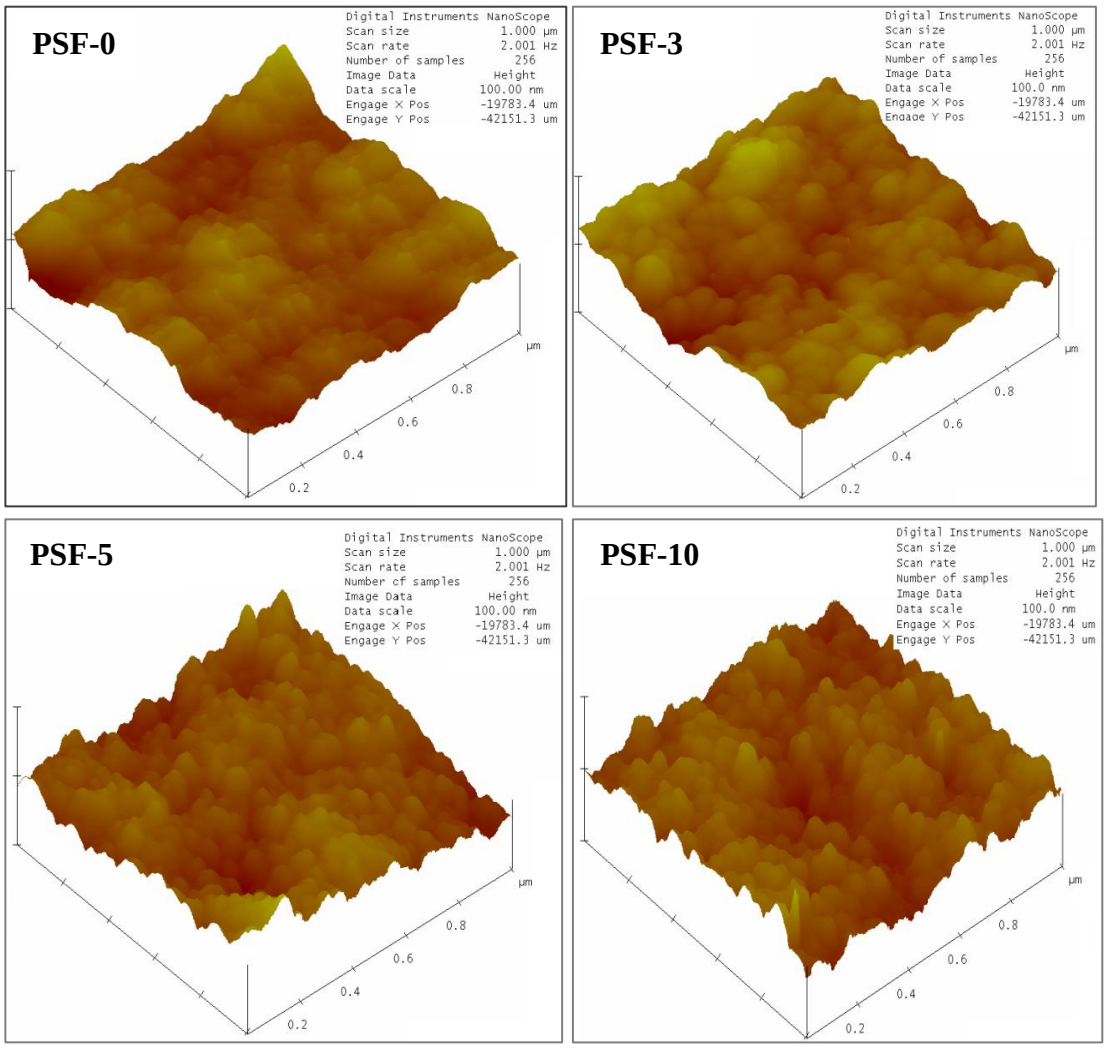


Figure 25 The 3D AFM images of the Ni-modified and unmodified PSF membranes

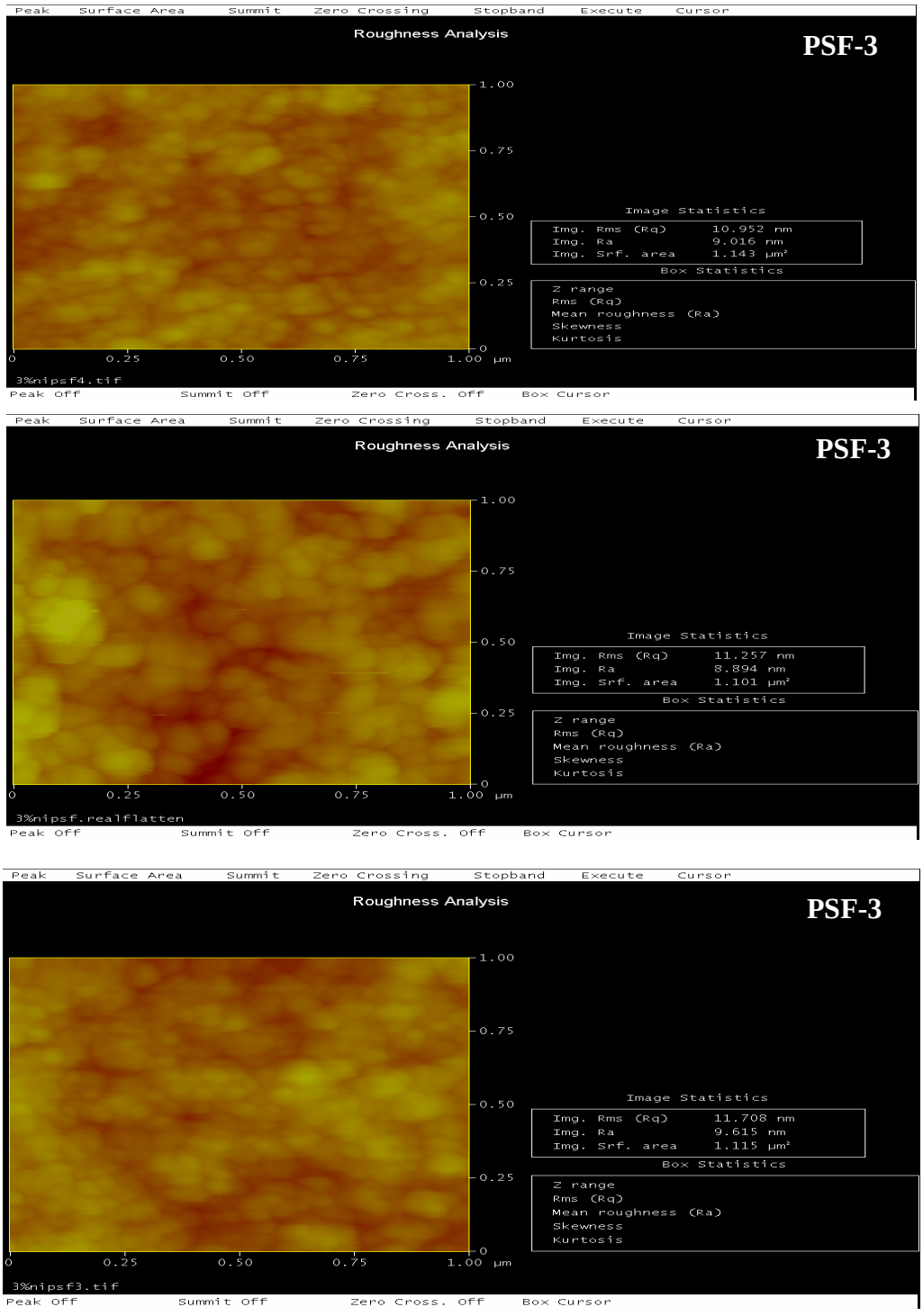


Figure 26 The 2D AFM images of the three different areas of the Ni modified PSF-3 membrane showing the quantitative roughness data of the membrane.

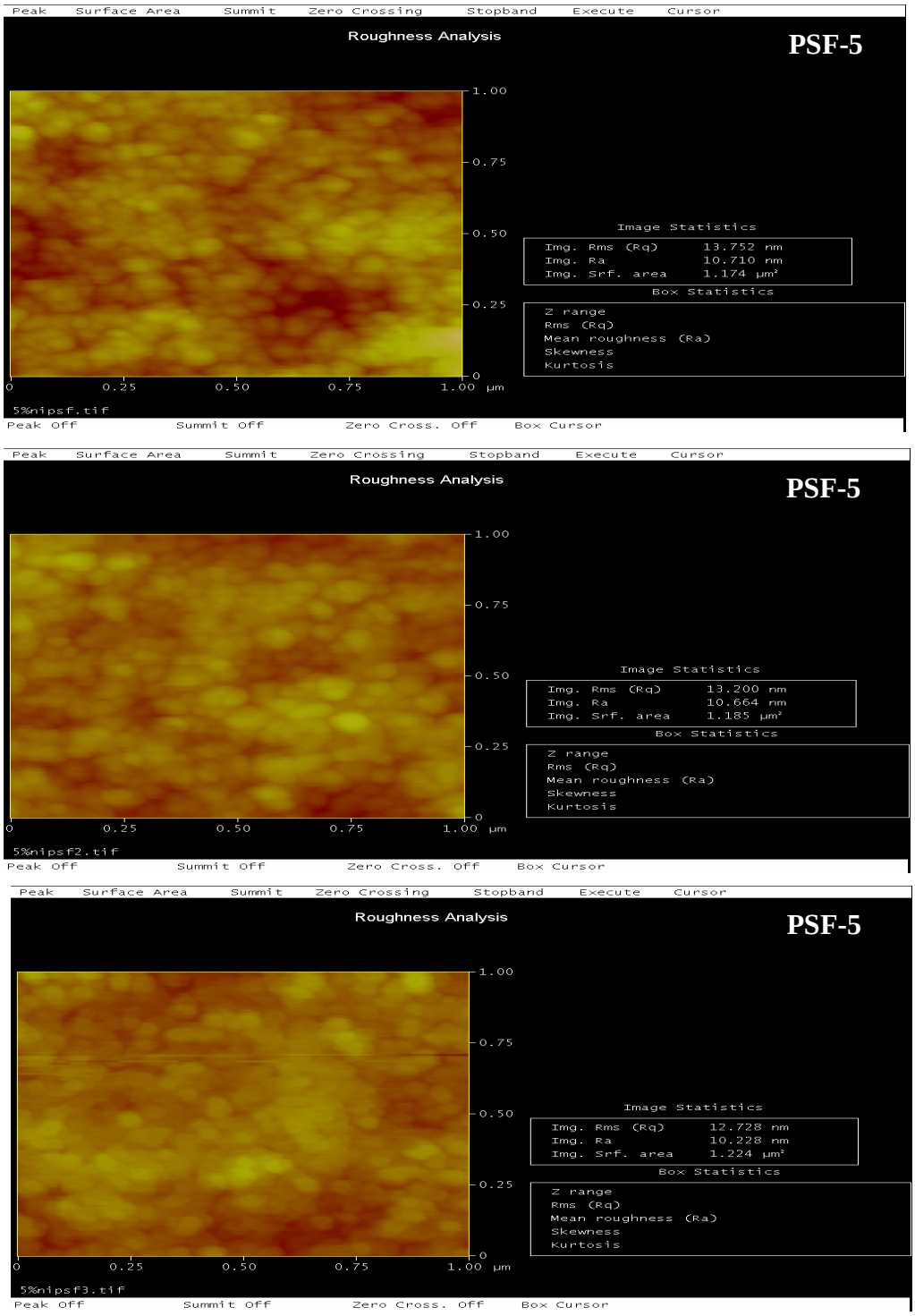
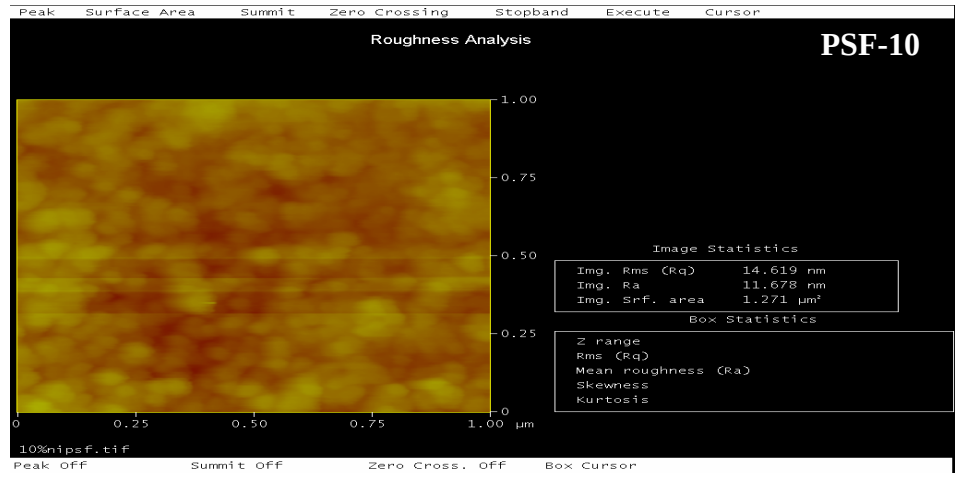
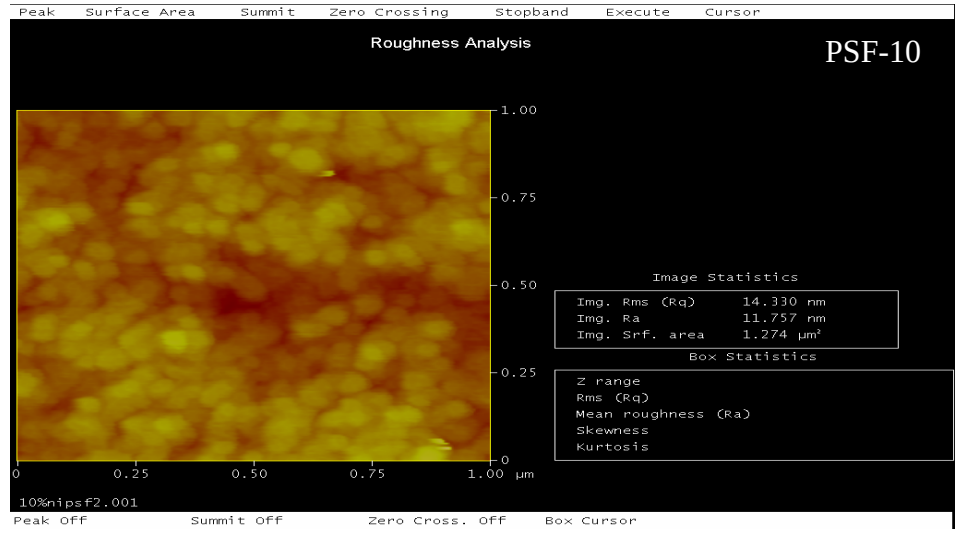


Figure 27 The 2D AFM images of the three different areas of the Ni modified PSF-5 membrane showing the quantitative roughness data of the membrane.





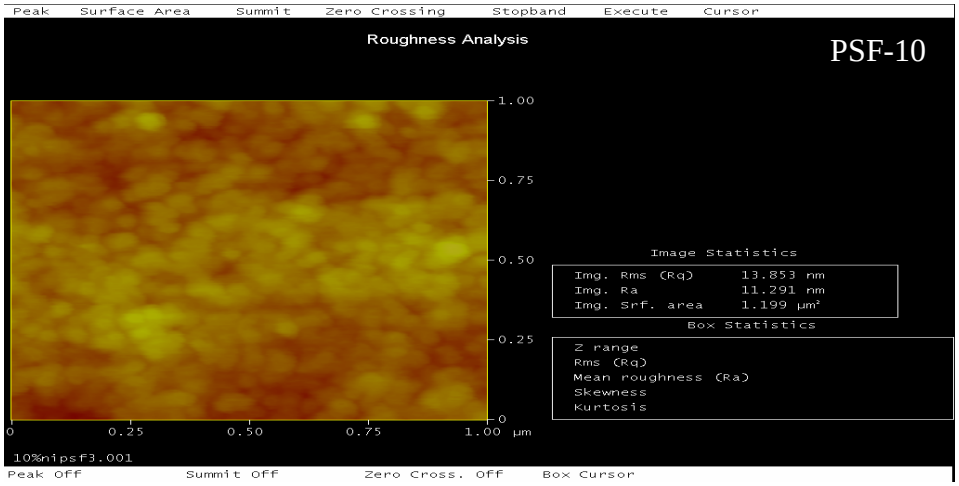


Figure 28 The 2D AFM image of the three different areas of the Ni modified PSF-10 membrane showing the quantitative roughness data of the membrane.

The AFM roughness data (R_a and R_{RMS} values) of the Ni-modified and unmodified membranes are also summarized in Table 7.

Table 7 The R_a and R_{RMS} values of the Ni-modified and unmodified PSF membranes.

Membranes	**R_a (nm)**	**R_{RMS}(nm)**
PSF-0	8.915	10.967
PSF-3	9.175±0.959	11.306±0.945
PSF-5	10.534±0.660	13.227±1.273
PSF-10	11.575±0.620	14.267±0.961

5.3.3 The FTIR result

The FTIR spectra of the Ni-modified and the unmodified PSF membranes are shown in Figure 29. The characteristic absorption peaks of polysulfone were obvious in all the membranes, however, the peaks of the incorporated nickel nanoparticles were not observed because of the small amount of the nanoparticles in the membrane matrix. A similar result was obtained in a silver modified PES membrane (Masheane 2016). The characteristic polysulfone absorption peak of 2969.57cm^{-1} corresponds to the C-H stretching vibrations. Other peaks at 1243.17cm^{-1} (C-O-C stretch), 1585.98, 1504.11 and 1488.30cm^{-1} (C=C stretching vibrations), and 1324.44 and 1294.79cm^{-1} (SO_2 symmetric stretch) were also seen.

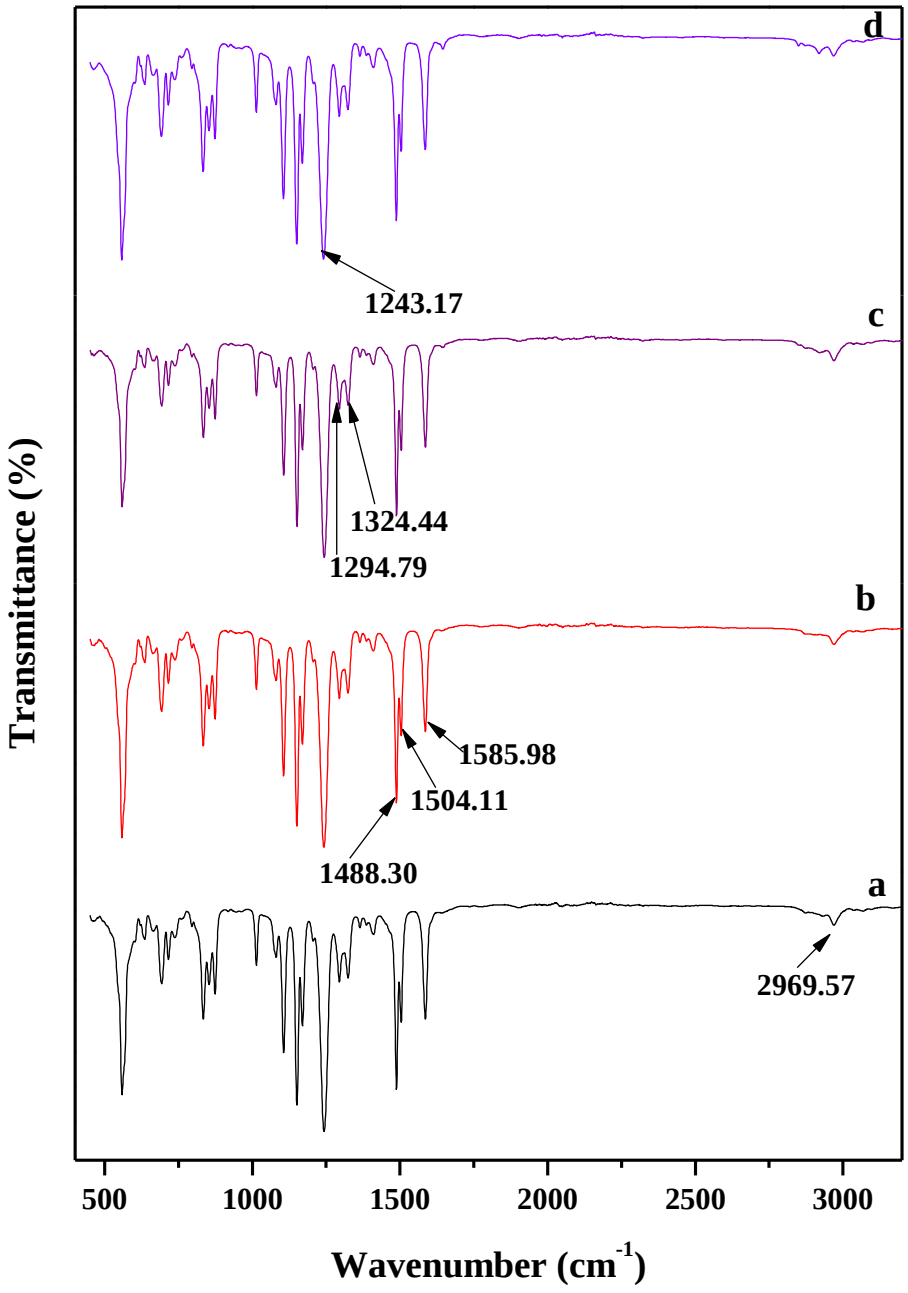


Figure 29 The FTIR spectra of (a) unmodified PSF-0, and the Ni modified (b) PSF-3,(c) PSF-5, and (d) PSF-10.

5.3.4 The TGA result

Figure 30 shows the TGA results. From the TGA curves, it can be seen that the incorporation of the nickel nanoparticles to the polysulfone membranes improves the thermal stability of the modified membranes. All the membranes have roughly the same onset and endset temperatures. At the endset temperature, 58.9% mass was lost by the unmodified-PSF membrane and the PSF-3 membrane showing that adding 3% Ni nanoparticles to the polysulfone matrix does not significantly affect the thermal stability of the PSF membrane. The PSF-5 and PSF-10 membranes lost 54.6% and 50.9% mass respectively. The reduced mass lost by the PSF-5 and PSF-10 membranes compared to the unmodified-PSF membrane can be explained by the interaction between the sulfone group of the polysulfone and the Ni-nanoparticles. This interaction inherently increases the strength of the bonds in the modified membranes, thereby increasing their thermal stability.

At the limit temperature of 800^{O}C, the residual mass for both the PSF-0 and the PSF-3 membranes are 34.6% while the PSF-5 and PSF-10 membranes have 38.3% and 42.7% residual masses respectively.

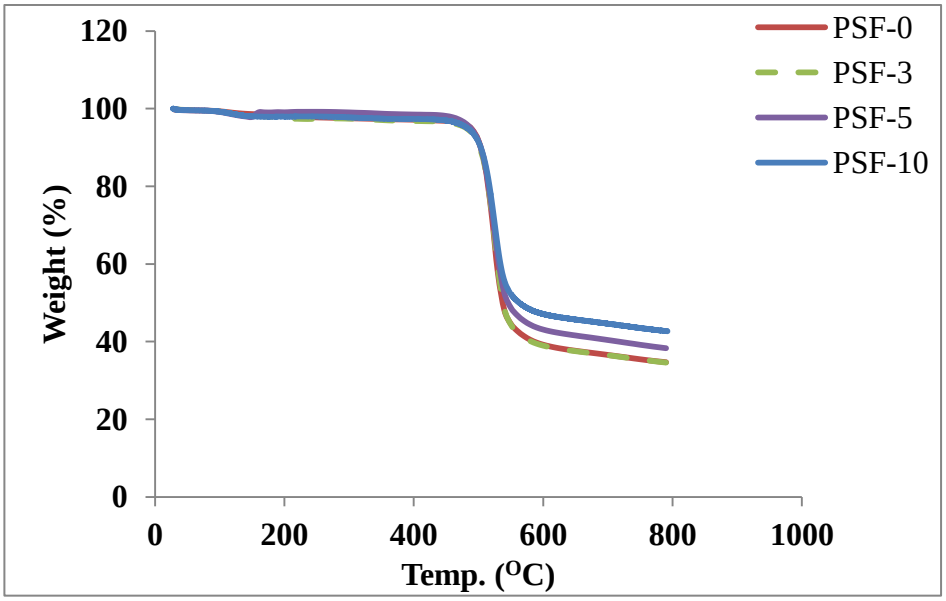


Figure 30 The TGA curve of the Ni-modified and unmodified PSF membranes.

5.3.5 The contact angle result

The influence of the embedded Ni nanoparticles on the hydrophilicity of the PSF membranes is presented in the contact angle result shown in Table 8 There was slight decline in contact angle of the Ni modified PSF-3 and PSF-5 compared to the unmodified membrane. The contact angle of the PSF-10 decreased significantly owing to the higher concentration of the Ni nanoparticles in the PSF-10 membrane.

Table 8 Contact angle results of the Ni-modified and unmodified PSF membranes.

Membranes	**Average contact angle (^{o})**
PSF-0	89.05
PSF-3	88.88
PSF-5	88.53
PSF-10	75.49

5.3.6 The flux result

The results of the various membranes flux is presented in Figure 31 and shows that the flux of the membranes was improved on modification of the membranes with the Ni nanoparticles. The improved flux was linked to the Ni nanoparticles which enhanced the hydrophilicity of the modified membranes and increased the membrane's attraction to water leading to faster passage of water through the membranes. The flux proportionally increased with the amount of the Ni nanoparticles embedded in the polymer matrix. The flux analysis was done in triplicates.

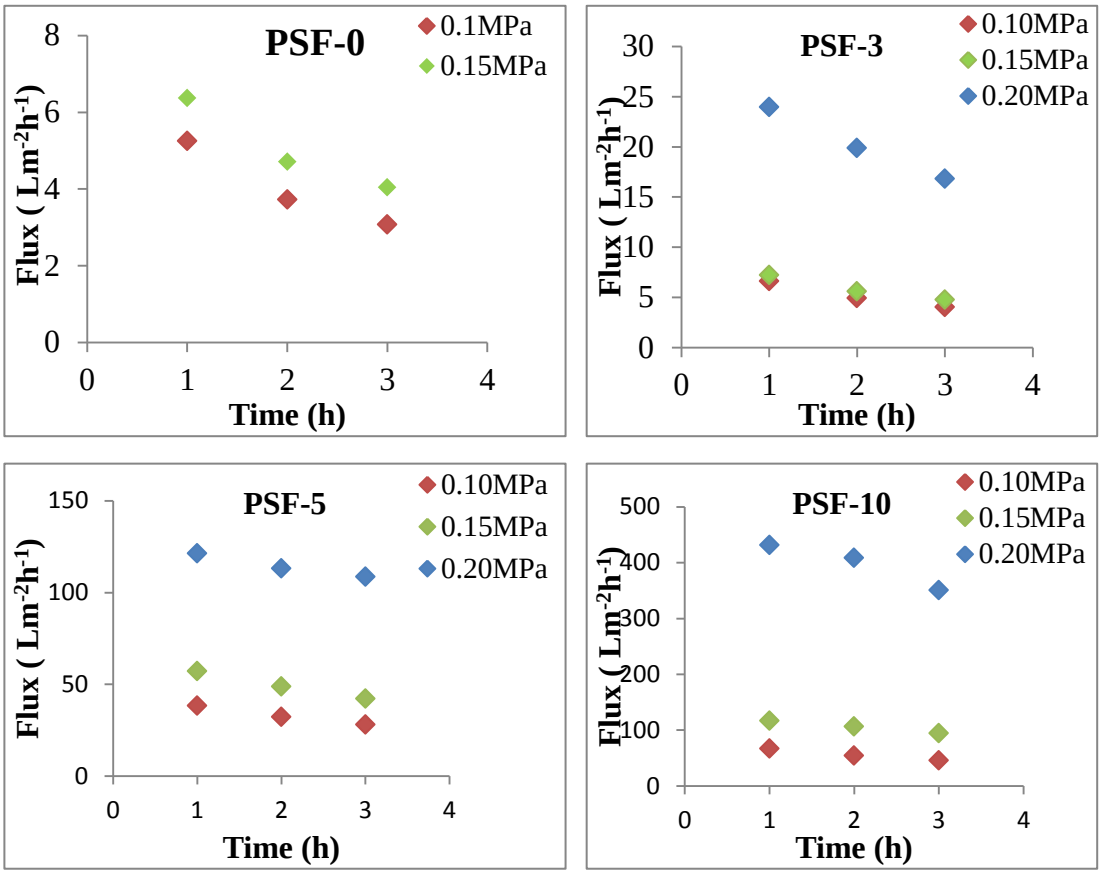
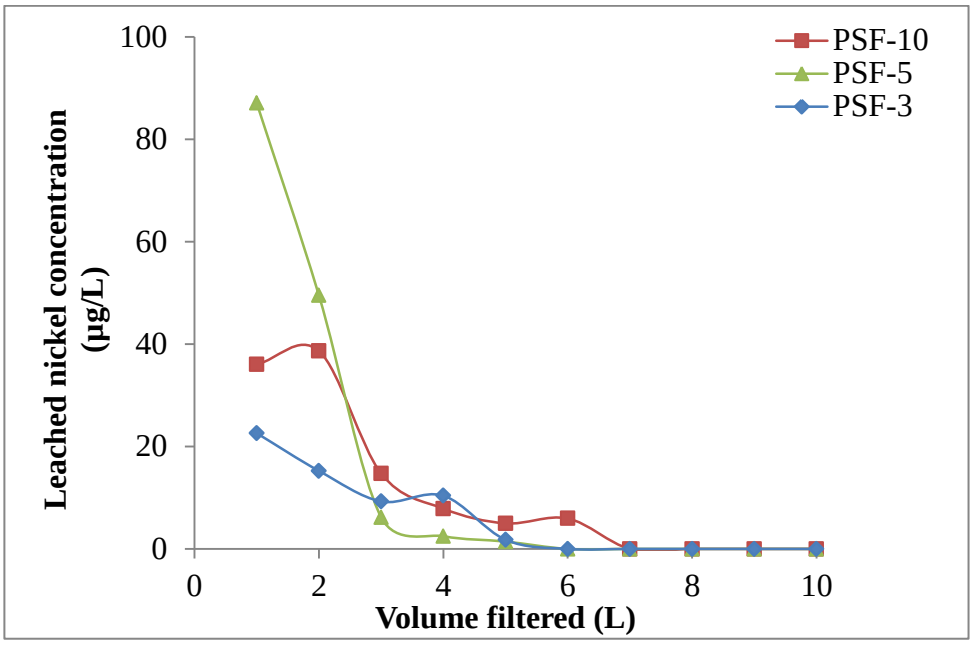


Figure 31 The flux of the Ni-modified and unmodified membranes at different pressures.

5.3.7 Leaching results

The result of the leaching of the embedded Ni nanoparticles is shown in Figure 32, and showed high initial leaching of the incorporated Ni nanoparticles from the membrane matrix. The leaching of the Ni nanoparticles was greatly reduced as more filtration was done. Similar trend was also observed by (Zhang et al. 2012d). The initially released Ni nanoparticles could be attributed to the unstable nanoparticles that were not properly bonded to the PSF matrix. The EDX of the membranes after filtration showed the presence of Ni nanoparticles in the modified PSF membranes after the leaching test was done, therefore the required attributes would be provided by the remaining Ni nanoparticles in the modified PSF membranes.



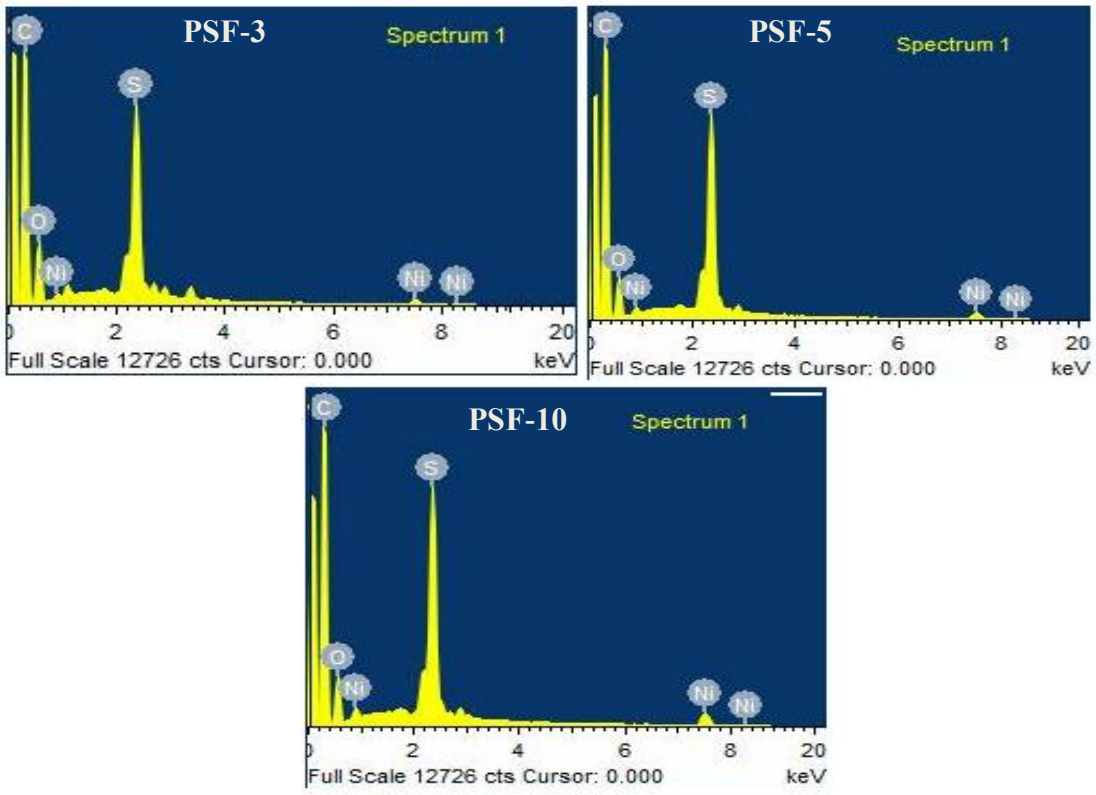


Figure 32 (a) Concentration of the released Ni nanoparticles, and (b) EDX of the "after leaching" membranes.

5.4 Characterization of the cobalt modified-PSF membranes

5.4.1 The SEM result

Similar to nickel modified-PSF membranes, the top surface of the cobalt modified-PSF membranes were relatively dense as can be seen in Figure 33. This is also as a result of the fact explained for the nickel modified-PSF membranes. Enhancement in the pore sizes and the porosity of the modified membranes can also be seen in the top surface as the embedded cobalt nanoparticles were increased. This is crucial to the selectivity of the modified membranes as the top surface of a membrane controls its selectivity.

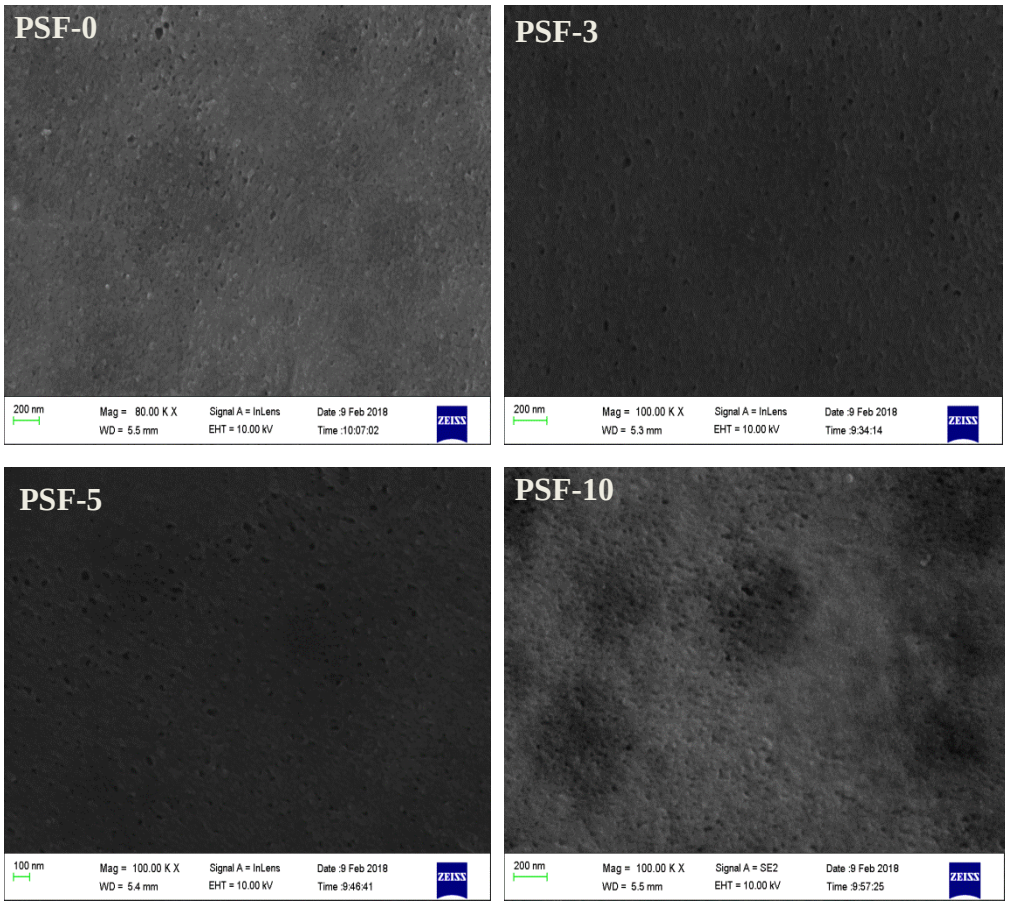


Figure 33 The SEM image of the top surface of the Co-modified and unmodified PSF membranes

The SEM image of the inner structure of the cobalt modified-PSF membranes is shown in Figure 34. The inner structure consists mainly of polymer-pore phases which are the pores of the membranes. The formation of the sponge-like highly porous structure can also be attributed to the relatively delayed phase inversion process that occurred in the inner structure unlike the top surface where the solvent-nonsolvent exchange was very fast. This delayed process gave enough time for the in-penetration of the nonsolvent and the out-transportion of the solvent resulting in a very porous structure.

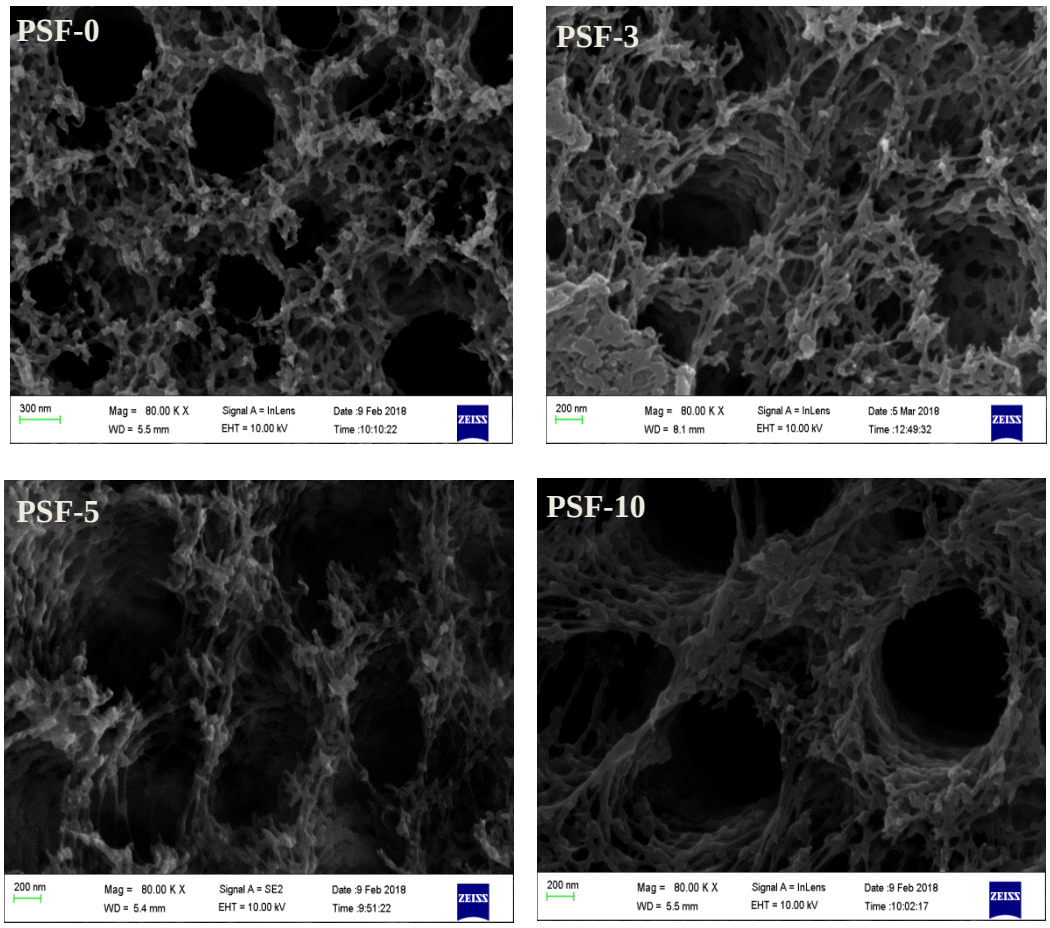


Figure 34 The SEM image inner structures of the Co-modified and unmodified PSF membranes

The pore sizes of the various Co-modified membranes seemingly increased as the amount of the incorporated Co nanoparticles was increased. However, the change in pore size was not quite significant in the PSF-3 membrane as compared to the unmodified membrane. An enormous increase in the pore size of the PSF-10 membrane was observed. This apparently shows that the pore size of polysulfone membranes can be significantly improved by embedding Co nanoparticles in the membrane matrix, and in our case, PSF-10 membrane gave the best result. Table 9 shows the pore sizes of the membranes.

Table 9 The pore sizes of the Co-modified and unmodified PSF membranes.

Membranes	**Pore size (μm)**
PSF-0	0.307
PSF-3	0.322
PSF-5	0.507
PSF-10	0.833

The EDX analysis result presented in Figure 35 confirms the presence of Co in the modified membranes matrix.

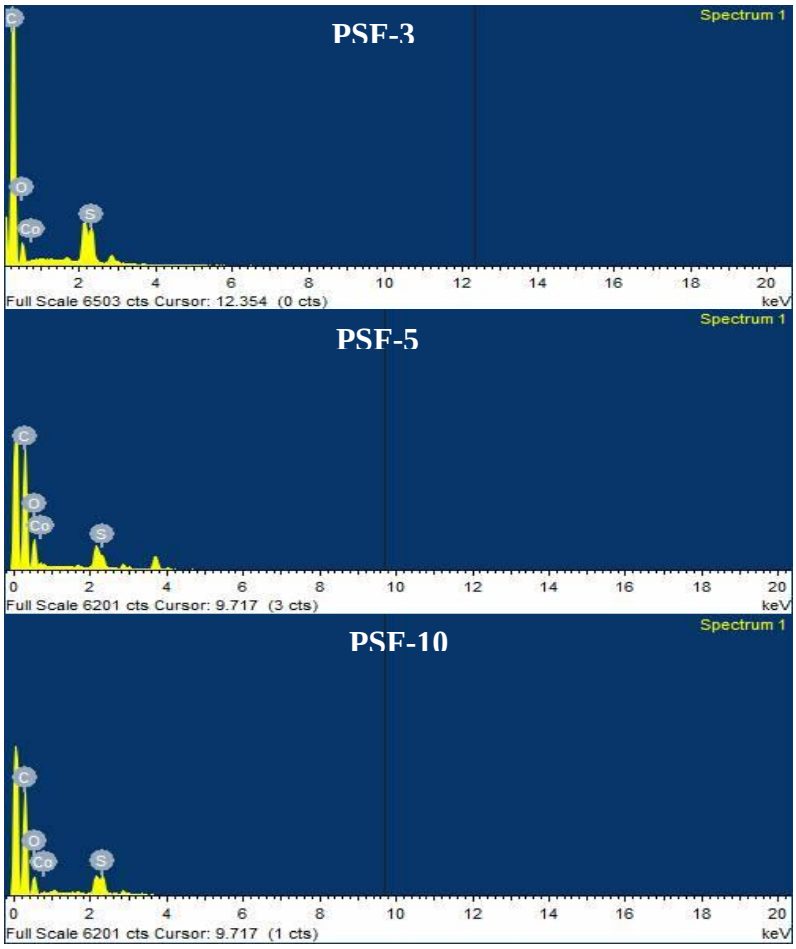


Figure 35 The EDX of the Co-modified PSF membranes

5.4.2 The AFM result

The graphical 3D images, as well as the quantitative AFM results were obtained as shown in figure 36 and table 10. There was an increment in roughness of the Co-modified membranes as the incorporated nanoparticles were increased. The PSF-10 membrane showed exhibited higher surface roughness while the PSF-3 has the least surface roughness. The increased surface roughness was expected to contribute in the enhancement of the flux of the membranes since the surface area was increased.

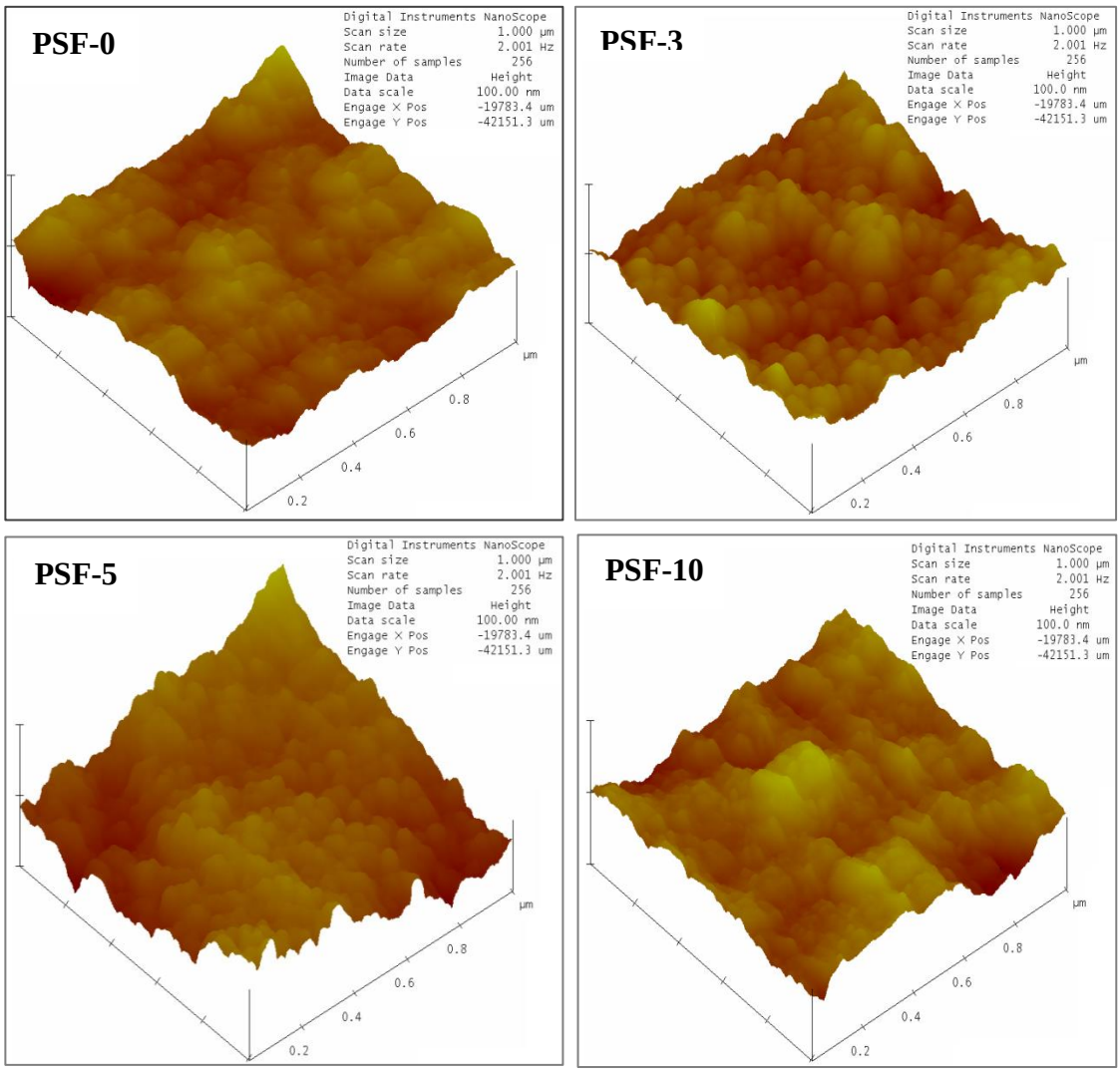


Figure 36 The 3D AFM image of the cobalt modified and unmodified PSF membranes.

The 2D AFM image and the quantitative roughness datails of the various Co-modified PSF membranes are shown in Figure 37, 38, and 39 respectively.

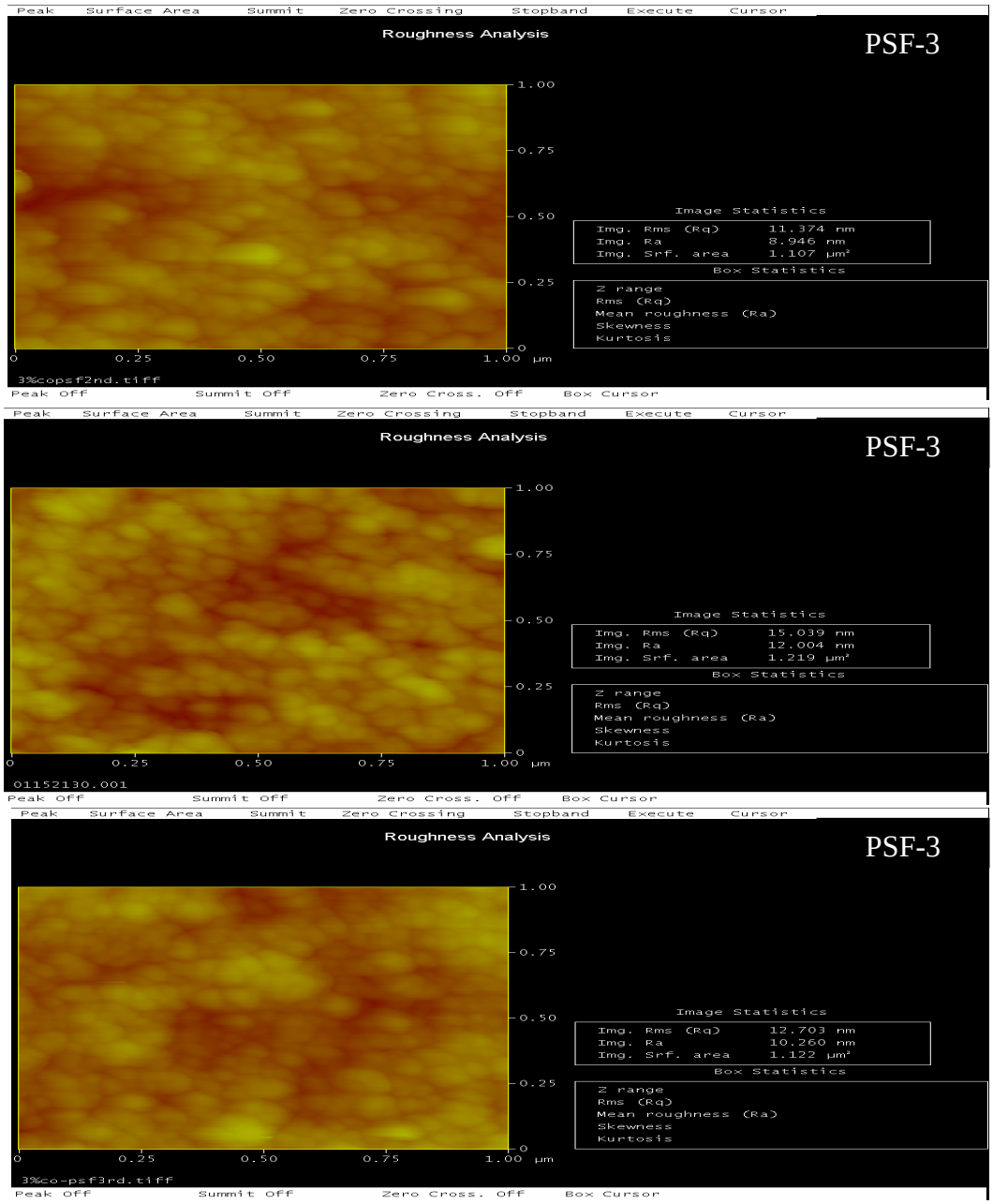


Figure 37 The 2D AFM image of the three different areas of the Co modified PSF-3 membrane.

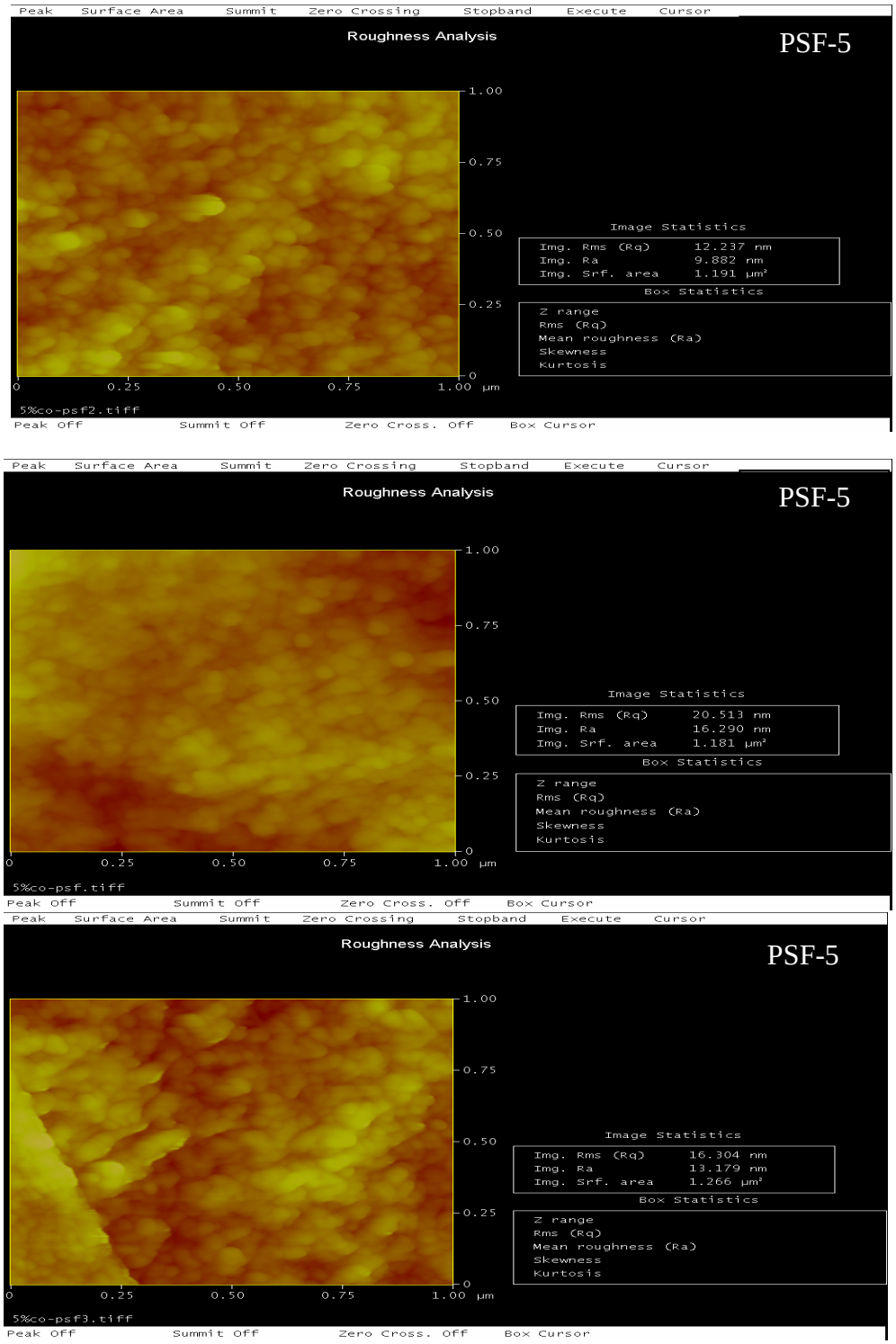


Figure 38 The 2D AFM image of the three different areas of the Co modified PSF-5 membrane.

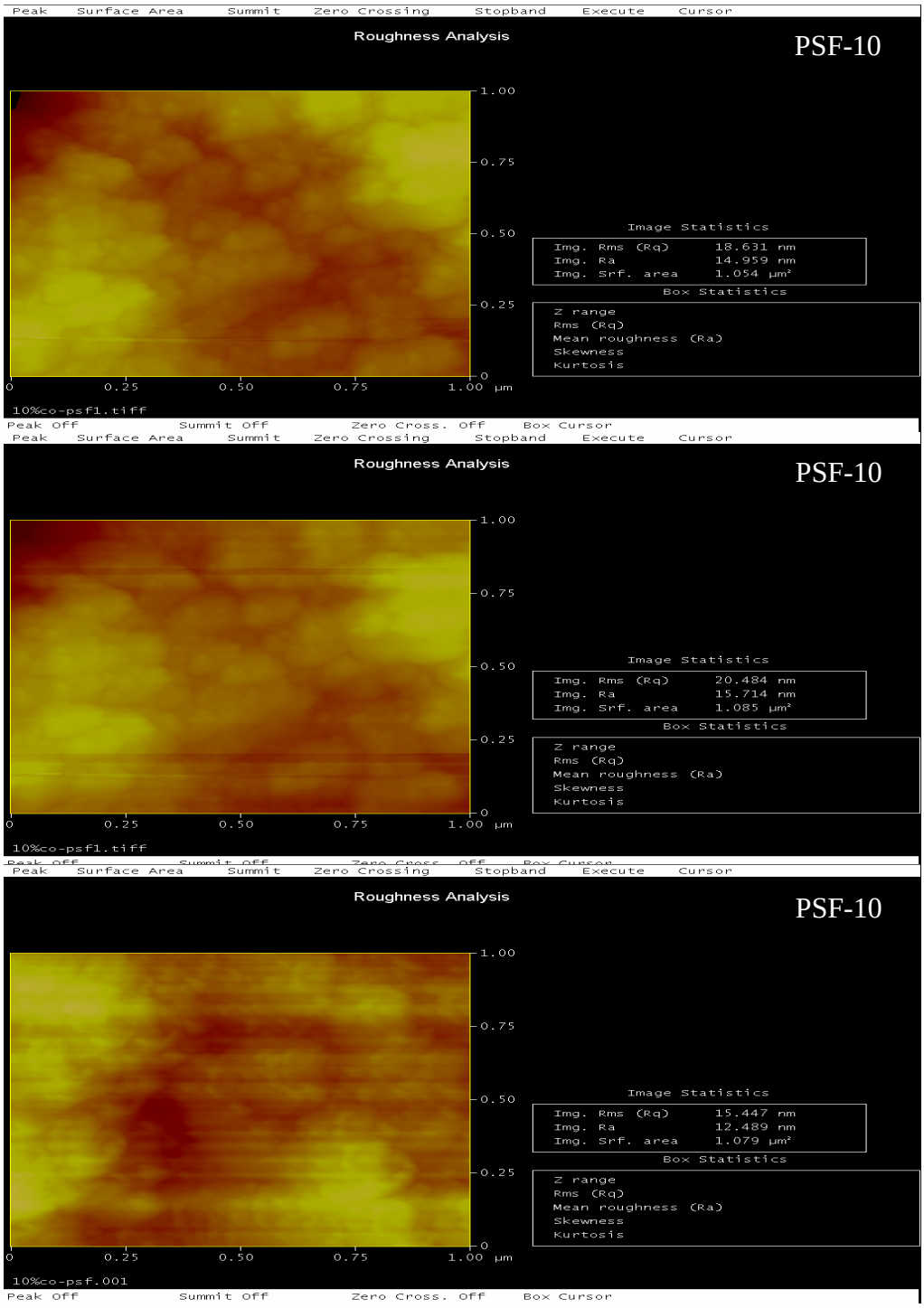


Figure 39 The 2D AFM image of the three different areas of the PSF-10 membrane.

The AFM roughness data (Ra and R_{RMS} values) of the Co-modified and unmodified PSF membranes are also summarized in Table 10.

Table 10 The R_a and R_{RMS} values of the Co-modified and unmodified PSF membranes.

Membranes	R_a(nm)	R_{RMS}(nm)
PSF-0	8.915	10.967
PSF-3	10.403±3.811	13.039±4.609
PSF-5	13.117±7.960	16.351±10.280
PSF-10	14.387±4.190	18.187±6.329

5.4.3 The FTIR result

The FTIR spectra of the Co-modified and the unmodified PSF membranes are presented in Figure 40. The characteristic absorption peaks of polysulfone were obvious in all the membranes, however, the peaks of the incorporated cobalt nanoparticles were not observed because of the small amount of the nanoparticles in the membrane matrix. A similar result was obtained in a silver modified PES membrane (Masheane 2016). The characteristic polysulfone absorption peak of 2969.57cm^{-1} corresponds to the C-H stretching vibrations. Other peaks at 1243.17cm^{-1} (C-O-C stretch), 1585.98, 1504.11 and 1488.30cm^{-1} (C=C stretching vibrations), and 1324.44 and 1294.79cm^{-1} (SO_2 symmetric stretch) were also seen.

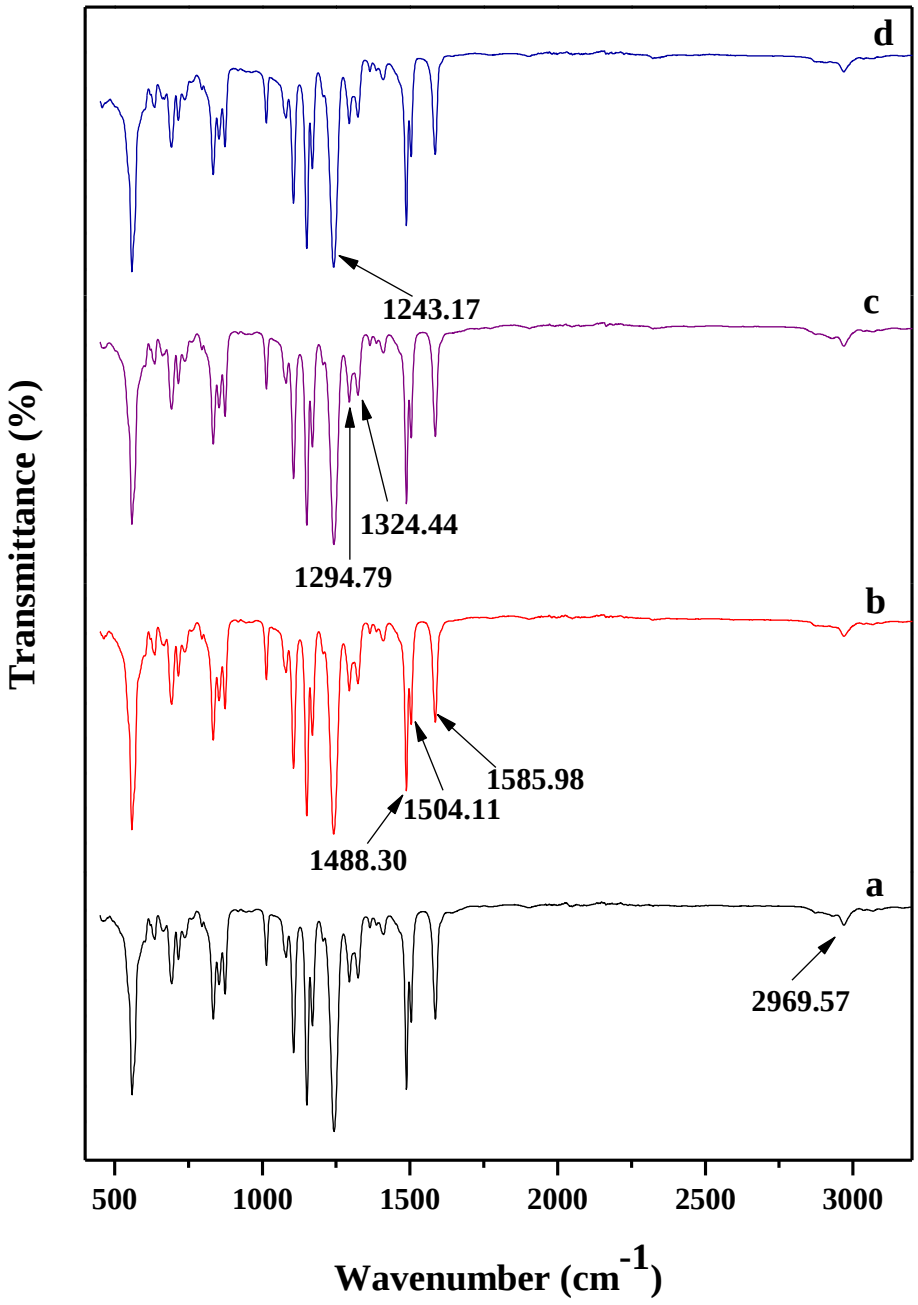


Figure 40 The FTIR spectra of (a) unmodified PSF-0, (b) Co modified PSF-3, (c) Co modified PSF-5, and (d) Co modified PSF-10.

5.4.4 The TGA result

The TGA result is presented in Figure 41, and it shows that the thermal stability of the Co-modified PSF membranes was improved with the incorporation of the Co nanoparticles.

Similar to Ni-PSF membranes, all the Co- modified PSF membranes have the same onset and endset temperatures. At the endset temperature, the mass loss of the PSF-0, PSF-3, PSF-5, and the PSF-10 membranes are 58.9%, 54.9%, 49.3%, and 43.1% respectively. The decrease in mass loss as the incorporated Co nanoparticles increases was attributed to the interaction in the nanocomposite matrix as explained in the case of Ni-modified PSF membranes. Contrary to Ni-PSF membranes, the mass loss of the Co modified PSF-0 and the PSF-3 are not the same.

At the limit temperatures, the residual masses of the Co modified PSF-3, PSF-5, and the PSF-10 membranes are 38.2%, 44.7%, 50.9% respectively.

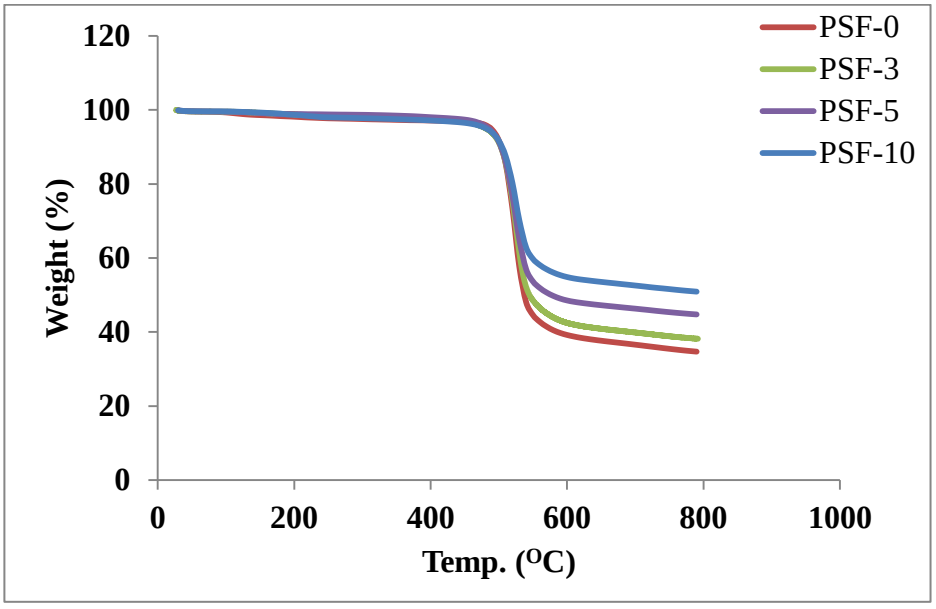


Figure 41 The TGA curve of the Co-modified and unmodified PSF membrane

5.4.5 The contact angle result

The hydrophilicity of the Co-modified PSF membranes and the unmodified membrane is shown in Table 11. There was an improvement in the hydophilicity of the Co modified PSF-3 and PSF-5 membranes as suggested by the decline in the contact angle of the membranes compared to the unmodified membrane. The contact angle of the PSF-10 membrane was unusually higher than the PSF-3 and PSF-5 membranes. The high contact angle of the PSF-10 membrane could be attributed to the agglomeration of the Co nanoparticles as a result of the higher concentration of the Co nanoparticles. At such high concentration, the interactions between the Co nanoparticles were quite significant leading to the clustering of the Co nanoparticles in the membrane solution. A similar observation was made in PSF membranes modified with carbon nanotubes (Qiu et al. 2009). The high contact angle of the PSF-10 correlates with the lower flux observed for the membrane as shown in the next subsection.

Table 11 Contact angle results of the Co-modified and unmodified PSF membranes.

Membranes	**Average contact angle (^{o})**
PSF-0	89.05
PSF-3	80.44
PSF-5	80.52
PSF-10	89.45

5.4.6 The flux result

The incorporation of the Co nanoparticles seemingly improved the flux of the PSF membranes at all the filtration pressures as shown in Figure 42. The incline in flux was attributed to the improved hydrophilicity of the various modified membranes as a

result of the embedded Co nanoparticles. The flux proportionally increased with the amount of the Co nanoparticles embedded, however, an exception was seen in PSF-10. At pressures of 0.10MPa and 0.15MPa, the flux of the PSF-10 membrane was lower than PSF-5 membrane flux. This is unusual since there were more of the hydrophilic nanoparticles in PSF-10. This decline in flux of the PSF-10 membrane at lower pressures was explained by the agglomeration seem in the PSF-10 membrane as shown below. The agglomerated Co nanoparticles in PSF-10 were as a result of the higher concentration of the nanoparticles in the PSF-10, and as a consequence, the pores of the membrane were blocked leading to the lower flux observed at these pressures. The high water contact angle of the PSF-10 membrane could also contribute to the lower flux. At pressure of 0.20MPa, the flux of the PSF-10 improved which could be attributed to the higher pressure that was sufficient to flush down the agglomerated nanoparticles blocking the pores of the membrane. For each of the pressures, there was a decline in flux with time. Similar result was obtained by (Zhang et al. 2012d). The PSF-0 and PSF-3 membranes could not withstand filtration at pressure of 0.20MPa as the membranes was torn during filtration at 0.20MPa, hence the flux results at this pressure was not obtained.

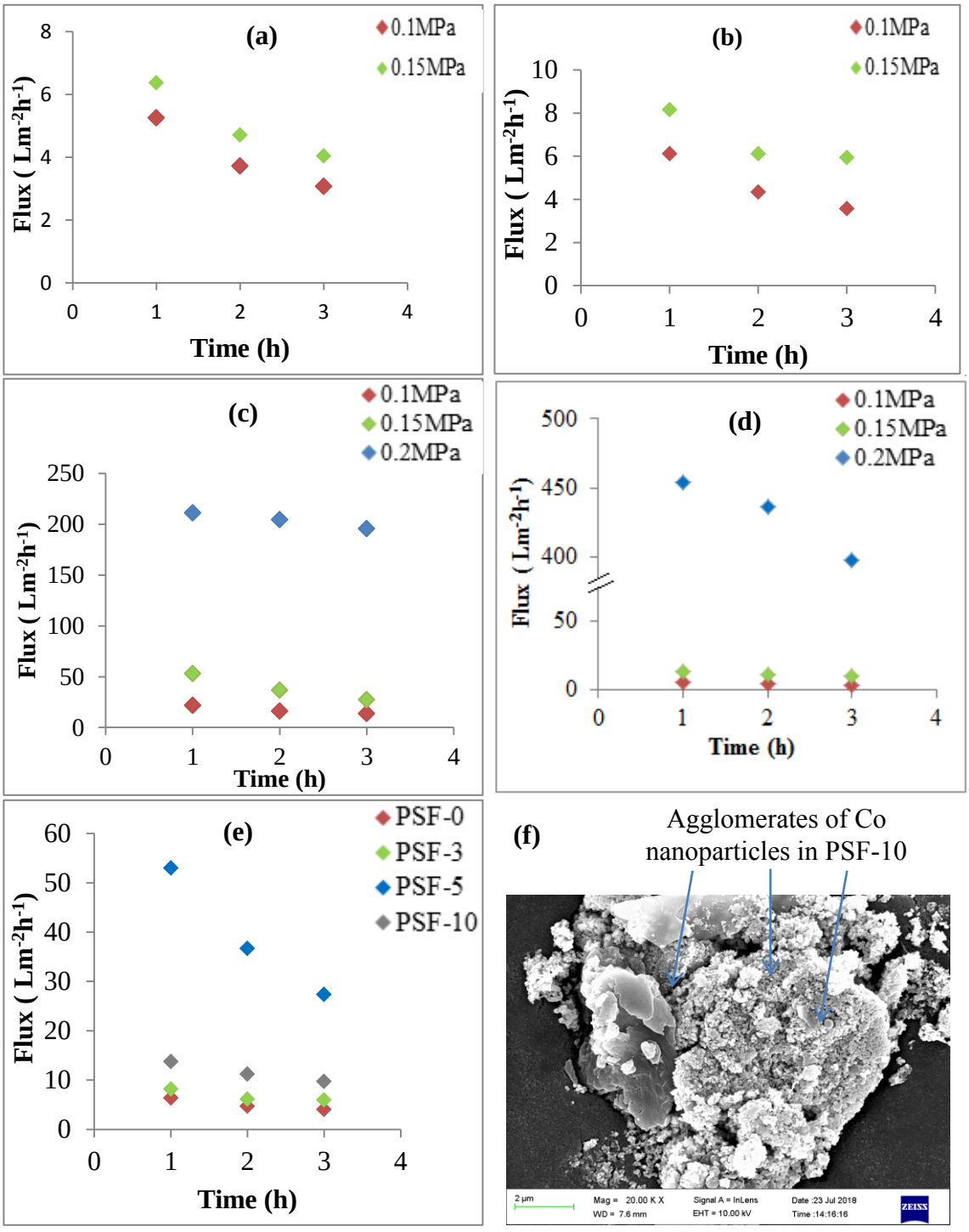


Figure 42 The flux of (a) unmodified PSF, (b) Co-modified PSF-3, (c) Co-modified PSF-5, (d) Co-modified PSF-10, (e) unmodified and modified Co-PSF membranes at 0.15MPa, and (f) agglomeration in PSF-10 membrane.

5.4.7 Leaching results

The result of the Co leaching is presented in Figure 43, and showed high initial leaching of the incorporated Co nanoparticles from the membrane matrix. The leaching of the Co nanoparticles was greatly reduced as more filtration was done. Similar trend was also observed by Zhang et al. (Zhang et al. 2012d). The initially released Co nanoparticles could be attributed to the unstable nanoparticles that were not properly bonded to the PSF matrix. The EDX of the membranes after filtration showed the presence of Co nanoparticles in the modified PSF membranes after the leaching test was done, therefore the required attributes would be provided by the remaining Co nanoparticles in the modified PSF membranes.

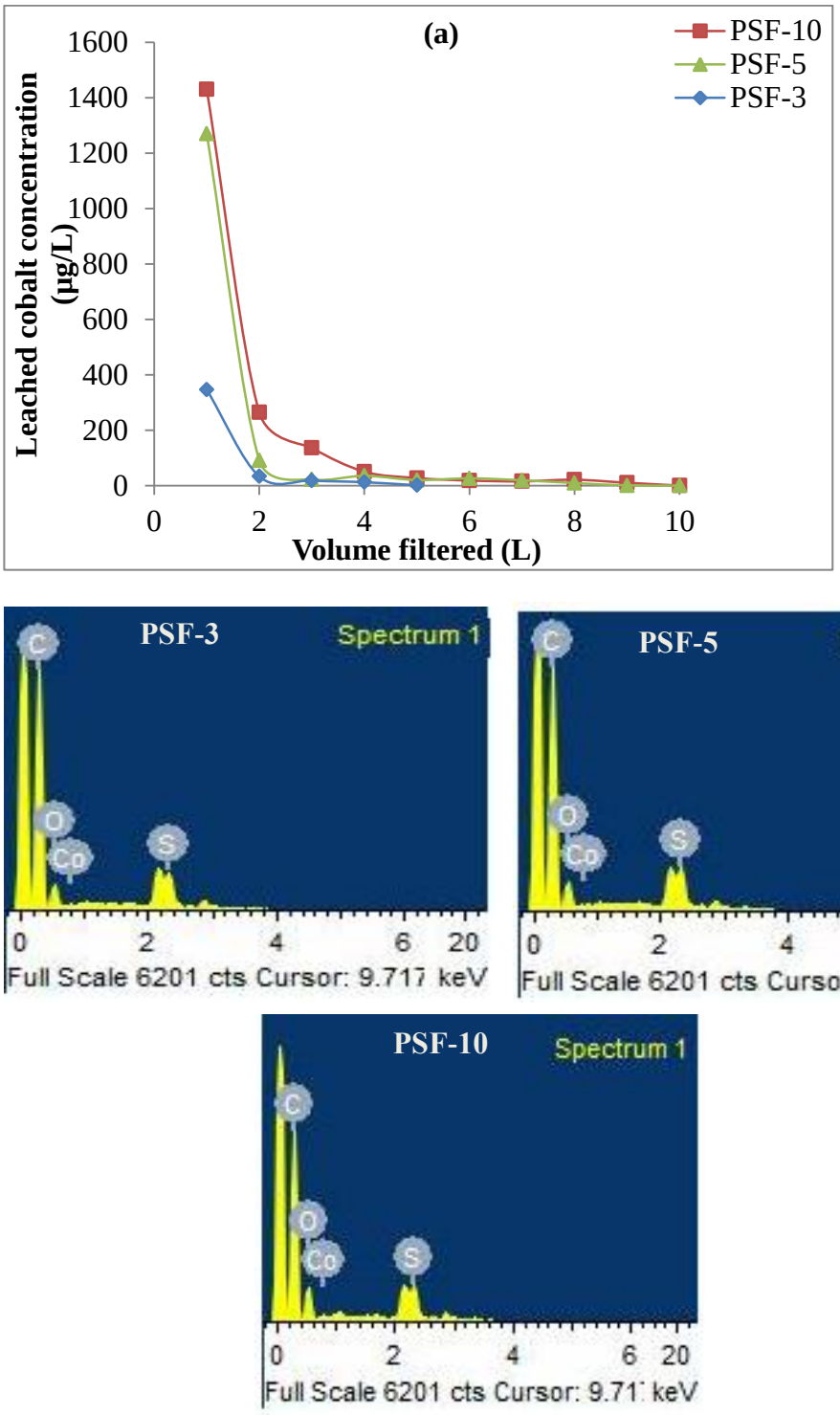


Figure 43 (a) The concentration of the released Co nanoparticles, and (b) EDX of the "after leaching" Co-PSF membranes.

CHAPTER 6

This chapter gives the conclusions and recommendations made from the findings of this research work.

6 CONCLUSIONS AND RECOMMENDATIONS

6.1 Conclusions

Ni and Co nanoparticles were successfully synthesized and used to modify PSF membranes. The embedment of the nanoparticles to the PSF matrix was found to have significant influence on the general characteristics and performance of the modified membranes. For all the modified membranes, the pore sizes were enhanced leading to improved flux of the membranes. The contact angle of the membranes modified with Ni nanoparticles was not improved significantly in the case of the PSF-3 and PSF-5, but a remarkable improvement was seen in the PSF-10 membrane. The improved contact angle of the Ni-modified PSF-10 membrane coupled with the enhanced pore size greatly improved the flux of the membrane. The leaching of the Ni nanoparticles from the modified membranes was not considered to be maximized as the amount of the embedded Ni nanoparticles was increased. For the Ni-modified nanocomposite membrane, the 10% Ni composition performed better.

For the membranes modified with Co, the pore sizes were enhanced as a result of the incorporated Co nanoparticles with the PSF-10 exhibiting the largest pore size. However, the contact angle of the Co modified PSF-10 was increased whereas a decline in the contact angle of PSF-3 and PSF-5 was observed. The increased contact angle of the Co modified PSF-10 membrane consequently led to a diminished flux of the membrane at lower pressures. The lower performance and agglomeration seen in the Co modified PSF-10 membrane shows that such amount of Co nanoparticles is not ideal for the modification of PSF membranes. The Co modified PSF-5 membranes exhibited the best consistent characteristic and performance results among the three Co modified membranes.

Generally, the stability of both the embedded Co and Ni nanoparticles was good as the leaching of the nanoparticles greatly decreased as the filtration progressed. The

high initial leaching was attributed to the nanoparticles that were not properly attached to the PSF matrix.

The results of this work proved that Co and Ni nanoparticles can be employed in the preparation of efficient modified PSF membranes, and the leaching of the nanoparticles will not limit the application of the modified membranes.

6.2 Recommendations

A concrete decision on the application of both the Co and Ni modified membranes for water treatment will be established if the membranes are employed for actual wastewater treatment. Hence it is recommended that the modified membranes are subjected to this test. This result of the analysis will help to ascertain whether the modified membranes are prone to fouling, their selectivity, and leaching at the pH of the various wastewater as they are exposed to realtime application.

The prospect of production of the modified Co and Ni PSF membranes at industrial level also needs to be investigated.

It may also be worthwhile to investigate the the use of other shapes and sizes of the Co and Ni nanoparticles in the modification of PSF membranes.

REFERENCES

Al Aani, S., Wright, C.J., Atieh, M.A., Hilal, N., 2017. Engineering nanocomposite membranes: Addressing current challenges and future opportunities. *Desalination*, 401, pp.1–15.

Ahmad, A.L., Ooi, B.S., Mohammad, A.W., Choudhury, J.P., 2004. Development of a highly hydrophilic nanofiltration membrane for desalination and water treatment. *Desalination*, 168, pp.215–221.

Allaker, R.P., 2010. The Use of Nanoparticles to Control Oral Biofilm Formation. *Journal of Dental Research*, 89(11), pp.1175–1186.

Amstad, E., Gopinadhan, M., Holtze, C., Osuji, C.O., Brenner, M.P., Spaepen, F., Weitz, D.A., 2015. NANOPARTICLES: Production of amorphous nanoparticles by supersonic spray-drying with a microfluidic nebulator. *Science*, 349(6251), pp.956–60.

Andrade, P.F., De Faria, A.F., Oliveira, S.R., Arruda, M.A.Z., Gonçalves, M.C., 2015. Improved antibacterial activity of nanofiltration polysulfone membranes modified with silver nanoparticles. *Water Research*, 81, pp.333–342.

Apel, P., 2001. Track etching technique in membrane technology. *Radiation Measurements*, 34(1–6), pp.559–566.

Bae, T. H., Kim, I.C., Tak, T.M., 2006. Preparation and characterization of fouling-resistant TiO2 self-assembled nanocomposite membranes. *Journal of Membrane Science*, 275(1–2), pp.1–5.

Bae, T.H., Tak, T.M., 2005. Effect of TiO2 nanoparticles on fouling mitigation of ultrafiltration membranes for activated sludge filtration. *Journal of Membrane Science*, 249(1–2), pp.1–8.

Barshik, C., Duckworth, D., Smith, D., 2000. Inorganic Mass Spectrometry: Fundamentals and Applications, New York: Marcel Dekker, Inc., pp.68-69.

Basile, A., Gallucci, F., 2011. Membranes for membrane reactors : preparation, optimization, and selection, Wiley, pp.2-10.

Beauchemin, D., 2010. Inductively Coupled Plasma Mass Spectrometry. *Analytical Chemistry*, 82(12), pp.4786–4810.

Beier, S.P., 2015. Pressure Driven Membrane Processes: Downstream Processing 3rd ed., London: Bookboon, pp.7-8.

Bhabra, G. et al., 2009. Nanoparticles can cause DNA damage across a cellular barrier. *Nature Nanotechnology*, 4(12), pp.876–883.

Bhushan, B., 2017. Handbook of Nanotechnology, 4th ed., Columbus: Springer, pp.1-2.

Bradley, L., Al-Shaeli, M.N.Z., 2017. Fundamentals of Membrane Bioreactors: Materials, Systems and Membrane Fouling, Singapore: Springer, pp.13-37.

Cao, G., Wang, Y., 2011. Nanostructures and Nanomaterials: synthesis, properties and applications, 2nd ed., Singapore: World Scientific, p.4.

Cao, X., Ma, J., Shi,X., Ren, Z., 2006. Effect of TiO2 nanoparticle size on the performance of PVDF membrane. *Applied Surface Science*, 253(4), pp.2003–2010.

Celik, E., Park, H., Choi, H., Choi, H., 2011. Carbon nanotube blended polyethersulfone membranes for fouling control in water treatment. *Water Research*, 45(1), pp.274–282.

Chin, A.B., Yaacob, I.I., 2007. Synthesis and characterization of magnetic iron oxide nanoparticles via w/o microemulsion and Massart's procedure. *Journal of Materials Processing Technology*, 191(1–3), pp.235–237.

Chin, S.F., Pang, S.C., Tan, C.H., 2011. Green Synthesis of Magnetite Nanoparticles (via Thermal Decomposition Method) with Controllable Size and Shape. *Journal of Material Environmental Science*, 2(3), pp.299–302.

Choi, I.H., Kima, I.C., Minb, B.R., Leea, K.H., 2006. Preparation and characterization of ultrathin alumina hollow fiber microfiltration membrane. *Desalination*, 193(1–3), pp.256–259.

Chou, W.L., Yu, D.G., Yang, M.C., 2005. The preparation and characterization of silver-loading cellulose acetate hollow fiber membrane for water treatment. *Polymers for Advanced Technologies*, 16(8), pp.600–607.

Chu, B., Hsiao, B., Fang, D., 2001. Apparatus and methods for electrospinning polymeric fibers and membranes. United States Patent.

Chun, Y., Mulcahy, D., Zou, L., Kim, I.S., 2017. A Short Review of Membrane Fouling in Forward Osmosis Processes. *Membranes*, 7(4), p.30.

Cui, Z.F., Muralidhara, H.S., 2010. Membrane Technology: A Practical Guide to Membrane Technology and Applications in Food and Bioprocessing, 1st ed., Oxford: Elsevier, p.6.

Dahe, G.J., Teotia, R.S., Bellare, J.R., 2012. The role of zeolite nanoparticles additive on morphology, mechanical properties and performance of polysulfone hollow fiber membranes. *Chemical Engineering Journal*, 197, pp.398–406.

Daraei, P., Madaeni, S.S., Ghaemi,N., Salehi, E., Khadivi, M.A., Moradian, R., Astinchap, B., 2012. Novel polyethersulfone nanocomposite membrane prepared by PANI/Fe3O4 nanoparticles with enhanced performance for Cu(II) removal from water. *Journal of Membrane Science*, 415–416, pp.250–259.

Department of Water Affairs (DWA), 2013. National Water Policy Review: Updated Policy Position to Overcome the Water Challenges of our Developmental State to Provide Access to Water, Equity and Sustainability, pp.5-25.

Du, W., Sun, Y., Ji, R., Zhu, J., Wub, J., Guo, H., 2011. TiO2 and ZnO nanoparticles negatively affect wheat growth and soil enzyme activities in agricultural soil. *Journal of Environmental Monitoring*, 13(4), p.822.

Eaton, P., West, P., 2010. Atomic Force Microscopy, 1st ed., New York: Oxford University Press, p.2.

Egerton, R.F., 2016. Physical Principles of Electron Microscopy: An Introduction to TEM, SEM and AEM, 2nd ed., Switzerland: Springer, p.17.

Elek, N., Hoffman, R., Raviv, U., Resh, R., Ishaaya, I., Magdassi, S., 2010. Novaluron nanoparticles: Formation and potential use in controlling agricultural insect pests. *Colloids and Surfaces A: Physicochemical and Engineering Aspects*, 372(1–3), pp.66–72.

Emadzadeh, D., Lau, W.J., Matsuura, T., Rahbari-Sisakht, M., Ismail, A.F., 2014. A novel thin film composite forward osmosis membrane prepared from PSf–TiO2 nanocomposite substrate for water desalination. *Chemical Engineering Journal*, 237, pp.70–80.

European Community, 2000. Directive 2000/60/EC of the European Parliament and of the Council of 23 October 2000 establishing a framework for Community action in the field of water policy. *Official Journal of the European Parliament*, L327(September 1996), pp.1–82.

Goldstein, J.I., Yakowitz, H., 1975. Practical Scanning Electron Microscopy: Electron and Ion Microprobe Analysis, 1st ed.,New York: Springer. p.2.

Goosen, M.F.A., Sablani, S. S., Al-Hinai, H., Al-Obeidani, S., Al-Belushi, R., Jackson, D., 2005. Fouling of Reverse Osmosis and Ultrafiltration Membranes: A Critical Review. *Separation Science and Technology*, 39(10), pp.2261–2297.

Gopal, R., Kaur, S., Ma, Z., Chan, C., Ramakrishna, S., Matsuura, T., 2006. Electrospun nanofibrous filtration membrane. *Journal of Membrane Science*, 281(1–2), pp.581–586.

Gu, H., Wang, C., Gong, S., Mei, Y., Li, H., Ma, W., 2016. Investigation on contact angle measurement methods and wettability transition of porous surfaces. *Surface and Coatings Technology*, 292, pp.72–77.

Guo, W., Ngo, H.H., Li, J., 2012. A mini-review on membrane fouling. *Bioresource Technology*, 122, pp.27–34.

Hainfeld, J.F., Slatkin, D.N., Smilowitz, H.M., 2004. The use of gold nanoparticles to enhance radiotherapy in mice. *Physics in Medicine and Biology*, 49(18), pp.309–315.

Hamid, N.A.A., Ismail, A.F., Matsuura, T., Zularisam, A.W., Lau, W.J., Yuliwati, E., Abdullah, M.S., 2011. Morphological and separation performance study of polysulfone/titanium dioxide (PSF/TiO2) ultrafiltration membranes for humic acid removal. *Desalination*, 273(1), pp.85–92.

Hernández-Sierra, J.F. et al., 2008. The antimicrobial sensitivity of Streptococcus mutans to nanoparticles of silver, zinc oxide, and gold. *Nanomedicine: nanotechnology, biology, and medicine*, 4(3), pp.237–40.

Herrera, A.P., Polo-Corrales, L., Chavezb, E., Cabarcas-Bolivar, J., Uwakweh, O.N.C., Rinaldi, C., 2013. Influence of aging time of oleate precursor on the magnetic relaxation of cobalt ferrite nanoparticles synthesized by the thermal decomposition method. *Journal of Magnetism and Magnetic Materials*, 328, pp.41–52.

Hoang, V.V., Ganguli, D., 2012. Amorphous nanoparticles — Experiments and computer simulations. *Physics Reports*, 518(3), pp.81–140.

Hołda, A.K., Vankelecom, I.F.J., 2015. Understanding and guiding the phase inversion process for synthesis of solvent resistant nanofiltration membranes. *Journal of Applied Polymer Science*, 132(27), p.42130.

Homayoonfal, M., Mehrnia, M.R., Shariaty-Niassar, M., Akbari, A., Ismail, A.F., Matsuura, T., 2014. A comparison between blending and surface deposition methods for the preparation of iron oxide/polysulfone nanocomposite membranes. *Desalination*, 354, pp.125–142.

Homayoonfal, M., Mehrnia, M.R., Rahmani, S., Mojtahedi, Y.M., 2015. Fabrication of alumina/polysulfone nanocomposite membranes with biofouling mitigation approach in membrane bioreactors. *Journal of Industrial and Engineering Chemistry*, 22, pp.357–367.

Hosokawa, M., Nogi, K., Naito, M., Yokoyama, T., 2012. *Nanoparticle technology handbook*, 2nd ed., Netherlands: Elsevier, p.5.

Houshiar, M., Zebhi, F., Razi, Z.J., Alidoust, A., Askari, Z., 2014. Synthesis of cobalt ferrite (CoFe2O4) nanoparticles using combustion, coprecipitation, and precipitation methods: A comparison study of size, structural, and magnetic properties. *Journal of Magnetism and Magnetic Materials*, 371, pp.43–48.

Jang, J.H., Lim, H.B., 2010. Characterization and analytical application of surface modified magnetic nanoparticles. *Microchemical Journal*, 94(2), pp.148–158.

Jenning, V., Gysler, A., Schafer-Korting, M., Gohla, S.H., 2000. Vitamin A loaded solid lipid nanoparticles for topical use: occlusive properties and drug targeting to the upper skin. *European Journal of Pharmaceutics and Biopharmaceutics*, 49(3), pp.211–218.

JEOL, Scanning Electron Microscope A To Z: Basic Knowledge For Using The SEM, p.3.

Jhaveri, J.H., Murthy, Z.V.P., 2016. A comprehensive review on anti-fouling nanocomposite membranes for pressure driven membrane separation processes. *Desalination*, 379, pp.137–154.

Jyothi, M.S., Nayak, V., Padaki, M., Balakrishna, R.G., Soontarapa, K., 2016. Aminated polysulfone/TiO2 composite membranes for an effective removal of Cr(VI). *Chemical Engineering Journal*, 283, pp.1494–1505.

Kamal, S.S.K., Sahoo, P.K., Premkumar, M., Rao, N.V.R., Kumar, T.J., Sreedhar, B., Singh, A.K., Ram, S., Sekhar, K.C., 2009. Synthesis of cobalt nanoparticles by a modified polyol process using cobalt hydrazine complex. *Journal of Alloys and Compounds*, 474(1–2), pp.214–218.

Khulbe, K.C., Feng, C.Y., Matsuura, T., 2008. Synthetic Polymeric Membranes: Characterization by Atomic Force Microscopy, 1st ed. Berlin: Springer, pp.6-7.

Kim, E.S., Hwang, G., El-Din, M.G., Liu, Y., 2012. Development of nanosilver and multi-walled carbon nanotubes thin-film nanocomposite membrane for enhanced water treatment. *Journal of Membrane Science*, 394–395, pp.37–48.

Kim, S.W., Jung, J.H., Lamsal K., Kim Y.S., Min, J.S., Lee, Y.S., 2012. Antifungal Effects of Silver Nanoparticles (AgNPs) against Various Plant Pathogenic Fungi. *Mycobiology*, 40(1), p.53.

Kim, Y., Kim, D., Lee, C.S., 2003. Synthesis and characterization of CoFe2O4 magnetic nanoparticles prepared by temperature-controlled coprecipitation method. *Physica B: Condensed Matter*, 337(1–4), pp.42–51.

Kodama, R., 1999. Magnetic nanoparticles. *Journal of Magnetism and Magnetic Materials*, 200(1–3), pp.359–372.

Kohli, R., Mittal, K.L., 2016. Developments in surface contamination and cleaning: Fundamentals and applied aspects, 2nd ed., London: Matthew Deans, p.452.

Koseoglu-Imer, D.Y., Kose, B., Altinbas, M., Koyuncu, I., 2013. The production of polysulfone (PS) membrane with silver nanoparticles (AgNP): Physical properties, filtration performances, and biofouling resistances of membranes. *Journal of Membrane Science*, 428, pp.620–628.

Kwok, D.Y., Gietzelt, T., Grundke, K., Jacobasch, H.J., Neumann, A.W., 1997. Contact Angle Measurements and Contact Angle Interpretation. 1. Contact Angle Measurements by Axisymmetric Drop Shape Analysis and a Goniometer Sessile Drop Technique. *Langmuir*, 13(10), pp.2880–2894.

Lakshmanan, R., Okoli, C., Boutonnet, M., Jara, S., Rajarao, G.K., 2014. Microemulsion prepared magnetic nanoparticles for phosphate removal: Time efficient studies. *Journal of Environmental Chemical Engineering*, 2(1), pp.185–189.

Lalia, B.S., Kochkodan, V., Hashaikeh, R., Hilal, N., 2013. A review on membrane fabrication: Structure, properties and performance relationship. *Desalination*, 326, pp.77–95.

Lee, S., Choi, In., Myung, S., Park, J., Kim, I., Kim, W., Lee, K., 2008. Preparation and characterization of nickel hollow fiber membrane. *Desalination*, 233(1–3), pp.32–39.

Leo, C.P., Cathie Lee, W.P., Ahmad, A.L., Mohammad, A.W., 2012. Polysulfone membranes blended with ZnO nanoparticles for reducing fouling by oleic acid. *Separation and Purification Technology*, 89, pp.51–56.

Li, X., Sotto, A., Li, J., Van der Bruggen, B., 2017. Progress and perspectives for synthesis of sustainable antifouling composite membranes containing in situ generated nanoparticles. *Journal of Membrane Science*, 524, pp.502–528.

Li, X., Fang, X., Pang, R., Li, J., Sun, X., Shen, J., Han, W., Wang, L., 2014. Self-assembly of TiO2 nanoparticles around the pores of PES ultrafiltration membrane for mitigating organic fouling. *Journal of Membrane Science*, 467, pp.226–235.

Liang, S., Xiao, K., Mo, Y., Huang, X., 2012. A novel ZnO nanoparticle blended polyvinylidene fluoride membrane for anti-irreversible fouling. *Journal of Membrane Science*, 394–395, pp.184–192.

Liesl K. Massey, 2003. Permeability Properties of Plastics and Elastomers : A Guide to packaging and barrier materials, 2nd ed., New York: William Andrew Publishing, p.295.

Luo, M., Zhao, J., Tang, W., Pu, C., 2005. Hydrophilic modification of poly(ether sulfone) ultrafiltration membrane surface by self-assembly of TiO2 nanoparticles. *Applied Surface Science*, 249(1–4), pp.76–84.

Mahmoudi, M., Sant, S., Wang, B., Laurent, S., Sen, T., 2011. Superparamagnetic iron oxide nanoparticles (SPIONs): Development, surface modification and applications in chemotherapy. *Advanced Drug Delivery Reviews*, 63(1–2), pp.24–46.

Malik, M.A., Wani, M.Y., Hashim, M.A., 2012. Microemulsion method: A novel route to synthesize organic and inorganic nanomaterials: 1st Nano Update. *Arabian Journal of Chemistry*, 5(4), pp.397–417.

Masheane, M., 2016. Greener synthesis of biopolymer-inorganic nanocomposite beads and membranes for use in water purification, pp.175-176.

Meyer, E., 1992. Atomic force microscopy. *Progress in Surface Science*, 41(1), pp.3–49.

Zhang, M., Li, C., Benjamin, M., Chang, Y.,2003. Fouling and Natural Organic Matter Removal in Adsorbent/Membrane Systems for Drinking Water Treatment. *Environmental Science Technology*, 37(8), pp.1663–1669.

Min, Y., Akbulut, M., Kristiansen, K., Golan, Y., Israelachvili, J., 2008. The role of interparticle and external forces in nanoparticle assembly. *Nature Materials*, 7(7), pp.527–538.

Miyazaki, T., Takenaka, M., 2017. Precise small-angle X-ray scattering evaluation of the pore structures in track-etched membranes: Comparison with other convenient evaluation methods. *Nuclear Instruments and Methods in Physics Research Section B: Beam Interactions with Materials and Atoms*, 394, pp.121–125.

Ng, L.Y., Mohammad, A. W., Leo, C. P., Hilal, N., 2013. Polymeric membranes incorporated with metal/metal oxide nanoparticles: A comprehensive review. *Desalination*, 308, pp.15–33.

Ning, R.Y., 2011. EXPANDING ISSUES IN DESALINATION, 1st ed., Croatia: Intech, pp. 66-78.

Oh, S.J., Kim, N., Lee, Y.T., 2009. Preparation and characterization of PVDF/TiO2 organic–inorganic composite membranes for fouling resistance improvement. *Journal of Membrane Science*, 345(1–2), pp.13–20.

Okoli, C., Boutonnet, M., Mariey, L., Järås, S., Rajarao, G., 2011. Application of magnetic iron oxide nanoparticles prepared from microemulsions for protein purification. *Journal of Chemical Technology & Biotechnology*, 86(11), pp.1386–1393.

Oxford University Press, 2004. *Oxford English Dictionary*, Oxford University Press.

Peinemann, K.V., Nunes, S.P., 2010. Membranes for water treatment, Weinheim: Wiley-VCH, p.237.

Petersen, R.J., 1993. Composite reverse osmosis and nanofiltration membranes. *Journal of Membrane Science*, 83(1), pp.81–150.

Phelane, L., Muya, F.N., Richards, H.L., Baker, P.G.L., Iwuoha, E.I., 2014. Polysulfone Nanocomposite Membranes with improved hydrophilicity. *Electrochimica Acta*, 128, pp.326–335.

Qiu, S., Wu, L., Pan, X., Zhang, L., Chen, H., Gao, C., 2009. Preparation and properties of functionalized carbon nanotube/PSF blend ultrafiltration membranes. *Journal of Membrane Science*, 342(1–2), pp.165–172.

Qu, X., Alvarez, P.J.J., 2013. Applications of nanotechnology in water and

wastewater treatment. *Water Research*, 47(12), pp.3931–3946.

Raaijmakers, M.J.T., Benes, N.E., 2016. Current trends in interfacial polymerization chemistry. *Progress in Polymer Science*, 63, pp.86–142.

Radjenović, J., Petrović, M., Ventura, F., Barceló, D., 2008. Rejection of pharmaceuticals in nanofiltration and reverse osmosis membrane drinking water treatment. *Water Research*, 42(14), pp.3601–3610.

Rajaeian, B., Rahimpour, A., Tade, M. O., Liu, S., 2013. Fabrication and characterization of polyamide thin film nanocomposite (TFN) nanofiltration membrane impregnated with TiO2 nanoparticles. *Desalination*, 313, pp.176–188.

Rajaeian, B., Heitz, A., Tade, M. O., Liu, S., 2015. Improved separation and antifouling performance of PVA thin film nanocomposite membranes incorporated with carboxylated TiO2 nanoparticles. *Journal of Membrane Science*, 485, pp.48–59.

Rana, D., Matsuura, T., 2010. Surface Modifications for Antifouling Membranes. *Chemical Reviews*, 110(4), pp.2448–2471.

Razmjou, A., Resosudarmo, A., Holmes, R. L., Li, H., Mansouri, J., Chen, V., 2012. The effect of modified TiO2 nanoparticles on the polyethersulfone ultrafiltration hollow fiber membranes. *Desalination*, 287, pp.271–280.

Razmjou, A., Mansouri, J., Chen, V., 2011. The effects of mechanical and chemical modification of TiO2 nanoparticles on the surface chemistry, structure and fouling performance of PES ultrafiltration membranes. *Journal of Membrane Science*, 378(1–2), pp.73–84.

Rugar, D. & Hansma, P., 1990. ATOMIC FORCE MICROSCOPY. *Physics Today*, 10, p.24.

Nunes, S.P., Peinemann, K. V., 2006. Membrane technology in the chemical

industry, 2nd ed., Weinheim: Wiley-VCH, p.99.

Saleh, T.A., Gupta, V.K., 2016. Nanomaterial and polymer membranes : synthesis, characterization, and applications, 1st ed., Amsterdam: Elsevier, p.170.

Sattler, K.D., 2011. Handbook of Nanophysics: Nanoparticles and Quantum Dots, London: CRC Press, pp.1-30.

Sawada, I., Fachrul, R., Ito, T., Ohmukai, Y., Maruyama, T., Matsuyama, H., 2012. Development of a hydrophilic polymer membrane containing silver nanoparticles with both organic antifouling and antibacterial properties. *Journal of Membrane Science*, 387–388, pp.1–6.

Sotto, A., Boromand, A., Zhang, R., Luis, P., Arsuaga, J. M., Kim, J., Van der Bruggen, B., 2011. Effect of nanoparticle aggregation at low concentrations of TiO2 on the hydrophilicity, morphology, and fouling resistance of PES–TiO2 membranes. *Journal of Colloid and Interface Science*, 363(2), pp.540–550.

South Africa Yearbook, 2015. *Land and it's people*, p.3.

Suh, S.K., Yuet, K., Hwang, D.K., Bong, K.W. Doyle, P.S. Hatton, T.A., 2012. Synthesis of Nonspherical Superparamagnetic Particles: *In Situ* Coprecipitation of Magnetic Nanoparticles in Microgels Prepared by Stop-Flow Lithography. *Journal of the American Chemical Society*, 134(17), pp.7337–7343.

Tartaj, P., Morales, M., Veintemillas-Verdaguer, S., Gonz lez-Carreno, T., Serna, C.J., 2003. The preparation of magnetic nanoparticles for applications in biomedicine. *Journal of Physics D: Applied Physics*, 36(13), pp.182–197.

Tian, Y., Wu, M., Liu, R., Li, Y., Wang, D., Tan, J., Wu, R., Huang, Y., 2011. Electrospun membrane of cellulose acetate for heavy metal ion adsorption in water treatment. *Carbohydrate Polymers*, 83(2), pp.743–748.

Toimil-Molares, M.E., 2012. Characterization and properties of micro- and nanowires of controlled size, composition, and geometry fabricated by electrodeposition and ion-track technology. *Beilstein journal of nanotechnology*, 3, pp.860–83.

United Nations Department of Social and Economic Affairs (UNDESA), 2014. International Decade for Action "Water for Life" 2005-2015. Focus Areas: Water scarcity.

Van Der Bruggen, B., Vandecasteele, C., Van Gestel, T., Doyen, W., Leysen , R., 2003. A review of pressure-driven membrane processes in wastewater treatment and drinking water production. *Environmental Progress*, 22(1), pp.46–56.

Vyazovkin, S., 2012. Thermogravimetric Analysis. In Characterization of Materials, New Jersey: John Wiley & Sons, Inc., pp. 1–12.

Wang, L.K., Kajitvichyanukul, P., Hung Y.T., 2011. Membrane and Desalination Technologies, *Handbook of Environmental Engineering*, The Humana Press Inc., NewYork Totowa, NJ: Humana Press, pp. 639-668

Water Research Commission (WRC), 2015. Water resource management, p.15.

Webb, J., Holgate, J.H., 2003. MICROSCOPY: Scanning Electron Microscopy. *Encyclopedia of Food Sciences and Nutrition*. Elsevier, pp. 3922–3928.

Weber, R., Chmiel, H., Mavrov, V., 2003. Characteristics and application of new ceramic nanofiltration membranes. *Desalination*, 157(1–3), pp.113–125.

Werber, J.R., Osuji, C.O., Elimelech, M., 2016. Materials for next-generation desalination and water purification membranes. *Nature Reviews Materials*, 1(5), p.16018.

WHO, 2006. Cobalt and Inorganic Cobalt Compounds, p.32

WHO, 2005. Nickel in Drinking-water Background document for development of WHO Guidelines for Drinking-water Quality, Geneva, p.16.

WHO, 2003. Silver in Drinking water: Background document for development of WHO Guidelines for Drinking-water Quality, Geneva, p.3.

World Health Organisation (WHO), 2001. Guidelines: the current position, pp.18-39.

World Health Organisation (WHO), 2017. WHO | Drinking-water, World Health Organization, pp. 1-7.

Wu, S.H., Chen, D.H., 2003. Synthesis and characterization of nickel nanoparticles by hydrazine reduction in ethylene glycol. *Journal of Colloid and Interface Science*, 259(2), pp.282–286.

Wu, Z.G., Munoz, M., Montero, O., 2010. The synthesis of nickel nanoparticles by hydrazine reduction. *Advanced Powder Technology*, 21(2), pp.165–168.

Yang, Y., Zhang, H., Wang, P., Zheng, Q., Li, J., 2007. The influence of nano-sized TiO2 fillers on the morphologies and properties of PSF UF membrane. *Journal of Membrane Science*, 288(1–2), pp.231–238.

Yin, J., Deng, B., 2015. Polymer-matrix nanocomposite membranes for water treatment. *Journal of Membrane Science*, 479, pp.256–275.

Zare, Y., 2016. Study of nanoparticles aggregation/agglomeration in polymer particulate nanocomposites by mechanical properties. *Composites Part A: Applied Science and Manufacturing*, 84, pp.158–164.

Zhang, F., Zhang, W., Yu, Y., Deng, B., Li, J., Jin, J., 2013. Sol–gel preparation of PAA-g-PVDF/TiO2 nanocomposite hollow fiber membranes with extremely high water flux and improved antifouling property. *Journal of Membrane Science*, 432, pp.25–32.

Zhang, G., Lu, S., Zhang, L., Meng, Q., Shen, C., Zhang, J., 2013. Novel polysulfone hybrid ultrafiltration membrane prepared with TiO2-g-HEMA and its antifouling characteristics. *Journal of Membrane Science*, 436, pp.163–173.

Zhang, M., Zhang, K., De Gusseme, B., Verstraete, W., 2012. Biogenic silver nanoparticles (bio-Ag0) decrease biofouling of bio-Ag0/PES nanocomposite membranes. *Water Research*, 46(7), pp.2077–2087.

Zhao, H., Qiu, S., Wu, L., Zhang, L., Chen, H., Gao, C., 2014. Improving the performance of polyamide reverse osmosis membrane by incorporation of modified multi-walled carbon nanotubes. *Journal of Membrane Science*, 450, pp.249–256.

Zodrow, K., Brunet, L., Mahendra, S., Li, D., Zhang, A., Li, Q., Alvarez, P. J.J., 2009. Polysulfone ultrafiltration membranes impregnated with silver nanoparticles show improved biofouling resistance and virus removal. *Water Research*, 43(3), pp.715–723.